Cross-shelf Transport and Exchange between a Temperate Shelf Sea and the North Atlantic Ocean

Thesis submitted in accordance with the requirements of the University of Liverpool for the degree of Doctor in Philosophy by

Eugenio Ruiz-Castillo

February 2019

Cross-Shelf Transport and Exchange between a Temperate Shelf Sea and the North Atlantic Ocean

Eugenio Ruiz-Castillo

Abstract

Shelf seas are relatively small regions. They account for 9% of the ocean's area and less than 0.5% of the ocean's volume (Simpson and Sharples, 2012). Despite their relatively small size shelf seas play a key role in global biogeochemical cycles. It is estimated that 20% of the global ocean annual primary production (Behrenfield et al., 2005) and 79% of the total CO_2 oceanic intake occurs in shelf seas (Jahnke, 2010). The physics governing cross-shelf transport and exchange between the shelf and the ocean impact the shelf sea biogeochemical cycles. For instance, the NW European shelf is generally seen as a net carbon sink (Hartman et al., 2018) with carbon thought to be exported from the shelf into the ocean (Thomas et al., 2004; Painter et al., 2017). In addition, it is estimated that globally about 56-58% and 85-90% of the phosphorus and nitrogen required by shelf seas to maintain high productivity are supplied from the ocean (Liu et al., 2010). Therefore, understanding the mechanisms governing transport, both within the shelf and in shelf-ocean exchange, will help to better comprehend how the high productivity of shelf seas is supported and how export of shelf seas contributes to the global carbon cycles.

This thesis focuses on the temperate and wide Celtic Sea, where it is unclear how nutrients supplied either at the shelf break or near the coast are transported into the interior of the shelf to sustain primary productivity or, conversely how carbon is exported from the shelf to drive net

shelf sea absorption of atmospheric CO_2. This research particularly focuses on the mechanisms supplying and transporting nutrients onto and across the Celtic Sea.

Results indicate that throughout summer, due to wind-driven dynamics, nutrients are chiefly supplied from the North Atlantic onto the outer Celtic Sea and on the shelf, nutrients are advected across the shelf in the bottom mixed layer. At the shelf edge off-shelf export in the bottom layer was found to be negligible. In the interior of the Celtic Sea evidence of stratification being maintained by wind-driven advection of relatively high salinity waters in the bottom layer was observed in late-autumn 2014 and spring 2015.

Declaration

I certify that the work described in this thesis is my own except where otherwise stated, and has not previously been submitted for any degree at this or any other University.

Eugenio Ruiz-Castillo

Acknowledgements

Firstly, I would like to express my deep gratitude to my supervisors Prof. Jonathan Sharples and Dr. Jo Hopkins for their time, guidance and patience over the last four years. Your feedback has improved my understanding of shelf sea science. I would also like to thank Jonathan Sharples for the support he has given me to carry out my PhD studies in Liverpool.

I must thank the National Council for Science and Technology (CONACyT) for supporting a scholarship which made possible the realisation of my PhD studies.

I am particular grateful for the friends I met in the last 4 years in and outside the University of Liverpool. Specially, Mila, Simeon, Arthur, Valerie, Charlotte and Dennis. It's been a pleasure.

Appreciation is due to Tony and Joan for all the Sunday roasts.

I would also like to thank Nealy for all the help she has given me, particularly in proof reading and making sure my English is clear. Also for the interesting discussions about shelf seas and biochemical processes and most important, for being there.

I wish to thank my family for their unconditional support.

Finally, I would like to thank Dr. Jose Gomez Valdes and Dr. Gilberto Jeronimo Moreno. Since I am an undergraduate, your passion for the oceanography has motivated me to pursue a career around the ocean sciences.

Contents

List of Figures

List of Tables

Chapter 1

Introduction

Shelf seas are characterised as shallow areas with depths typically less than 200 m and smooth sloping seabed. These regions account for only 7% of the ocean's area and 0.5% of the ocean's volume (Simpson and Sharples, 2012). However, despite their relatively small size, about 20% of the global ocean annual primary production is estimated to occur in shelf seas (Behrenfield et al., 2005; Jahnke, 2010). Primary production is controlled by the role that the physics of stratification and mixing plays in controlling phytoplankton access to light and nutrients. A key event in the seasonality of primary production is the spring bloom, triggered by the onset of stratification (Pingree et al., 1976; 1977; Poulton et al., 2018).

The general view is that stratification over most of the shelf is triggered by atmospheric heat input. However, the vertical distribution of salinity may be important in generating a stable water column (Pingree et al., 1976; Hill et al., 1997). Once the water column stabilises in spring, phytoplankton located above the pycnocline in the euphotic zone increase their biomass whilst nutrients are available (Pingree et al., 1976, 1977; Hickman et al., 2018). About 56-58% and 85-90% of the phosphorus and nitrogen required to maintain high productivity in shelf seas are thought to be supplied from the open ocean (Liu et al., 2010). The total dissolved

inorganic nitrogen supply to shelf seas has been estimated to be 27-40 Tmol N yr^{-1} (Walsh 1991). Globally rivers are estimated to supply 2.5-3.5 Tmol N yr^{-1} and 0.68-0.71 Tmol P yr^{-1} accounting only for 10-14 and 42-44% of the shelf sea needs for N and P, respectively (Liu et al., 2010). The role of riverine nutrients in fuelling shelf sea primary production is less well understood. Processing of nutrients within estuaries and the coastal zone will reduce the effects of riverine nutrients further out in the shelf sea (Sharples et al., 2017).

The physical mechanisms governing the nutrient supply from rivers and the ocean set the nutrient budget available for biological processes. They also affect the fate of the primary production, i.e. the transport of carbon within the shelf system and between the shelf and the open ocean. Temperate shelf seas are generally seen to be net sinks for atmospheric CO_2 (Thomas et al., 2004; Chen, 2010; Jahnke, 2010), driven by a combination of carbon fixation by the shelf phytoplankton and seasonal temperature changes (Liu et al., 2010). For instance, in winter the shelf-water column absorbs a larger influx of atmospheric CO_2, due to greater solubility of the water column, that remains in the bottom mixed layer once stratification is established again (Chen, 2010; Liu et al., 2010). Shelf seas account for 79% of the total CO_2 oceanic intake (Jahnke, 2010) resulting in 0.23-0.28 Pg C yr^{-1}. Therefore, understanding the mechanisms governing transport, both within the shelf sea and in shelf-ocean exchange, will help to better comprehend how the high productivity of shelf seas is supported and how shelf sea primary production contributes to the global carbon cycle.

The focus of this thesis is on the Celtic Sea of the NW European shelf, a wide shelf sea, where it is unclear how nutrients supplied either at the

shelf edge or near the coast are transported into the interior to sustain primary productivity or, conversely, how carbon is exported from the shelf to drive net shelf sea absorption of atmospheric CO_2. This research particularly focuses on the mechanisms supplying and transporting nutrients onto and across the temperate and wide shelf of the Celtic Sea. In the following introduction the processes that govern transport across shelf seas and exchange with the open ocean are described, followed by a broad description of the oceanography of the Celtic Sea.

1.1 Theoretical Background

1.1.1 Taylor-Proudman Theorem

Exchange between the ocean and shelf seas is hindered by the nature of geostrophic flows. If we consider a steady flow, the frictional forces are negligible, e.g. far from the seabed and with no stress applied at the sea surface, and at relatively long spatial scales, leading to a small Rossby number (Ro), so the non-linear terms ($(\mathbf{u}\nabla)\mathbf{u}$) can be disregarded from the equations of motion, we get a balance between the pressure gradient force and the Earths rotation. If we assume hydrostatic pressure variation in the vertical the equations of motion are reduced to:

$$-fv = -\frac{1}{\rho_0}\frac{\partial P}{\partial x} \tag{1.1}$$

$$fu = -\frac{1}{\rho_0}\frac{\partial P}{\partial y} \tag{1.2}$$

$$0 = -\frac{1}{\rho_0}\frac{\partial P}{\partial z} - g \tag{1.3}$$

and the continuity equation is:

$$\frac{\partial u}{\partial x} + \frac{\partial v}{\partial y} + \frac{\partial w}{\partial z} = 0 \tag{1.4}$$

Some of the constraints on geostrophic flows can be understood by eliminating the pressure terms by taking the y-derivative of eq. (1.1) and adding it to the x-derivative of eq. (1.2) as follows:

$$\frac{\partial u}{\partial x} + \frac{\partial v}{\partial y} = \frac{1}{f\rho_0}\left(-\frac{\partial^2 P}{\partial y \partial x} + \frac{\partial^2 P}{\partial y \partial x}\right) \tag{1.5}$$

leading to:

$$\frac{\partial u}{\partial x} + \frac{\partial v}{\partial y} = 0 \tag{1.6}$$

and the continuity eq. (1.4) requires that:

$$\frac{\partial w}{\partial z} = 0 \tag{1.7}$$

This is the Taylor-Proudman theorem, which applies to slowly varying flows in a homogeneous, rotating, inviscid fluid. The last restriction (1.7) implies that geostrophic flow cannot cross isobaths and must flow along them. Thus cross-shelf exchange is limited by the tendency of geostrophic flows to follow bathymetric contours (Allen et al., 2009). If isobaths converge the flow will accelerate (e.g. Oke and Middleton, 2000). Thus, topography combined with the Earths rotation constrains large-scale flows from crossing the shelf edge. Geostrophic currents present zero divergence. Transfer across isobaths is enabled only when the flow is not geostrophic, in the boundary layers near the surface and seabed where frictional effects are important, or at large Rossby numbers giving rise to non-linear flow. All mechanisms that exchange water across the shelf break require one or more assumptions underlying geostrophy to be invalid.

1.1.2 Cross-slope exchange mechanisms

Wind-driven exchange

Wind stress acting on the sea surface, combined with the Earths rotation, leads to a net transport of upper ocean water (the "Ekman Layer") to the right of the wind direction (northern hemisphere) (Ekman, 1905). In terms of exchanging water between the shelf and the open ocean, we can consider a wind stress parallel with the coast or shelf edge aligned along the y-axis as described in Figure 1.1. As the wind stress starts, water in the surface layer will initially accelerate in the same direction of the wind. Where depth allows the existence of a surface boundary layer, after 1 inertial period the Coriolis force balances the frictional force of the wind stress. Subsequently the alongshore transport is deflected offshore in the surface Ekman layer (Fig. 1.1). Transport (U) within the Ekman layer can be quantified as:

$$U = \frac{\tau_y}{f\rho} \tag{1.8}$$

and if we vertically integrate the continuity eq. (1.4) we get:

$$\frac{\partial U}{\partial x} = -w \tag{1.9}$$

Thus the divergence of flow near the coast results in vertical velocities (eq. 1.9) and generates upwelling of relatively cold and nutrient-rich waters from the subsurface to replenish waters transported offshore (Fig.1.1). Along with the upward flow, mass conservation triggers a compensatory onshore current below the surface Ekman layer as described in Figure 1.1. Once the water from the lower layer is advected onshore by the upwelling mechanism, its shoreward motion is abruptly halted (Austin and Lentz, 2002; Tilburg, 2003), and the cold water remains at the inner shelf where it is subject to an advective-diffusive balance (Austin and Lentz, 2002). In contrast, wind stress aligned with the coast but in the

opposite direction generates convergence at the coast and leads to downwelling of surface waters. During downwelling events the water column becomes unstable because cross-shelf circulation forces lighter water under denser water, driving convection and turbulent mixing occurs (Austin and Lentz, 2002; Pedlosky, 2007).

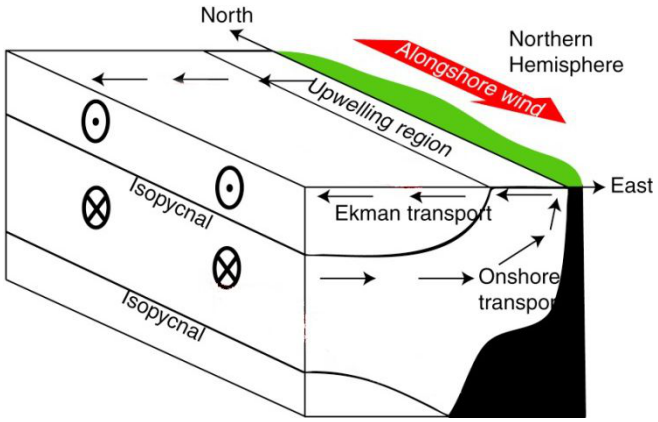

Figure 1.1: Wind-driven upwelling schematics. Modified from Talley et al. (2011).

Bottom Ekman transport

Far from the sea bed friction between geostrophic flows and the bottom is negligible. However, friction governs dynamics within the bottom boundary layer (D_B) resulting in a gradual decrease of the velocity close to the seabed. Similar to the cross-slope wind driven flow that is caused by an external stress, cross-slope flow within the bottom boundary layer is generated by the drag of the bottom on an along-slope geostrophic flow (Simpson and Sharples, 2012). The stress is proportional to the squared geostrophic current above the bottom boundary layer. In the northern hemisphere the flow within the bottom boundary layer is deflected to the left of the direction of the geostrophic current. The cross-slope transport (U_B) can be calculated using the velocity of the geostrophic flow (v_g) as follows (Cushman-Roisin and Beckers, 2009; Simpson and Sharples,

2012):

$$U_B = \frac{v_g}{2} D_B \tag{1.10}$$

Transport in the bottom boundary is replenished above the bottom boundary layer by flow in the opposite direction.

Cross-slope transport within the bottom boundary layer is an important shelf-deep ocean exchange mechanism that has been seen in several regions. For example, along the eastern edge of the Yucatan shelf, Moliniari and Morrison (1988) reported encroachment of the Yucatan Current upon the shelf. During these events the current was topographically controlled along the eastern shelf break resulting in an ageostrophic flow enhancing transport across isobaths through the bottom boundary layer. Oke and Middleton (2000) in the eastern shelf of Australia reported that the alongshelf flow accelerates as a consequence of the narrowing of the shelf. This increase in velocity enhances the bottom stress, generating a stronger onshore flow through the bottom boundary layer and transporting nutrient-rich waters from the subsurface to the surface. On the other hand, an example of downwelling or Ekman drainage has been described on the NW European shelf (Souza et al., 2001; Holt et al., 2009; Simpson and Mcandliss, 2013). The geostrophic flow heads poleward along the shelf break slope and exports shelf waters into the North Atlantic Ocean in the bottom layer. The Ekman drainage is an important mechanism for export of carbon from shelf seas into the ocean (Simpson and Mcandliss, 2013; Painter et al., 2017), in contrast to the upwelling case which is important for nutrient supply.

Cascading

An efficient process in transporting water through the bottom boundary layer into the ocean is cascading (Huthnance, 1995). Cascades occur

when dense water formed on the continental shelf become unstable, spills over the shelf edge and descends down the shelf slope as a gravity current near the bottom (Cooper and Vaux, 1949; Hill et al., 1998; Ivanov et al., 2004). Cascading events have been reported on several shelves all around the world (Ivanov et al., 2004). However it is possible that these events occur only once per year for short periods (few days), when the environmental conditions are favourable for cascading, and that they are highly intermittent (Huthnance et al., 2009).

Several mechanisms contribute to the formation of relatively dense water on the shelf and depend on the local environmental conditions. For instance, in the Gulf of California strong summer evaporation (1 m yr^{-1}) and moderate winter cooling occur (Ivanov et al., 2004). High salinity waters are found throughout the shallow northern gulf in summer and autumn. During winter, the water temperature cools, further increasing the water density and triggering a density current. In this case, temperature and salinity contribute equally to the initiation of the cascade (Lavin et al., 1995). Another example has been reported off the west coast of Scotland in the Malin Shelf (Hill et al., 1998). In winter convection occurs up to 200 m on the shelf whilst in the adjacent ocean penetrated up to at least 500 m. However, the temperature difference between the ocean and the slope, where a poleward current occurs and transports waters with relatively high salinity, is not enough to onset the cascading mechanism. The high salinity of the slope current combined with the relatively cold waters trigger the cascading event.

Internal waves

Cross-slope exchange can also be produced by the action of internal tidal waves. These internal waves are generated by the barotropic tide flowing

over steep topography, onto and off the shelf (Fig. 1.2). In a stratified water column, the pycnocline is uplifted and depressed as the barotropic tidal flow moves on- and off-shelf. The vertical movement of the pycnocline results in the generation of waves propagating onto the shelf and into the open ocean in the tidal frequency. In the Celtic Sea internal waves can propagate up to 170 km from the shelf edge (Inall et al., 2011). The periodicity of this motion is rapid enough to not be limited by geostrophic constraints (Simpson and Sharples, 2012).

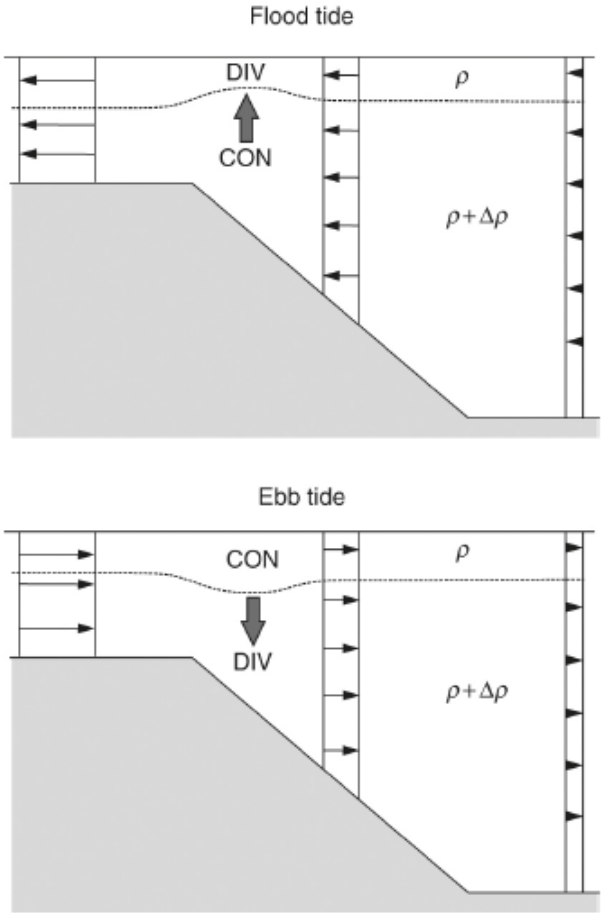

Figure 1.2: Generation of internal waves by the barotropic tidal flow. From Simpson and Sharples (2012).

Internal waves generate enhanced turbulence and mixing (Simpson and Sharples, 2012) that modify the vertical flux from the nutrient-rich bottom waters onto the surface layer (Sharples et al., 2001; Sharples et al., 2007). In addition, propagation of these waves results in baroclinic flows

that may contribute to net exchange between the shelf and the ocean. For instance, Inall et al (2001) described off-shelf flow in the bottom layer of 5 m^2 s^{-1} for 1.5 hours sustained by internal waves. Another example was reported by Hopkins et al. (2012) in the Celtic Sea. Lenses of relatively high salinity water from the North Atlantic intruded up to 100 km on-shelf within the pycnocline layer. The intrusion of high salinity was attributed to the second baroclinic mode of an internal wave.

Non-linear flow

Geostrophic currents flow along isobaths. However, sharp changes in topography may result in large radial accelerations resulting in the non-linear terms to be significant (Simpson and Sharples, 2012). To describe geostrophic flows, we assumed that the rotation of the Earth and the pressure gradient force dominated the dynamics of the flow and hence we neglected the non-linear terms from the equation of motion. In order to discern whether these terms should be neglected we used the spatial Rossby number (Ro) defined as follows:

$$Ro = \frac{u}{fL} \tag{1.11}$$

where u is the along-slope current speed and L is the length scale over which the flow has to vary. In the context of geostrophic flows along the shelf slope, L would be the radius of curvature of the bathymetry. Ro compares the relative importance between the Coriolis and inertial acceleration as the flow attempts to remain parallel to the isobaths. If >0.1 the flow is ageostrophic (Simpson and Sharples, 2012) and therefore the non-linear terms cannot be neglected. An example of non-linear flow can be seen in the Kuroshio region where the Kuroshio current crosses the 200 m isobath (Hsueh et al., 1996; Centurioni et al., 2004) and is controlled by sharp changes in topography giving rise to the non-linear

terms (Hsueh et al., 1996).

1.1.3 Oceanography of the Celtic Sea

The Celtic Sea is a wide shelf sea (>500 km) and can be considered a transition zone between the oceanic Atlantic waters at the margins of the European Continental shelf and the low salinity waters of the Bristol Channel and the Irish Sea (Brown et al., 2003; Uncles, 2010). Winter is the wettest period (Pingree, 1980) and results in the maximum riverine discharge into the Bristol Channel (Uncles and Rashford, 1980; Uncles, 2010). Compared to winter, freshwater input is a minimum throughout the rest of the year (Uncles and Rashford, 1980; Uncles, 2010). Low salinity waters from the Bristol Channel are supplied into the Celtic Sea (Uncles, 2010) and are directed northward towards the Irish Sea (Uncles, 2010). Therefore, the effects of the low salinity water from the Bristol Channel further into the interior of the shelf are expected to be limited. Off the mouth of the Bristol Channel, low salinity may contribute up to 50% of the buoyancy input in summer (Brown et al., 2003; Young et al., 2004).

In winter the Celtic Sea is fully mixed. A combination of heat loss, intensified wind stress and tides generate a homogenous water column (Pingree et al., 1976; Pingree, 1980; Simpson, 1981; Wihsgott et al., 2019). Across the shelf a salinity and temperature gradient occurs, with saltier and warmer waters at the shelf edge (Pingree, 1980). This salinity gradient is intensified in the north of the Celtic Sea by the low salinity waters supplied from the Bristol Channel (Uncles, 2010). Across the shelf it is thought that horizontal gradients in temperature and salinity at least partially compensate in their effect on density, as the water is cooler and fresher towards the coast (Pingree, 1980). In summer, away from the

coasts and the influence of estuaries, surface heating is the predominant factor (85-90%) in determining the density of the water column (Brown et al., 2003) and the onset of stratification (Wihsgott et al., 2019). Over large areas of the shelf the mean annual contribution of salinity to surface buoyancy is relatively small. Nonetheless, in the early part of the stratified period, when the rate of surface heating is low, the relative importance of salinity differences may be important in determining the density structure (Pingree et al., 1976; Hill et al., 1997; Horsbourgh et al., 1998).

In summer the circulation in the Celtic Sea is governed by a cyclonic baroclinic jet associated with a dense (cold and saline) pool of bottom water at the boundary between the Irish Sea and the Celtic Sea (Horsbourgh et al., 1998; Brown et al., 2003; Young et al., 2004). The low temperature feature is localized in summer and generated when saline and cold winter water is left at the bottom in a depression (the Celtic Deep) after the formation of the pycnocline (Young et al., 2004). The cyclonic circulation transports relatively high salinity waters from the south. It has been inferred that high salinity waters from the North Atlantic are transported across the shelf eventually reaching the Irish Sea (Hydes et al., 2004; Bowers et al., 2013) and are gradually diluted as they move northward (Brown et al., 2003; Gowen and Stewart, 2005). In addition, low salinity waters from the Bristol Channel are transported into the north western region of the Celtic Sea, off the coast of Ireland, by the cyclonic circulation (Horsburgh et al. 1998; Brown et al., 2003). East of the Celtic Sea, the English Channel is supplied with relatively high salinity waters originated in the North Atlantic through the Celtic Sea (Uncles and Stephens, 2007) and probably are transported by an eastward flow near the shelf edge of the Celtic Sea (Pingree and Le Cann,

1989).

Along the shelf break a poleward along-slope current centred on the 500 m isobath has been observed in the NW European shelf (Souza et al., 2001; Simpson and Mcandliss, 2013). This current has a maximum flow in winter (0.05 m s^{-1}) (Pingree and Le Cann, 1989). Nonetheless, the flow may reverse and head southward in summer (Porter et al., 2016). The poleward along-slope flow transports warmer and saltier waters from the south (Hill et al., 1998; Pingree et al., 1999). Associated with this flow, long term simulations have calculated a net downwelling along the European shelf break in the bottom boundary layer (1.2 sv) leading to export of shelf waters from the Hebridean shelf into the North Atlantic (Holt et al., 2009; Simpson and Mcandliss, 2013). In the Celtic Sea evidence of exchange with the North Atlantic has been observed at the shelf break. The prevailing winds are from the west-southwest with a tendency for more south westerly winds (Pingree, 1980) and are favourable for surface off-shelf transport. Pingree and LeCann (1990) observed wind-driven southward surface currents at the shelf edge. Cross-slope exchange generated by internal waves has also been reported at the shelf break of the Celtic Sea (Inall et al., 2001; Hopkins et al. 2012). Nonetheless internal waves can be generated in the interior of the shelf as well (Palmer et al., 2013), as sharp changes in topography occur across and along the Celtic Sea (e.g. Jones Bank). Due to transport generated by internal tides oceanic waters may intrude up to 100 km on-shelf within the pycnocline (Hopkins et al., 2012). The general view is that transport between the Celtic Sea and the North Atlantic is governed by nonlinear waves generated by the internal tide (Sharples et al., 2007; Hopkins et al., 2012), wind-driven Ekman transport (Huthnance et al., 2009) and transport in the bottom boundary layer (Huthnance et al., 2009; Porter et al., 2016).

1.1.4 Shelf Sea Biogeochemistry programme and project data

The Shelf Sea Biogeochemistry programme was developed to understand the influence of shelf seas in the wider and global biogeochemical cycles. The programme aims to better comprehend the role of shelf seas in processes such as carbon storage, cycling of key nutrients and determining primary and secondary production. A specific objective of the programme is to assess the role of cross-slope exchange mechanisms between the shelf seas and the ocean. Assessment of the cross-slope exchange mechanisms will identify the relative importance in carbon storage and cycling of oceanic water supply onto the shelf and export of shelf waters into the ocean.

Within the Shelf Sea Biogeochemistry programme 9 oceanographic campaigns were carried out between March 2014 and August 2015 to assess the vertical and horizontal distribution of sea water properties of the Celtic Sea. The study of the shelf sea was complemented with time series of salinity and temperature and current measurements from moorings across the shelf. In addition, autonomous vehicles (gliders) sampled the Celtic Sea in-between oceanographic cruises.

For the development of this thesis, CTD and nutrient data sampled during 9 oceanographic cruises were combined with hydrographic data from the shelf slope collected by gliders. Temporal variability was analysed by using the time series of freshwater discharge, salinity, temperature and horizontal velocities. The atmospheric influence on the water column was assessed with meteorological buoys and remote sensing data.

1.1.5 Thesis structure

Chapter 2 uses a series of cross-shelf CTD section in the Celtic Sea to provide a seasonal summary of how the hydrographic and nutrient (nitrate) structure of the Celtic Sea changes. The amount of nutrients supplied from riverine discharge and the shelf edge are estimated. Evidence of nutrients being advected across the shelf is presented and is used to provide an estimate of the relative importance of physical advection and remineralisation of nutrients. This chapter is an overview of the oceanographic features that will be analysed and explained in more detail throughout the thesis.

In chapter 3 some of the oceanographic features described in chapter 2 are elucidated. These features include the dynamics behind exchange between the Celtic Sea and the North Atlantic Ocean within the pycnocline and the mechanisms driving cross-shelf advection. A particular focus is on the relative roles of wind-driven transports and transport associated with internal tidal waves in summer.

Chapter 4 explains the physical processes driving the supply of nutrients from the North Atlantic Ocean onto the Celtic Sea and under which forcing mechanisms cross-slope exchange is inhibited in autumn and winter. The implications of this inhibition on the dynamics of the Celtic Sea are explained. In addition, input of fresher waters from the Bristol Channel and exchange at the shelf edge in winter are assessed. It is found that nutrients are supplied from the ocean onto the Celtic Sea throughout summer and that cross-slope exchange is minimum in late-autumn and winter.

In chapter 5 the driving mechanisms and the effects of cross-shelf trans-

port on the onset and maintenance of stratification in spring are elucidated. A comparison between spring 2014 and 2015 is carried out, illustrating that the general view that spring stratification is triggered by surface heating does not always hold; wind stress combined with the horizontal salinity gradient can also play a role.

Chapter 2

Seasonality in the Cross-Shelf Physical Structure of a Temperate Shelf Sea and the Implications for Nitrate Supply

This chapter is an article currently in press. The full citation is:

Ruiz-Castillo, Eugenio, Jonathan Sharples, Jo Hopkins, Malcolm Woodward. 2018. Seasonality in the Cross-Shelf Physical Structure of a Temperate Shelf Sea and the Implications for Nitrate Supply. Progress in Oceanography. In press. https://doi.org/10.1016/j.pocean.2018.07.006

Abstract

We address a long-standing problem of how nutrients are transported from the shelf edge and from rivers to support regular, seasonal primary production in the interior of a wide, temperate, shelf sea. Cross-shelf sections of hydrography and nutrients, from a series of cruises between March 2014 and August 2015, along with time series of river discharge and river nutrient load are used to assess the seasonality of cross-shelf transports. Riverine nitrogen inputs are estimated to account for 30% of the nitrate available for the spring bloom on the inner shelf, and 10% in the mid- to outer-shelf. In the bottom layer in summer, high salinity, nutrient-rich waters are transported on-shelf as a result of wind-driven

Ekman transport, cross-shelf pressure gradients and/or internal tidal wave Stokes drift. In the centre of the shelf this advection is responsible for 25% of the increase in bottom water nitrate seen between April and November 2014. The remaining nitrate increase suggests that about 50-62% of the nitrogen fixed into organic material during spring, summer and autumn phytoplankton growth is recycled in the bottom water over the 12 months between March 2014 and March 2015. In winter, when the water column is vertically mixed, there is a weak net off-shelf transport of about 1 m^2 s^{-1}, possibly driven by a reversal of the horizontal density gradient caused by excess cooling of shallower shelf waters. Overall, shelf nitrate concentrations are maintained by a combination of riverine supply, recycling of organic material, and summer on-shelf transports. We suggest that the main driver of inter-annual variability in pre-spring nitrate concentrations is variability in the depth of the winter mixed layer over the shelf slope.

2.1 Introduction

Compared to their relatively small size, continental shelves are highly productive regions. Despite accounting for only 9% and 0.5% of the oceans area and volume respectively (Simpson and Sharples, 2012), it is estimated that 20% of the global ocean annual primary production takes place on continental shelves (Behrenfeld et al., 2005; Jahnke, 2010). Globally, rivers supply about 1.6 Tmol of dissolved inorganic nitrogen (DIN: NO_2, NO_3 and NH_4) per year with about 25% of this thought to be used by biogeochemical processes on the shelf (Sharples et al., 2017). However, DIN supplied from rivers is generally low compared to oceanic input. The open ocean is generally viewed as the dominant source of nutrients to the shelf, supplying between 85-90% of the nitrogen and 56-58% of the phosphorus required by shelf seas (Liu et al., 2010).

For a wide continental shelf sea it is unclear how nutrients supplied at the coastal and ocean boundaries are transported into the interior of the shelf to drive primary production. The concept of a down-welling circulation as a mechanism for driving the continental shelf pump (Holt et al., 2009), where waters enter the shelf at the surface and leave at depth, is able to account for the export of carbon off-shelf but does not provide a physical means of nutrient supply to bottom waters. The nutrient distribution along and across a shelf will be controlled by the particular seasonal dynamics of the shelf (e.g. Liu et al., 2000; Roughan and Middleton, 2002). The question we address here concerns how nutrients supplied either at the open ocean or coastal boundaries of a wide, temperate shelf system are able to penetrate into the interior of the shelf sea to support the regular seasonal high primary production (e.g.Seguro et al.,2017; Hickman et al., 2018).

The focus of this study is the Celtic Sea (Fig. 2.1), an approximately 500 km wide section of the Northwest European Shelf (Huthnance et al. 2009). It is supplied with low salinity water from the Bristol Channel (Uncles, 1984; Hydes et al., 2004), as seen in Figure 1, and is connected to the deep Northeast Atlantic Ocean across a steep shelf edge. The hydrography of the Bristol Channel is mainly linked to seasonal variability in the riverine flows, (e.g. Uncles, 2010). Winter is the wettest season in the region (Pingree, 1980) and the freshwater flow into the Bristol Channel is a maximum during this period (Uncles and Radford, 1980; Uncles, 2010). The shallow water depth and strong tidal currents within the Bristol Channel ensure that the water column is mixed throughout the year (Uncles, 2010). During the summer near the mouth of the Bristol Channel, freshwater may contribute to 50% of the buoyancy input

(Brown et al., 2003; Young et al., 2004). Beyond the mouth, the fresher waters strengthen horizontal gradients in the northern Celtic Sea (Brown et al., 2003; Young et al., 2004). However, the buoyant low salinity water from the Bristol Channel is mainly diverted northward by the effect of the Earths rotation, so its influence across the wider Celtic Sea to the south is likely to be limited. In contrast, it has been inferred that high salinity water from the Atlantic Ocean makes its way across the Celtic Sea and into St. Georges Channel (e.g. Hydes et al., 2004; Bowers et al., 2013). Thus, the Celtic Sea is a wide transition zone where oceanic waters with initially high salinity are gradually diluted as they progress northwards, eventually entering the Irish Sea (Brown et al., 2003; Gowen and Stewart, 2005).

Away from the influence of the Bristol Channel, the Celtic Sea is a typical temperate shelf system, where the seasonal changes in water column structure are governed by a competition between surface heating and vertical mixing, the latter formed by varying contributions from tidal currents, wind stress and convective mixing (e.g. Simpson, 1981). In winter, convection (surface heat loss), the tide, and enhanced winds vertically mix the water column. In spring vertical stratification begins once the rate of heating is able to overcome the ability of tidal and wind mixing in redistributing the heat. This seasonally-stratifying region is bounded to the north by the Irish Sea. Most of the Irish Sea remains fully mixed all year, due to shallow water and strong tidal currents, with a tidal mixing front in St. Georges Channel separating the Irish Sea from the stratified Celtic Sea in summer (Simpson, 1976; Horsburgh et al., 2000). East of the Celtic Sea is the English Channel with relatively high salinity originating from the North Atlantic Ocean via the Celtic Sea (Uncles and Stephens, 2007).

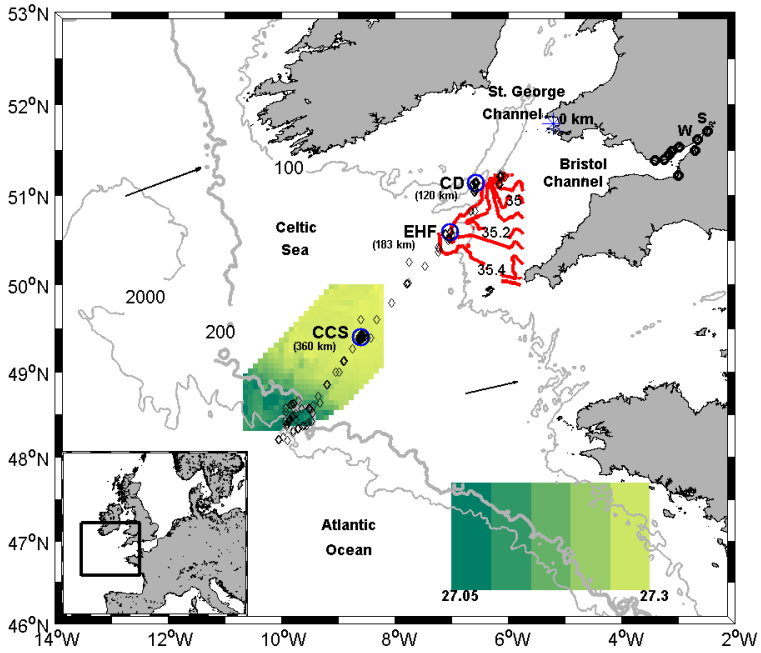

Figure 2.1: Map of the Celtic Sea. Black diamonds show the location of CTD casts. Black circles indicate the location of rivers discharging into the Bristol Channel where nutrient data was available. S and W stand for the Severn and Wye Rivers, respectively. The blue asterisk is the reference used in the hydrographic sections. Locations of the Celtic Deep (CD), East of Haig Fras (EHF) and Central Celtic Sea (CCS) moorings are marked by blue circles and in parenthesis distance to the blue asterisk. The density at 75 m between the shelf edge and central shelf is based on interpolation of 8 towed undulating CTD transects in June 2010. Red contours, every 0.1 g kg^{-1}, are the surface salinity in May 2015 constructed from the ships underway sampling. Vectors indicate the average wind speed (4.41 m s^{-1} in the north and 3.06 m s^{-1} in the south) from 1st January 2014 to 31st December 2015 from Era-interim data.

To the south and west the Celtic Sea is bounded by the shelf edge and the adjacent Northeast Atlantic Ocean. The shelf edge and slope region guide a slope current of generally salty water (Pingree and Le Cann, 1989; Holt et al., 2009), with strong internal mixing over the 200 meters isobath caused by a breaking internal tide during the stratified season (New, 1988; New and Pingree, 1990).

In this chapter it is demonstrated that seasonality in the outflow from the Bristol Channel combined with the high salinity boundary of the Northeast Atlantic Ocean set up cross-shelf gradients in density that

drive shelf-wide circulation and important cross-shelf transports. We show that despite the dilution of riverine water, the rivers supply an important fraction of the nutrients to the Celtic Sea. However, we find that the nutrients available to each years spring bloom are a combination of ocean-supplied nutrients and recycled material from the previous year.

2.2 Methods

We combine hydrographic and nutrient data collected by the UK Shelf Sea Biogeochemistry (SSB) Programme along with river flow and nutrient time series from tributaries of the Bristol Channel to build a seasonally resolved understanding of shelf-scale density distributions, circulation and nutrient transports.

2.2.1 CTD transects

Hydrographic data were collected between March 2014 and August 2015 during 9 oceanographic cruises on board the ships RRS Discovery and RRS James Cook. On each cruise a Seabird 911plus CTD (Conductivity, Temperature and Depth) system collected full water column profiles of temperature, conductivity and pressure. Raw data was processed onto a 1 db grid using standard Seabird Data Processing Software and customized quality control routines. Derived salinity was subsequently calibrated against in situ samples analysed on a Guildline Autosal salinometer. The TEOS-10 functions (IOC et al., 2011) were used to derive thermodynamic properties. A total of 315 CTD casts were performed along the track shown in Figure 1, and used to construct cross-shelf sections of conservative temperature, absolute salinity and potential density during each cruise. The main cross-shelf CTD transect was set orthogonal to the shelf edge and the general slope of the continental shelf.

Spatial interpolation of bottom water density measurements made from a towed undulating CTD package in June 2010 across a 284 km by 146 km area (Fig. 2.1) also confirmed that the transect was orthogonal to the typical orientation of bottom water isopycnals. The distance along each hydrographic transect is measured from the eastern side of St. Georges Channel, north of the Bristol Channel mouth (blue asterisk at 51.79^{o}N, 5.2^{o}W; 0 km in Fig. 2.1). The distance between CTD stations was on average 25 km and a minimum of 5 km, much greater than (on average), or as a minimum equal to the spatial scale of semi-diurnal tidal excursions in the Celtic Sea (Polton, 2015). Although each CTD transect was typically completed over 2-4 weeks, given our focus on low frequency and seasonal variability each transect was assumed to be a synoptic picture of that month. Evolution of the hydrographic structures was consistent with the long-term mooring time series of velocity and hydrography, described later in section 2.4, confirming that each transect represents a synoptic picture on the time scales of interest. The coarser spatial resolution of the sampling in March 2014 and 2015 on the shelf, between 250 km and 450 km distance from the coast, was augmented by using surface temperature and (calibrated) salinity data (from 6 metres depth) recorded continuously along the ships path. The water column is vertically mixed during these months (Huthnance et al., 2001; Whisgott et al., 2019), as will be described in the hydrographic sections, therefore the surface temperature and salinity values are representative of the whole water column.

Absolute salinity is used as a conservative tracer to track the movement of the waters in the Celtic Sea. The 35.2 and 35.7 g kg^{-1} isohalines were used to identify the influence of fresher water from the Bristol Channel and high salinity Atlantic Water, respectively. In previous studies

around the Bristol Channel mouth and south of St. Georges Channel (e.g. Brown et al., 2003) salinities below 35 have been used to describe waters from river origin. In this research the salinity chosen (<35.2 g kg^{-1}) to represent the fresher water influence is based on the new equation of state (IOC et al., 2010), where Absolute Salinity shows an increase of about 0.17 units compared to practical salinity.

2.2.2 CTD nutrient data

Water samples were collected on average from 6 depths between the surface and near bed on each CTD cast and analyzed onboard for dissolved inorganic nutrients using a 5-channel Bran and Luebbe AAII segmented flow auto-analyser following the molybdenum blue method. For further details can be found in Woodward (2016) and Poulton et al. (2018). Our focus here is on nitrite (NO_2) plus nitrate (NO_3) (referred to for the rest of this chapter as nitrate), with nitrogen generally being the limiting nutrient for new primary production in this system (Holligan et al., 1984; Pemberton et al., 2004; Davis et al., 2014).

Supported by measurements taken during the cruises (e.g. Garcia-Martin et al., 2017; Poulton et al., 2018; Hickman et al., 2018), we assume that nitrate at 80 metres depth, i.e. below the seasonal pycnocline and much deeper than the euphotic zone (1% light level is 46 metres), is largely unaffected by phytoplankton consumption, and therefore nitrate can be considered a quasi-conservative tracer. The nitrate-salinity relationship from March 2014 was used as the pre-spring bloom state of shelf nitrate distributions, and to provide estimates of the physical transport of nitrate in bottom waters at CCS throughout the rest of the stratified period of the year by tracking the movement of isohalines. Subsequent increases

in bottom water nitrate concentrations above the values estimated from the conservative behavior based on the March nitrate-salinity relationship are then assumed to indicate addition of deep shelf water nitrate caused by regeneration of organic material.

2.2.3 River discharge and nutrient load

Daily river flow data, provided by Natural Resources Wales and the National River Flow Archive, from 33 tributaries that discharge into the Bristol Channel were added together to quantify the total freshwater input into the Bristol Channel between the 1st of July 2013 and the 30th of September 2015. After analysing the hydrographic data, the Bristol Channel was identified as the main source of fresher water; therefore only tributaries that discharge directly into the channel were considered (Fig. 2.1). Although data were not available for all, the Severn and the Wye Rivers are included which are the main freshwater suppliers accounting for about 54% of the total input of freshwater (Uncles and Radford, 1980; Jonas and Millward, 2010).

Time series data provided by Cefas (courtesy of Dr. Sonja van Leeuwen) were used to assess the total inorganic nitrogen (NH_4, NO_2 and NO_3) input into the Bristol Channel from 9 tributaries (black circles in Fig. 1). Water samples were analysed for NH_4, NO_2 and TON (Total Oxidised Nitrogen) using a Konelab discrete analyser at the National Laboratory Service (http://natlabs.co.uk). NO_3 was then calculated from TON and NO_2 (TON - NO_2= NO_3). NH_4 is not included in CTD nutrient data.

As reported in Jonas and Millward (2010) the contribution to the total inorganic nitrogen load made by each tributary scales with their freshwater discharges. Of the total inorganic nitrogen input supplied by the

9 tributaries summed here, the Severn and Wye Rivers account for 43% of the 2013-2014 winter total. Additional contributions from the Bristol Avon, Cadoxten, Parrett, Rhymney, Taff, Thaw and Usk, many of which are identified as significant contributors to both the freshwater and total inorganic nitrogen load by Jonas and Millward (2010) are also accounted for. Data in the period between the 1st of October 2013 and the 30th of September 2014 are used here. The impact of the offset between riverine time series and Celtic Sea is negligible as the effects of freshwater input are expected to be observed after March.

2.2.4 Moorings

Salinity time series from moorings located in the central Celtic Sea (CCS) and the Celtic Deep (CD) (Fig. 2.1) were available with temporal resolutions of 5 and 30 minutes respectively (Wihsgott et al., 2016; Hull et al., 2017). The surface salinity time series at CD was collected between the 23rd March 2014 and the 8th July 2015. At CCS two salinity time series were used to compare the hydrographic conditions in the upper and bottom layers, at 20 metres and 120 metres below the sea surface, between the 26th March 2014 and the 23rd of August 2015. The salinities were calibrated against in-situ samples analysed on a Guildline Autosal Salinometer with a stated accuracy of $<$ 0.002 psu. All three salinity time series were filtered using a low-pass Lanczos filter (Thompson and Emery, 2014) with a cut-off frequency of 1/24 h^{-1}, so only fluctuations with periods longer than 1 day were considered.

ADCP velocity time series at CCS, Celtic Deep and at a site referred to as East of Haig Fras (Fig. 2.1) are used to assess the speed and direction of bottom water currents. Near full water column velocity time series were available at CCS between the 22nd June 2014 and the 25th

July 2015, with a 57 day gap during early summer 2014 (Wihsgott et al., 2018). Velocities were recorded in 2.5 metres vertical bins between 7.5 metres and 127.5 metres above the seafloor (mean total water depth of 147 metres), over 2.5 min ensembles. At East of Haig Fras (EHF) and at the Celtic Deep, velocities were recorded every hour within the bottom 40 m of the water column only, at a vertical resolution of 0.5 m (Thompson et al., 2017; 2018). Data was successfully returned at EHF from 22nd March 2014 to 24th October 2014 and then from 17th March 2015 to 30th August 2015. At the Celtic Deep velocities were recorded from autumn 2014 until spring 2015 (23rd October 2014 to 8th May 2015), with a short 22 day gap starting mid-February 2015.

A depth mean of the instantaneous velocities within the bottom 40 metres of the water column at all sites was calculated. Temporal averaging was then performed within a moving window of twenty M_2 tidal periods (10.3 days). These time series reveal the net movement of near bottom water across the shelf on an approximate 10 day time scale and are used to independently support the estimates of transport inferred from the movement of isohalines across the shelf.

2.3 Results

2.3.1 Shelf-wide seasonal hydrogrpahy

In March 2014 and 2015 the Celtic Sea was vertically mixed with cross-shelf horizontal gradients in conservative temperature (Fig. 2.2a and 2.2e). Relatively cold waters with values below 10 ^{o}C were located over the central Celtic shelf while slightly warmer waters were located near the shelf break. In April and May 2015 the water column gained heat and the upper 30 metres warmed up across the entire shelf (Fig. 2f and

2g). A two-layer system had developed by May (Fig. 2.2g) with a weak thermocline at a depth of about 50 metres separating upper and lower layers with temperatures of 11.5^{o}C and 10 ^{o}C respectively. Throughout summer, June to August (Fig. 2.2b, 2.2c, 2.2h, and 2.2i), vertical thermal stratification strengthened. Maximum near surface temperature of 16 ^{o}C occurred in August (Fig. 2.2c and 2.2i). In November (Fig. 2.2d), the thermocline deepened below 50 metres, as the surface layer cooled and generated convective vertical mixing. Throughout the year water near the shelf break (approximately 450 km from the coast; depth of 200 m) remained warmer than bottom water across the rest of the shelf, probably because of the along-slope (poleward) flow of warmer waters originating from more southerly latitudes as well as strong internal tidal mixing acting to redistribute heat vertically.

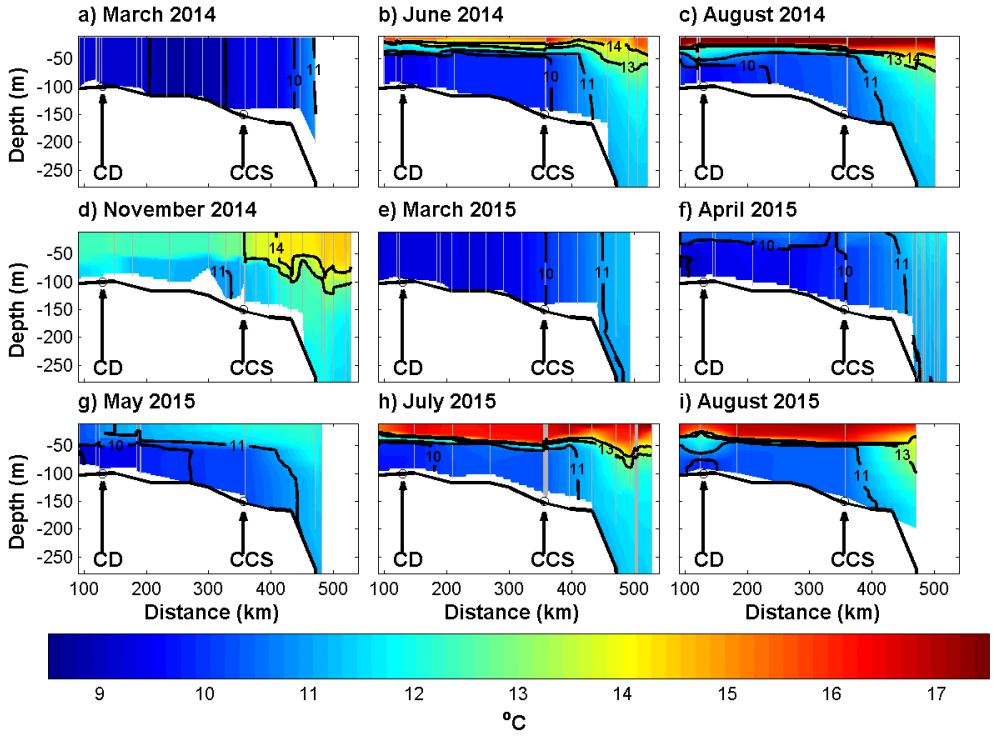

Figure 2.2: Conservative temperature sections across the Celtic Sea. Vertical gray lines indicate the location of the CTD casts. Gray circles at the bottom show the position of the moorings at Celtic Deep (CD) and the central Celtic Sea (CCS).

In March 2014 and 2015 the vertical isohalines across the whole shelf

reflected the vertically well-mixed, isothermal conditions (Fig. 2.3a and 2.3e). A horizontal cross-shelf salinity gradient was maintained between the low salinity input of the Bristol Channel in the north and the high salinity (> 35.7 g kg^{-1}) oceanic water near the shelf edge. In April 2015 (Fig. 2.3f) a band of low salinity water (35.2 g kg^{-1}) was observed in the northern Celtic Sea and remained within 100-150 km of St. Georges Channel. The 35.2 g kg^{-1} isohaline was vertically sheared, with lower salinity water extending further offshore above the thermocline. Noting that isohalines during the previous winter were vertical, this suggests an off-shore transport of low salinity surface water. Through late spring and summer of both years (Fig. 2.3b, 2.3c, 2.3g, 2.3h, 2.3i) this suggestion of differential transport between surface and bottom layers strengthened, with marked shear also observed in the 35.4 and 35.45 g kg^{-1} isohalines further out across the central shelf.

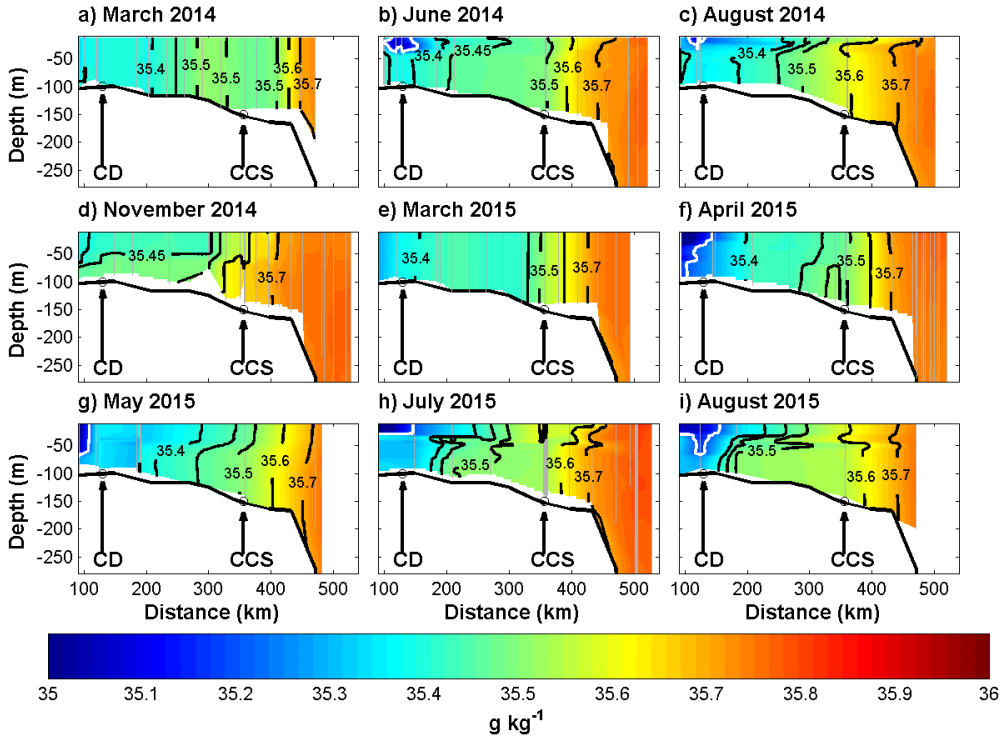

Figure 2.3: Absolute salinity sections across the Celtic Sea. CTD casts and mooring locations marked as per Figure 2. White contours represent the 35.2 g kg^{-1} isohaline that indicates the presence of fresher water.

The salinity of bottom water across the Celtic Sea increased from March

into late autumn (Fig. 2.4a). Between March and August 2014, the 35.6 g kg^{-1} isohaline at the sea bed moved from the shelf edge to just beyond CCS, a distance of approximately 100 km. This isohaline was initially vertical in March, but sheared in August, suggesting a persistent on-shelf transport of bottom water over the summer and autumn months. In 2015 the 35.6 g kg^{1} isohaline did not move as far. Instead, evidence of on-shelf bottom water transport is found in the 35.5 g kg^{-1} isohaline that moved 120 km on-shore between March and August 2015. In 2014 and 2015 the mean on-shore flows inferred from isohaline displacement were about 1 km day^{-1} (Fig. 2.4b). Maximum velocities above 1.5 km day^{-1} occurred in November 2014 and August 2015. The ingression of more saline oceanic water onto the shelf beneath the thermocline and the off-shore spread of fresher water above it ensured that much of the Celtic Sea was vertically stratified in salinity as well as temperature throughout the summer.

Between November 2014 and March 2015 there is an indication of water moving from mid-shelf towards the outer shelf and shelf edge. All isohalines in November 2014 make some progress towards the shelf edge (Fig. 2.3d, e). A consistent off-shelf movement occurred (0.8 km day^{-1}) from December 2014 to April 2015 (Fig. 2.4b) of bottom water salinity as a part of the broader seasonal cycle of salinity variations (Fig. 2.4). However, the extent of the apparent movement will be altered due to vertical mixing from mid-December through to March (Fig. 2.4a).

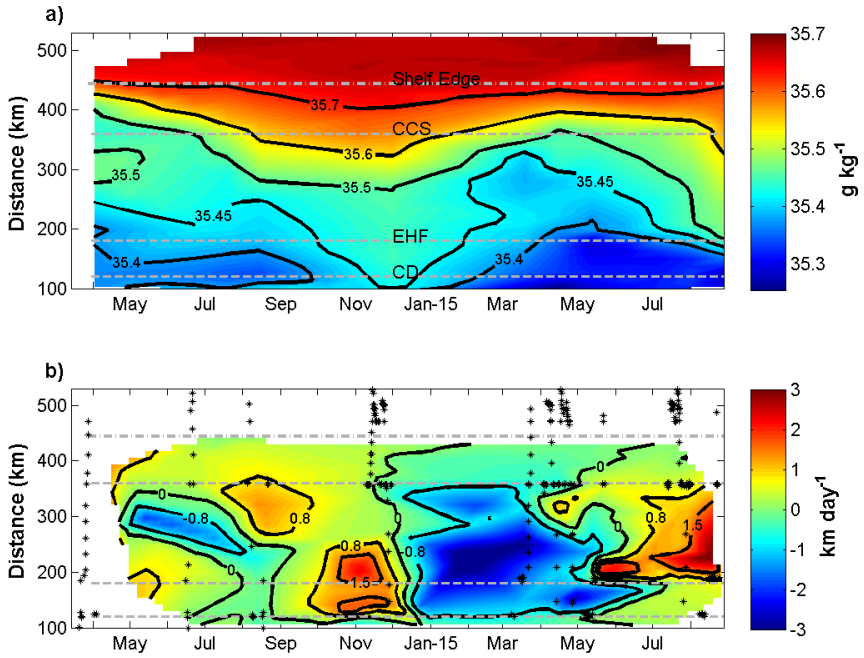

Figure 2.4: Bottom water absolute salinity (at 80 metres) along the CTD transect and b) velocities calculated from the isohaline displacement along the CTD transect. Gray dashed lines show the location of CD, EHF and CCS. Location of the shelf break is represented by -.- gray line. Black asterisks in b) indicate where CTD casts were carried out.

Together, the temperature and salinity structures determined the vertical and horizontal density gradients across the Celtic Sea (Fig. 2.5). From May to August (Fig. 2.5b, 2.5c, 2.5g, 2.5h, 2.5i) the bottom-surface density difference across most of the shelf was 1 to 1.2 kg m^{-3}. June, July and August were the most strongly stratified (Fig. 2.5b, 2.5h and 2.5i). The pycnocline, over both the shelf and the deep ocean, was defined by the 1026.8 and 1027 kg m^{-3} isopycnals. The development of a low salinity surface plume in April 2015 (Fig. 2.5f) once weak vertical thermal stratification had started was reflected in a 30-40 metres thick anomalously low density surface layer in the north of the Celtic Sea.

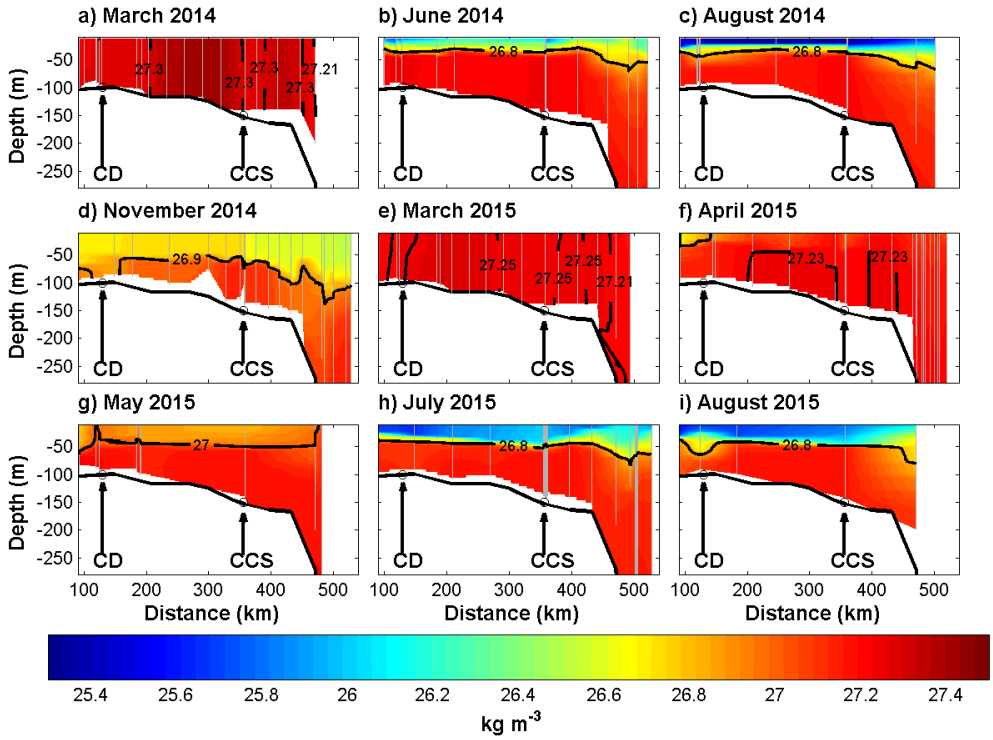

Figure 2.5: Potential density sections across the Celtic Sea. CTD casts and mooring locations marked as per Figure 2.2.

Beneath the pycnocline there were important cross-shelf gradients in bottom water density (Fig. 2.6). Throughout the year, the bottom water density from CCS towards the shelf-edge typically decreases; this gradient intensifies during the latter half of the summer and into autumn as water at the shelf edge becomes increasingly warmer compared to the central shelf. Moving on-shelf from CCS towards the coast there is also a general decrease in density with a persistent mid-shelf maximum in bottom water density varying seasonally between about 200 and 350 km from the northern end of the transect line.

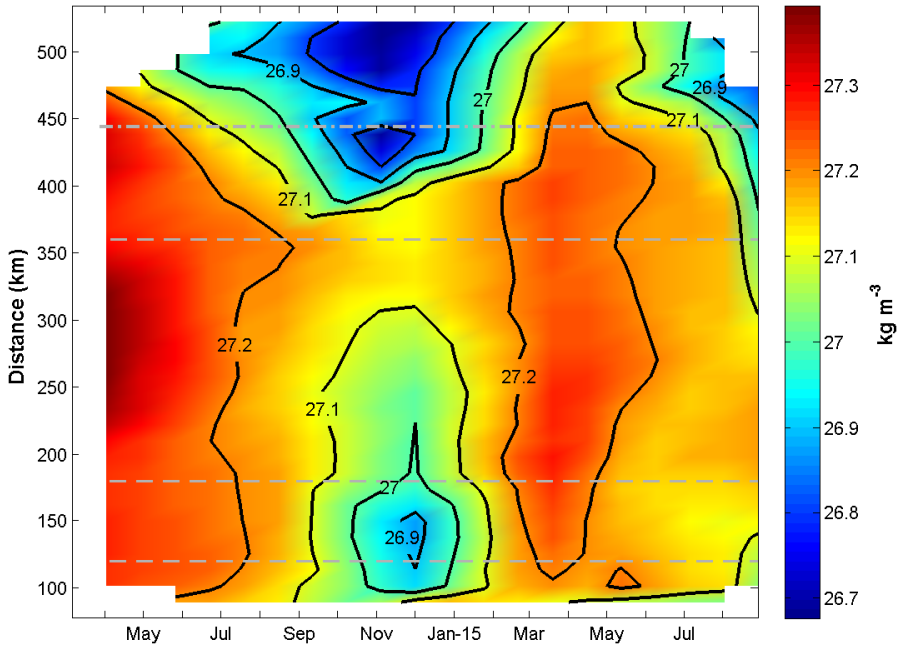

Figure 2.6: Bottom water density (at 80 metres) along the CTD transects. Shelf edge, CD, EHF and CCS locations indicated as per Figure 2.4a.

2.3.2 Near bed ADCP velocities

The direction and magnitude of near bed velocities recorded at CCS, East of Haig Fras (EHF) and at the Celtic Deep (CD) are supportive of the direction and magnitude of flows inferred from the movement of isohalines (Fig. 2.7). During April at CCS there was on average a 1 km day^{-1} current directed increasingly on-shelf in the bottom 40 metres of the water column (Fig. 2.7a). At the end of April strong, on-shelf northeastward velocities of 1.8 km day^{-1} were recorded. Much weaker on-shelf flows were observed at CCS throughout July and early August, in agreement with the 0(0.5 km day^{-1}) velocities predicted from the isohaline movement (Fig. 2.4b). During the second half of August, however velocities increase to on average 1.7 km day^{-1} and the current turns towards the northeast (on-shelf), the timing of which is consistent with the

predicted increase in on-shelf flow at this time (Fig. 2.4). Throughout September, October and early November episodes of opposing strong (1-3 km day^{-1}) on-shelf and off-shelf flow occur. The net result is a weak (0.1 km day^{-1}) east-northeast flow, which is supportive of the reduced on-shelf movement of isohalines over this period at CCS. Isohaline movements at CCS during 2015 predict on-shelf transport from May onwards, increasing to 0.8 km day^{-1} in early August 2015 (Fig 2.4b). Bottom currents from the ADCP at CCS average 0.6 km day^{-1} north-east, directly on-shelf between 1st May 2015 and the end of July 2015.

As is observed at CCS, the latter half of April 2014 at Haig Fras is dominated by strong on-shelf bottom water flows, peaking at 3 km day^{-1} (Fig. 2.7b). The predicted off-shelf movement during August 2014 (Fig. 2.4b) is supported by a period of sustained 0.5 km day^{-1} off-shelf flow recorded by the ADCP at Haig Fras. In 2015 the latter stages of significant off-shelf winter transport at Haig Fras estimated from the isohaline displacement is supported by an average flow of 1.2 km day^{-1} southward between 22nd March and 13th April 2015.

The ADCP record at CCS over the winter months confirms the anticipated off-shelf movement of bottom water. Between the 26th November 2015 and 26th January 2015 the bottom water currents averaged 0.9 km day^{-1} towards the south (Fig. 2.7a). During the remainder of the well mixed period at CCS bottom water currents oscillated between being on- and off-shelf, suggesting that the majority of the off-shelf transport over the outer shelf likely occurred during early winter, a detail that is reflected by the sharp decrease in bottom water salinity recorded during December 2014 at CCS (Fig. 2.8c). Further on-shelf at the Celtic Deep near bed currents over the winter were stronger and more persistently

off-shelf (Fig. 2.7c), averaging 1.2 km day^{-1} southwest between 5th December and 1st May 2015, and in agreement with the greater cross-shelf displacements estimated for lower value isohalines.

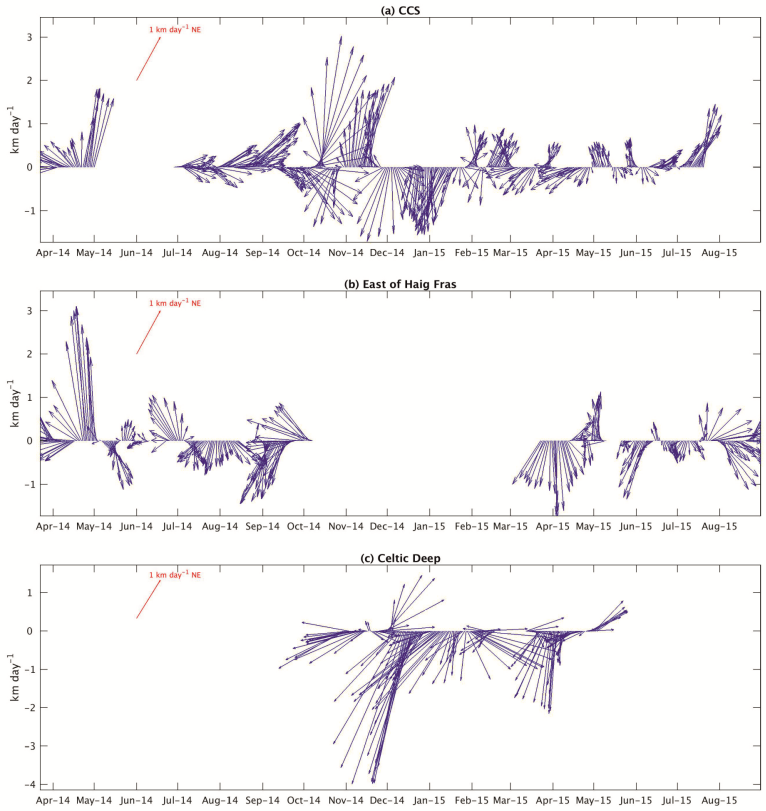

Figure 2.7: Mean velocities within the bottom 40 metres of the water column at (a) CCS, (b) East of Haig Fras and (c) Celtic Deep. At each location, the instantaneous velocities were averaged within a running window of 20 x M2 tidal periods (10.3 days). For clarity, one vector every 24 hours in plotted. Note that panel (c) has a different vertical scale.

2.3.3 River flow,nutrient and salinity time series

River discharge into the Bristol Channel was greatest during winter (Fig. 2.8a). Maximum flows of 1800 m^3 s^{-1} and 1200 m^3 s^{-1} were reached during the winters of 2013/2014 and 2014/2015, respectively. Relatively high discharge was sustained throughout most of the 2013/2014 winter period (December to March), whereas 2014/2015 was characterized by a series of smaller peaks (below 950 m^3 s^{-1}) from October onwards. After March, the river discharge decreased significantly and remained

low throughout spring and summer.

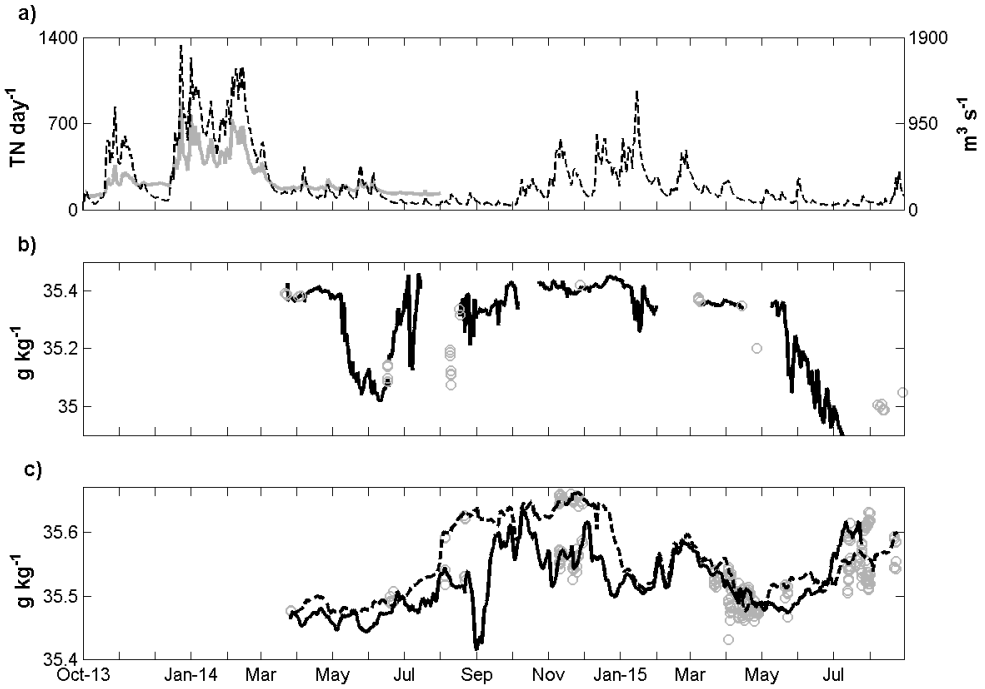

Figure 2.8: (a) River discharge in m^3 s^{-1} (dashed line) and nutrient input in Tonnes of Nitrogen per day^{-1} (gray) into the Bristol Channel. Peak winter river discharge occurs on 23rd December 2013 and 15th January 2015. (b) Surface salinity at the Celtic Deep mooring (solid line). Following peak river discharge the salinity starts to decrease on 6th May 2014 and 13th May 2015. (c) Surface (20 m, solid line) and near bottom (140 m, dashed line) salinity at the central Celtic Sea (CCS) mooring. Open gray circles in (b) and (c) are the salinities measured independently from the CTD during the cruises and validate the quality of the salinity time series at each mooring.

The total nitrogen supply into the Bristol Channel is strongly correlated with the freshwater discharge (Fig. 2.8a) with a Pearson correlation coefficient (R^2) of 0.97. Maximum input was during winter with peak values above 700 tonnes of nitrogen day^{-1}, decreasing to values below 200 tonnes of nitrogen day^{-1} in spring and summer. We can estimate the nitrate contribution from rivers by assuming that the total nitrogen (the sum of nitrate, nitrite and ammonium) indicates the potential nitrate as the nitrogen enters the coastal sea, ammonium would rapidly be turned into nitrite by bacteria. Taking a mean winter discharge rate of 1200 m^3 s^{-1}, or $1{\times}108$ m^3 day^{-1}, combined with a mean total nitrogen load of 550

tonnes per day suggests that the freshwater total nitrate concentration during the winter preceding spring 2014 was about 390 mmol m^{-3}.

At the Celtic Deep, in the northern Celtic Sea, the surface salinity decreased from 35.4 g kg^{-1} in early May to 35 g kg^{-1} in mid-June 2014 (Fig. 2.8b). A pronounced 0.4-0.5 g kg^{-1} decrease in salinity also started in mid-May 2015 and continued until the end of the record (July 2015). For context, the range in surface water salinity experienced over a spring tidal cycle at the Celtic Deep is 0.03 g kg^{-1} an order of magnitude less than the May decrease. These trends are consistent with the perspective provided by the CTD transects (Fig. 2.3) and support the idea of low salinity water spreading out over the northern Celtic Sea. Throughout the latter half of summer 2014 the surface salinity at the Celtic Deep increased and remained around values of 35.4 g kg^{-1} from October onwards.

In the central Celtic Sea the bottom water salinity increased over the summer and reached a maximum in November/December (Fig. 2.8c). This pattern is again consistent with the seasonal hydrographic sections, which we interpret as indicating a near-bed transport of high salinity water across the shelf. Sustained periods of time between July 2014 and January 2015, where the top to bottom salinity difference was 0.05 to 0.1 g kg^{-1}, reveal prolonged episodes of vertical salinity stratification on the central shelf.

2.3.4 Nitrate distribution across the Celtic Sea

The distribution of nitrate across the shelf is shown in Figure 2.9. During both March 2014 and March 2015 (Fig. 2.9a and 2.9e), when the water column was vertically well mixed, nitrate was also homogeneously distributed throughout the water column. Across the shelf there was a

horizontal nitrate gradient with higher concentrations at the shelf edge (8-9 mmol m^{-3}) decreasing to about 6 mmol m^{-3} in the Celtic Deep. Following the onset of stratification in April (Fig. 2.9f), nitrate concentrations rapidly reduced to near zero in the surface layer due to uptake by primary producers (Garcia-Martin et al.,2017; Poulton et al., 2018). The surface layer remained depleted in nitrate until the onset of surface layer deepening arising from convective and wind-driven mixing in autumn (Wihsgott et al., 2019). It is clear that convection entrained deep-water nutrients up into the autumn surface layer (Fig. 2.9d, November 2014), when nitrate reached 2-3 mmol m^{-3}.

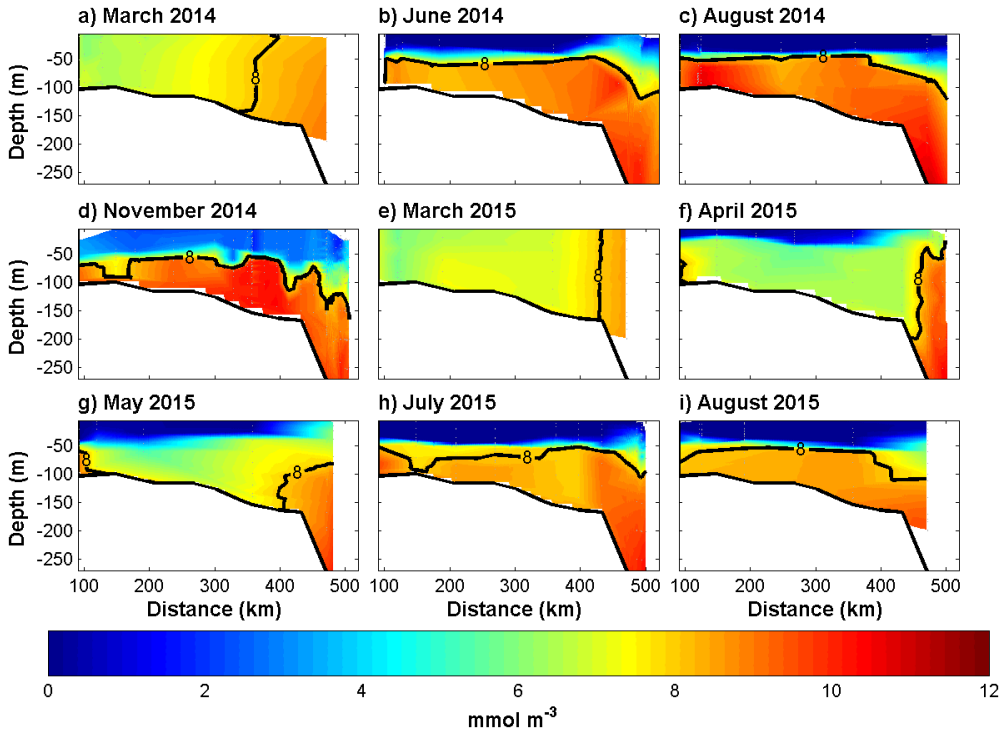

Figure 2.9: Nitrate sections across the Celtic Sea. The black line represents the 8 mmol m^{-3} contour.

In April 2015 (Fig. 29f) the bottom water nitrate concentration across the shelf was 6 mmol m^{-3}. A higher pool of nitrate (> 8 mmol m^{-3}) was located seaward of the shelf-break. A pool of higher bottom water nitrate (> 7 mmol m^{-3}) was also observed at the northern end of the section, coincident with lower salinity water (Fig. 2.3f), thought to originate from

the Bristol Channel. Throughout the stratified months (Fig. 2.9b-d and 2.9g-i) the bottom water nitrate concentration across the whole shelf increased, typically reaching 9-10 mmol m^{-3} by August. The on-shelf movement of the 8 mmol m^{-3} contour between April 2015 and May 2015 (Fig. 2.9f and 2.9g) appears to imply that there was a physical transport across the shelf-break.

2.4 Discussion

Based on the patterns of the isohalines from the CTD sections (Fig. 2.3 and Fig. 2.4) and the salinity time series at the mooring sites (Fig. 2.8) the results indicate several important aspects of cross-shelf flows. In particular, (1) offshore surface flow of low density water in the north of the transect in spring, (2) onshore flows of bottom water in the central Celtic Sea and near to the shelf edge during summer, and (3) off-shelf flows of bottom water across the shelf and towards the shelf edge during winter. We will now consider each of these aspects of mean flow to assess the likely driving force and also to consider the consequences for the transports of nutrients. While we lack data to track how the shelf evolved over winter, we can make some assessment of the net changes to the shelf system between November 2014 and March 2015 which are relevant to understand whether or not the shelf receives new nutrients from the ocean during winter. Finally, we will consider the implications for nutrient supplies to the central Celtic Sea.

2.4.1 Surface offshore flow in the northern Celtic Sea

The low density, low salinity water exiting the Bristol Channel has typically been assumed to mainly head north towards the Irish Sea as a

buoyancy-driven flow influenced by Coriolis (Uncles, 2010). However, salinity transects (Fig. 2.3) suggest a gradual freshening in the northern Celtic Sea, and a sharpening of the horizontal salinity gradient, from November 2014 through to April 2015. Riverine input from the southern coast of Ireland into the Celtic Sea is minor and flows westward within a coastal current (Brown et al., 2003). Freshening of the northern Celtic Sea between winter and spring is therefore more likely to be associated with elevated winter discharge from the Bristol Channel.

In April 2015, significant shear in the salinity structure is clear, with a plume-like low-salinity layer in the northern Celtic Sea developed coincident with the thermally-stratified surface layer (Fig. 2.2). Over most of the Celtic Sea in spring, surface salinity tends to reduce compared to the bottom water, indicating an offshore transport that sets up a haline stratification across the shelf that persists until winter re-mixing. The shear of the 35.2 g kg^{-1} isohaline in April 2015 suggests a relative movement of the surface layer offshore by about 35-40 km over the bottom layer. Assuming that this shear must have developed after the March 2015 survey suggests a mean surface layer flow relative to the bottom layer of at least 1.4 km day^{-1} (1-2 cm s^{-1}). The position of the 35.2 g kg^{-1} isohaline stayed roughly constant after this April 2015 event. The speed of the flow, followed by the halt of further offshore progression, suggests initial relaxation of the horizontal density gradient triggered by the spring thermal stratification switching off mixing between surface and bottom waters. This is akin to the estuarine-style baroclinic circulation described by Linden and Simpson (1988) for a number of shallow seas and estuaries worldwide. As fresh water from the Bristol Channel is allowed to extend towards the northern Celtic Sea it is continually mixed with (and freshens) surrounding water, a non-reversible process that extends

the southward influence of the Bristol Channel.

The width of the surface relaxation should equal a few internal Rossby (Ro) :

$$Ro = \frac{\sqrt{g h_s \frac{\triangle \rho}{\rho_0}}}{f} \tag{2.1}$$

where $g = 9.81$ m s^{-2}, $\triangle \rho$ is the bottom-surface density difference (1 kg m^{-3}), ρ_0 the reference density (1027 kg m^{-3}), f the Coriolis parameter and h_s the surface layer thickness of about 40 metres. Using these typical values Ro is 5.5 km. The scaling between the width of the fresher water plume (40 km) and Ro is 7.2. The width of the relaxation is therefore about 7 times Ro (7×5.5 km $= 38.5$ km), a scaling that lies within the range of values reported by Sharples et al. (2017) for the width of a fresh water plume. The width of the relaxation will vary depending on the prevailing wind conditions, the strength of the river discharge, the level of tidal mixing and the strength of the existing horizontal salinity gradient. Once the surface plume has reached its maximum southward extent it will feel the effects of rotation and the low salinity water will join the cyclonic geostrophic gyre circulation described by Horsburgh et al. (1998) and Brown et al. (2003).

The potential for nutrient supply from rivers to support the Celtic Sea spring bloom can be considered by noting the dilution of the salt content and the initial river nitrate concentration of 390 mmol m^{-3} which will be modified by biogeochemical processing during transit from the rivers to the Celtic Sea. An estimate of the transit time of fresh water from the Severn Estuary and Bristol Channel to the Celtic Sea can be made by considering the time between peak river discharge and the sharpening of the horizontal salinity gradient and drop in surface salinity in the northern Celtic Sea, i.e. assuming changes in salinity are only due to

freshwater flow. In 2013/2014 the decrease in salinity at the Celtic Deep (on 6th May 2014) takes place 4.5 months after peak river discharge (on 23rd December 2013). In 2014/2015 a drop in salinity at the Celtic Deep starts just 3.5 months after the peak in river input (on 15th January 2015), or a more conservative 4.5 months if the earlier secondary peak in discharge during December 2014 is considered. On average therefore, it takes about 4 months for fresh water to reach the northern Celtic Sea. For context, Uncles and Radford (1980) estimate the residence time of the Severn Estuary (from Maisemore Wier north of Gloucester to Minehead) to be about 100 days (3.3 months) in the winter, a timescale well aligned with the evidence presented here.

A 4 months transit time, based on the time between the peak of freshwater input and the minimum in salinity time series at Celtic Deep, would imply a mean flow of about 2-3 cm s^{-1}, which is a reasonable value for a mean surface flow in the Bristol Channel (Uncles, 2010). Removal of nitrogen by biogeochemical processing over 4 months will reduce the riverine nitrate concentration. Based on data collected from lakes, rivers, estuaries and continental shelves Seitzinger et al. (2006) established a relationship between the removal of DIN (by de-nitrification) from aquatic systems and the residence time of water within them whereby the percentage (%) of DIN removed, DIN_{rem}, is related to the residence time T_{res} (months) by $DIN_{rem} = 23.4T_{res}^{0.204}$. This empirical relationship suggests that about 30% of the total riverine nitrate will be removed over 4 months. It is less clear how long the riverine influence would take to reach the CCS mooring site. Bottom onshore transport was 1-1.5 m^2 s^{-2} throughout summer, as will be described in the following section. A transport of 1.25 m^2 s^{-2} in a 50-60 m layer thickness leads to velocities of 1.7-2.1 km day^{-1} and therefore fresher waters from the Bristol Channel

would take at least 6 months to reach CCS. Assuming 6-12 months, and again using the relationship from Seitzinger et al. (2006) would mean a reduction in the original riverine nitrogen input of between 34% and 40%. Taking the oceanic salinity to be 35.7 g kg^{-1}, and the spring salinities in the northern Celtic Sea and at the CCS mooring site to be 35.4 and 35.55 g kg^{-1} respectively, results in the freshwater fraction to be 0.8% in the north and 0.4% at CCS, based on dilution of North Atlantic waters. Thus the contribution of river nitrate load to the nitrate observed at the Celtic Deep in spring is about 2.2 mmol m^{-3} of the observed 7 mmol m^{-3}, so about 30% of the nitrate available to the spring bloom in the Celtic Deep is riverine in origin. In the Central Celtic Sea, by the CCS mooring site, the same calculation (denitrification and percentage of freshwater that reaches CCS) suggests 0.9-1.0 mmol m^{-3} of river-sourced nitrate out of a total of 8 - 9 mmol m^{-3}, so approximately 10% of the nitrate available to the spring bloom at CCS is riverine.

2.4.2 On-shelf bottom water flows

In March 2014 the 35.6 g kg^{-1} isohaline was situated at the shelf edge. During summer 2014 this water in the bottom layer moved approximately 100 km onto the shelf by August 2014. In spring-summer 2015 the same isohaline remained almost fixed, just 30 km onto the shelf from the shelf edge. The 35.5 g kg^{-1} isohaline, initially 25 km on-shelf from CCS, had moved about 120 km further onto the shelf by July-August 2015. Bottom water transports can be estimated by taking the mean flow implied by the isohaline movement and the thickness of the layer. For March to August 2014 the movement of the 35.6 g kg^{-1} isohaline (speed approximately 0.87 km day^{-1} (1 cm s^{-1}), layer thickness 150 metres) suggests a transport of 1.5 m^2 s^{-1}. For March to July 2015, the movement of the 35.5 g kg^{-1} isohaline (speed approximately 0.87 km day^{-1}, layer thick-

ness 100 metres) suggests a transport of 1 $m^2 s^{-1}$.

There are several potential mechanisms for driving this bottom water across the shelf. We consider here: (1) horizontal dispersion down the horizontal salinity gradient, (2) a compensating on-shore transport for a surface off-shore Ekman transport, (3) a mean density-driven (or pressure gradient) transport, (4) the Stokes drift of an on-shore propagating internal tidal wave, and (5) on-shore baroclinic transport of high salinity lenses in the pycnocline (Hopkins et al., 2012).

(1) Horizontal dispersion

The timescale for horizontal dispersion can be estimated as $k_h \frac{\triangle s}{\triangle y}$ where $\frac{\triangle s}{\triangle y}$ is the horizontal salinity gradient and k_h is a horizontal dispersion coefficient. Observations of dispersion coefficients in shelf seas are typically 10 - 600 m^2 s^{-1} (Sanders and Garvine, 2001; Houghton et al., 2009). Taking a high value of 10^3 m^2 s^{-1} suggests a timescale of over 1 year for the observed bottom layer isohaline shifts in 2014 and 2015, much slower than the observed transport.

(2) Ekman transport

For the surface Ekman transport we take the mean cross-shelf Ekman transport between March and September 2014 and 2015 calculated as $\frac{\tau_w}{f\rho_0}$ with τ_w the averaged along-shelf edge wind stress (0.01 and 0.02 N m^{-2} in 2014 and 2015 respectively),ρ_0 1027 kg m^{-3} and f the Coriolis parameter at latitude 48^oN. In both years we find a weak net off-shelf wind-driven surface Ekman transport of 0.1-0.2 m^2 s^{-1}, which would drive a weak compensating on-shelf return flow in the bottom layer.

(3) Pressure-gradient flow

A consistent feature of all of the CTD sections is a cross-shelf horizontal density gradient (Fig. 2.6) set up by the salinity gradient (Fig. 2.4a), and modified by seasonal changes in the horizontal temperature structure. The pressure gradients associated with contrasts in density across the outer shelf are conducive to driving on-shelf transports in the bottom layer (Fig. 2.10). Outside of the bottom turbulent boundary layer the pressure gradient will be balanced by Coriolis, and there would be no net transport down the density gradient. However, this balance breaks down in the bottom boundary layer, allowing down-gradient transport. We assume a simple balance between the horizontal pressure gradient ($\frac{1}{\rho_0}\frac{\partial P}{\partial y}$) and stress ($\tau$), to occur within a bottom turbulent boundary layer of thickness h_{BL}:

$$\frac{1}{\rho_0}\frac{\partial P}{\partial y} = \frac{1}{\rho_0}\frac{\partial \tau}{\partial z} \tag{2.2}$$

Taking the vertical gradient in stress ($\frac{\partial \tau}{\partial z}$) to be approximated by the effect of bed friction, $\tau_b = k_b \rho_0 v^2$ with k_b 0.0025 the bottom drag coefficient, ρ_0 the average density and v the mean current speed in the bottom layer, distributed through the bottom boundary layer,

$$\frac{1}{\rho_0}\frac{\partial P}{\partial y} = \frac{1}{\rho_0}\frac{k_b \rho_0 v^2}{h_{BL}} \tag{2.3}$$

for the total transport in the bottom boundary layer(h_{BL}), we have:

$$v h_{BL} = \sqrt{\frac{h_{BL}^3}{k_b}\frac{1}{\rho_0}\frac{\partial P}{\partial y}} \tag{2.4}$$

For h_{BL} we take the height above the seabed within which most of the velocity shear was located. Based on the current meter data available from the mooring at CCS this was 40 metres. Density was depth averaged from the surface to 80 metres depth for each oceanographic survey

every 25 km between 100 km and the Central Celtic Sea mooring site. The depth averaged density was used to calculate the pressure gradient force at 80 metres along the hydrographic transect. In both years, the typical mean near bed pressure gradient term,$(\frac{1}{\rho_0}\frac{\partial P}{\partial y})$, across the central shelf (between 100 and 350 km) from April to August was about 0.7-1.2 $\times 10^{-7}$ m s^{-2}. Using these values in eq. (2.3) gives velocities between 2.9 - 3.8 km day^{-1} (0.03 - 0.045 m s^{-1}), which are of the same order to the ones calculated following the salinity contours (Fig. 2.4b), and a transport 1.3-1.8 m^2 s^{-1}. This should be viewed as an upper limit, as we would expect the flow within the bottom boundary layer to be diverted across the pressure gradient by Coriolis.

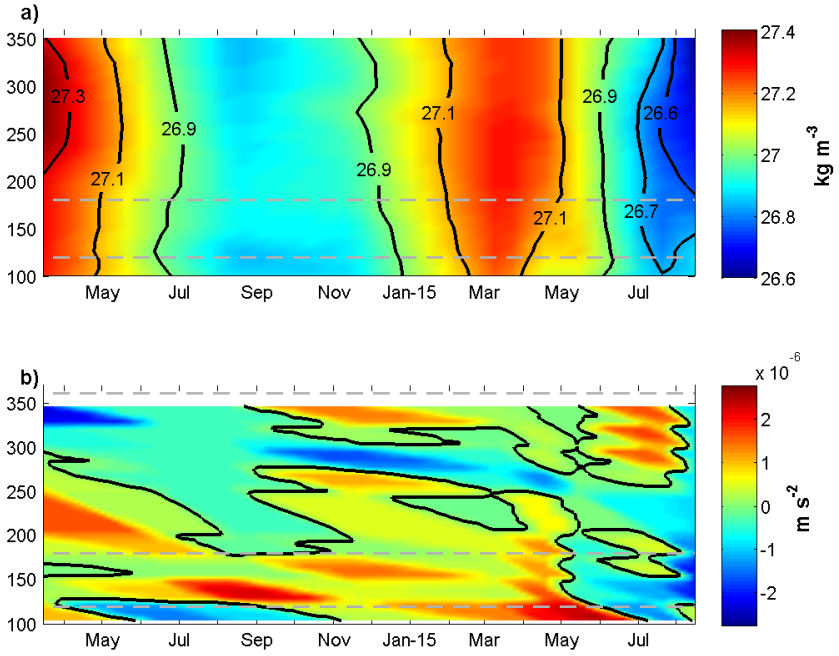

Figure 2.10: (a) Depth averaged density across the Celtic Sea between CCS and CD. (b) Pressure gradient across the Celtic Sea. The black contour in (b) represents the 0 m s^{-2} pressure gradient. Positive values indicate on-shelf acceleration.

(4) Internal tide Stoke's Drift

The Celtic Sea is influenced by internal tidal waves, generated at the shelf slope and propagating at least 170 km into the Celtic Sea (Inall et al., 2011). At CCS semi-diurnal isopycnal displacements characteristic of a propagating internal tide first appear in April, shortly after the onset of stratification, and persist until December when the water column becomes isothermal again (Wihsgott et al., 2019). Evidence of isotherm displacement can also be found at the Celtic Deep, over 300 km from the shelf edge (not shown). The bottom layer Stokes drift volume transport (V_{St}) associated with a propagating internal tidal wave is estimated from:

$$V_{St} = \frac{1}{2} K A_0^2 c \coth(K h_b) \tag{2.5}$$

with K m^{-1} the wavenumber, A_0 (m) the wave amplitude and h_b the bottom layer thickness (Simpson and Sharples, 2012). The wave speed is estimated from:

$$c = \sqrt{g \frac{\triangle \rho}{\rho_0} h_b} \tag{2.6}$$

where g=9.81 m s^2, and $\triangle \rho$ is the bottom-surface density difference (1 kg m^{-3}). Using typical values for the wavelength (35 km) and amplitude (15 metres) for the internal tidal wave on the shelf (Inall et al, 2011) eq. (2.5) suggests a volume transport of about 1 m^2 s^{-1}. This on-shore Lagrangian transport has to be balanced by an off-shore flow. Where in the water column that balancing return flow occurs will affect the net effect that the Stokes transport has on bottom layer scalar distributions. If the return flow occurs within the pycnocline (e.g. Henderson, 2016) then 1 m^2 s^{-1} would represent a reasonable estimate for the onshore bottom layer transport. Salinity transects suggests for both summer 2014 and 2015 (Fig. 2.3) that there is offshore transport within the pycnocline layer, which would be consistent with this mechanism.

(5) High Salinity Lenses

High salinity lenses of water have been identified moving on-shore within the pycnocline of the Celtic Sea (Hopkins et al., 2012), driven by non-linear second-mode internal waves. Combined with diapycnal mixing between the base of the pycnocline and the bottom layer, these would provide a mechanism for evolving the cross-shelf salinity gradient by transporting salt onto the shelf during the summer. An estimate of the volume flux driven by these lenses can be made by considering the mean flows associated with their on-shore propagation (0.02 m s^{-1}) and the typical lens thickness (30 metres) (Hopkins et al., 2012). This yields a transport of 0.6 m^2 s^{-1}, which will be an upper limit due to the likely temporal patchiness in the generation of the internal waves and lenses (Hopkins et al., 2012). Whilst there is some evidence in August 2014 of higher salinities within the pycnocline near the shelf edge (Fig. 2.3c), there are also examples throughout the summers of both 2014 and 2015 of lower salinities than either the upper or lower layers (Fig. 2.3).

The above estimates suggest that the bulk of the on-shelf bottom layer flow may be a result of wind-driven Ekman transports, near bed pressure gradients and/or internal tide Stokes drift. It seems unlikely that horizontal dispersion is able to contribute significantly to the on-shelf transport observed during early summer, and while high salinity lenses could in principle contribute we cannot find persistent evidence of the required salinity signal in the summer of 2014 and 2015.

2.4.3 Offshore transports during winter

There is an indication in the salinity transects and evidence from the near bed currents recorded by the ADCPs across the shelf that water moves off-shelf between November 2014 and March 2015. While we lack

CTD transect data through this period, we can make an assessment of the net effects of winter on the system by considering the changes in the horizontal salinity structure. The November CTD transect took place as the shelf water was quickly becoming fully-mixed by a combination of convection due to surface cooling and wind-driven mixing, and we know from the CCS mooring data that the shelf was vertically homogeneous by about mid-December (Wihsgott et al., 2019). The depth-mean salinity structure in November 2014 should therefore be very similar to that about 3 weeks later in mid-December, and we can compare that with the pre-spring salinity in March 2015 (Fig. 2.11). The 35.45 g kg^{-1} isohaline moves across the shelf by about 180 km between November and March, implying a cross-shelf flow of about 2 cm s^{-1} and a transport over 110 metres depth of 2.2 m^2 s^{-1}. Cross-shelf displacements of the higher value isohalines are less, 70 km for 35.6 g kg^{-1}, 40 km for 35.7 g kg^{-1}. With mean depths associated with these isohaline movements of about 160 metres and 170 metres, this suggests transports of 1.4 and 0.9 m^2 s^{-1}. At CCS evidencefrom ADCP indicates an off-shore flow with mean velocities above 1 km day^{-1} between mid-November and February 2015. Similarly, at CD an off-shore flow occurred between mid-November and April 2015, with maximum velocities ($>$ 3 km day) in December. Without more information over the winter it is difficult to be confident of the mechanisms driving these isohaline movements, but we can indicate the likely causes.

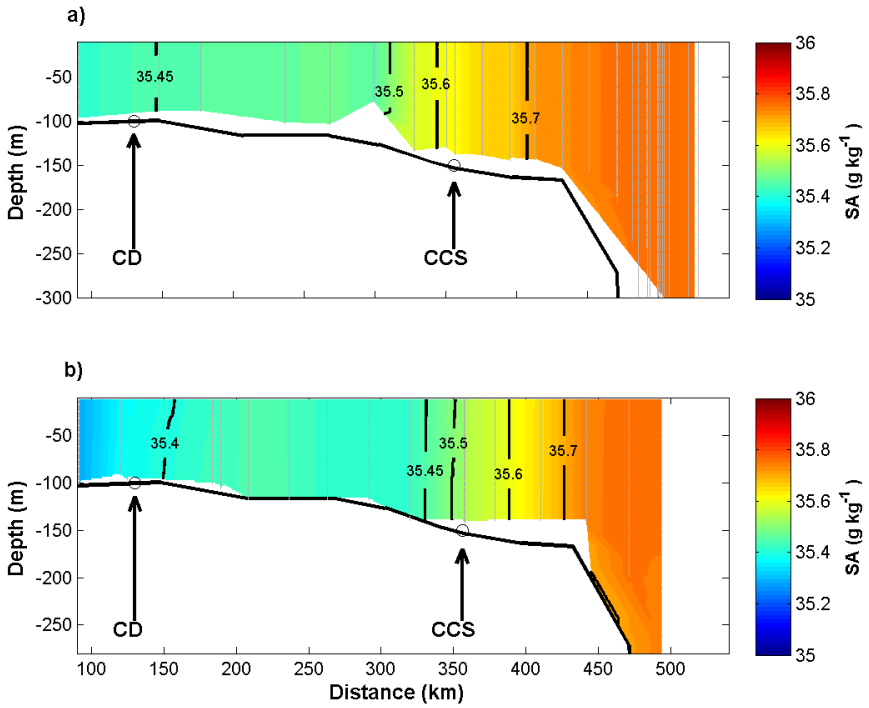

Figure 2.11: (a) Depth-mean salinity in autumn (November 2014) and (b) Salinity distribution in late winter (March 2015).

The simplest explanation of the overall reduction in shelf salinity between November and March is rainfall, with the strong winter mixing redistributing the freshwater vertically. Considering the mid-shelf between distances of about 150 and 300 km, the salinity decreased by about 0.1 g kg^{-1} over a mean depth of 100 metres. Assuming no horizontal transport, and that the total mass of salt in the water column is conserved, then a precipitation of 31 cm would be sufficient to produce the observed salinity change. Between November and March the precipitation based on ERA-interim reanalysis was 16 cm at CCS and 18 cm at the Celtic Deep. Taking account of the ERA-interim precipitation over the ocean to be typically 0.3 mm day^{-1} higher than observations (Dee et al., 2011) reduces the precipitation by about 3 cm over the period November - March, suggesting that about 42- 48% of the observed salinity change can be attributed to rainfall. At the outer shelf, between a distance of about 330 and 440 km, the observed salinity changes would need a rain-

fall of 50 cm and so about 26% of the salinity change is likely due to precipitation.

Based on the analysis of the effects of precipitation above, there remains a consistent off-shelf transport of about 1 m^2 s^{-1} occurring over winter that needs to be explained. The along-shelf edge wind stress over the winter was seen to be consistently driving surface water off-shelf, with a mean Ekman transport of 0.45 m^2 s^{-1}. Considering the cross-shelf horizontal salinity gradient this off-shelf flux would drive a decrease in surface salinity, with the compensating return flow increasing deeper water salinity. Towards the outer shelf the effect of depth-mean salinity can be estimated by taking a mean horizontal salinity gradient of 1×10^{-6} g kg^{-1} m^{-1} and assuming that the surface Ekman layer is about 30 metres thick, with the return flow occurring in the lower 120 metres. Over 3 months advection of the salinity gradient then yields a surface salinity decrease of 0.12 g kg^{-1}, and a bottom water salinity increase of 0.03 g kg^{-1}. Weighting these contributions by the layer thicknesses suggests almost zero change of the depth mean salinity. Taking into account the non-linearity of the horizontal salinity gradient, with the gradient tending to steepen at depth near the shelf edge, would lead to a slight salinity increase in the depth mean salinity of O(0.001 g kg^{-1}). It is therefore unlikely that wind-driven Ekman transport can explain the overall reduction of shelf salinity and the implied off-shelf flux of 1 m^2 s^{-1}. One possible candidate mechanism for this transport could be a flux through the bottom boundary layer driven by a cross-shelf pressure gradient. Assessing this is difficult without further data between November and March: the problem largely depends on whether the excess cooling in the shallower water on the shelf, compared to the deeper outer shelf, can reverse the horizontal density gradient set up by the horizontal salinity

gradient across the shelf.

2.4.4 Implications for nitrate sources to the central Celtic Sea

The time series of nitrate at CCS allows us to make some inferences on the fate of nitrate throughout the year, and how the shelf is set up with nitrate ready for the spring bloom.

We have suggested, based on dilution and processing of riverine nitrogen, that the major riverine sources of nitrogen in the Bristol Channel could be responsible for about 1 mmol m^{-3} of the nitrate in the central Celtic Sea. There are two sources of error to these estimates. There is an uncertainty of about 15% in the empirical fit linking nitrate removal to transport timescale (Sharples et al., 2017), and there is uncertainty in the time it takes riverine water to be transported to the central Celtic Sea.

The on-shelf flow of bottom water during summer will also supply nitrate to the shelf. We can quantify this by using the time series of salinity from CTD at 80 metres depth at CCS (Fig. 2.12) combined with a relationship between salinity and nitrate concentration at 80 m depth across the shelf in March 2014, i.e. before the spring bloom and any biogeochemical modification of nitrate. The salinity-nitrate relationship implies that horizontal movement of the isohalines indicates a similar displacement of the background concentration of nitrate (Fig. 2.13). There is a near linear increase in observed bottom water nitrate between April and November 2014, from 8 mmol m^{-3} to 9.7 mmol m^{-3} (Fig. 2.12b, dashed line). Of this 1.7 mmol m^{-3} increase, 0.4 mmol m^{-3} or 25% can be attributed to on-shelf transport in the bottom layer between March and August (Fig 2.12b. solid line) using the nitrate-salinity relationship. The total depth

at CCS was 145 metres, which in summer we will assume was made up of a 40 metres surface layer and a 105 metres bottom layer. Within the bottom layer a 0.4 mmol m^{-3} nitrate increase, suggests a transport contribution to total water column nitrate at CCS of about 40 mmol m^{-2}. The on-shelf movement of isohalines at CCS slows between August and November (Fig. 2.4a) and only an additional 0.05-0.1 mmol m^{-3} nitrate is supplied by advection during this period. From late summer onwards the surface layer deepens, and by November has reduced the depth of the bottom layer to 85 metres (Wihsgott et al. 2019). Therefore approximately 7 mmol m^{-2} of nitrate is transported to CCS in the bottom water during this later summer and early autumn period.

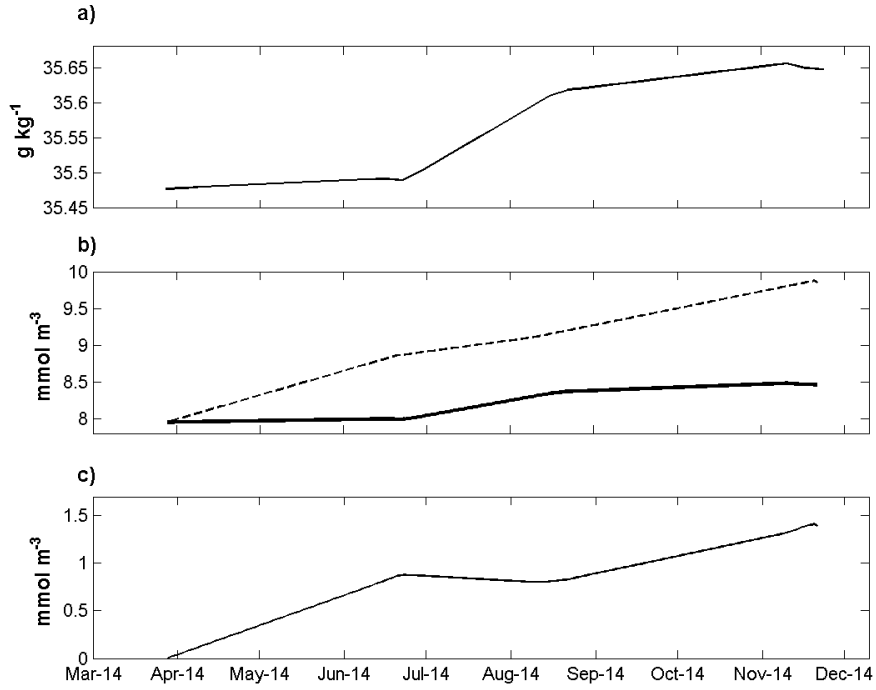

Figure 2.12: (a) Bottom water salinity at CCS from CTD casts. (b) Observed nitrate concentration in CCS bottom water (dashed line) and nitrate concentration (black line) inferred from the movement of isohalines from the March 2014 nitrate-salinity relationship. (c) Difference between observed nitrate and the predicted supply from physical transport.

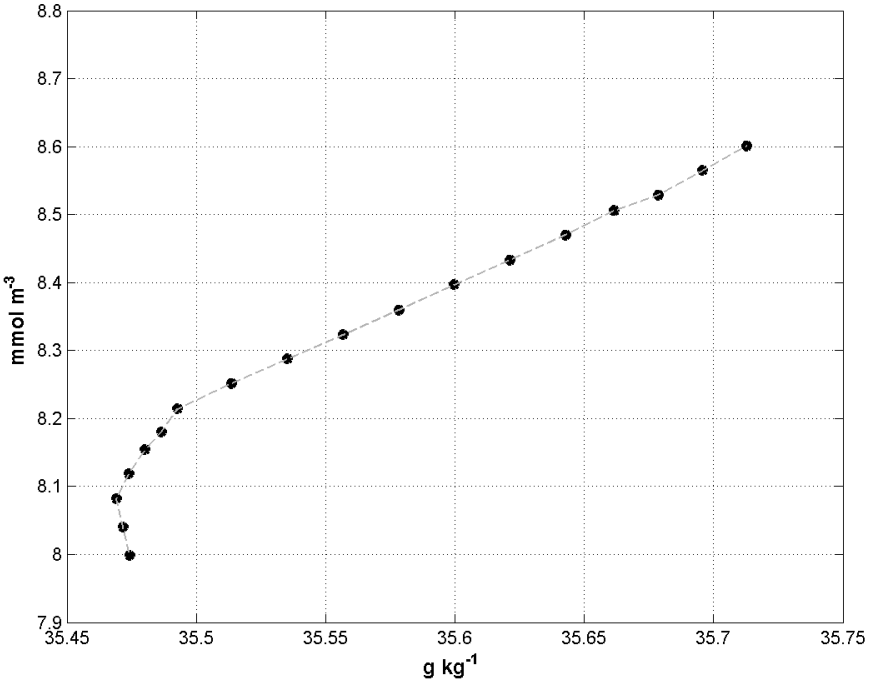

Figure 2.13: Nitrate-salinity relationship from CCS to the North Atlantic Ocean at 80 m depth in March 2014. The relationship was obtained from interpolated cross-shelf sections of nitrate and absolute salinity.

Pre-spring nitrate concentration at CCS in 2014 was 8 mmol m^{-3} in a water column of 145 metres, so a total of 1160 mmol m^{-2} (Fig. 2.14a). At the end of August 2014 the 40 metres deep surface layer was completely depleted in nitrate whereas the bottom 105 metres saw an increase in nitrate concentration to 9 mmol m^{-3}, equating to a total water column DIN content of 945 mmol m^{-2} (Fig. 2.14b). The generation of organic material during the spring bloom, vertical fluxes of nitrate into the base of the thermocline sustaining a subsurface chlorophyll maximum during the summer months, on-shelf transport in the bottom layer and the re-generation of organic material all contribute to the 215 mmol m^{-2} total water column decrease in nitrate during this period. Firstly, the spring bloom nitrate use is taken as the surface mixed layer thickness (40 metres) multiplied by the initial pre-bloom nitrate concentration of 8 mmol m^{-3}, contributing a 320 mmol m^{-2} reduction. The diapycnal nitrate flux to the subsurface chlorophyll maximum, that we assume is all consumed, is

estimated by using measurements of vertical eddy diffusivity made close to CCS by Williams et al. (2013). Wind stress pulses generate dyapicnal mixing and supply nutrients across the pycnocline from the bottom layer. For the 4 months of May-August based on Williams et al. (2013) fluxes, we assume a background 1.5 mmol m^{-2} d^{-1} for 110 days and storm driven fluxes of 20 mmol m^{-2} d^{-1} for 10 days using ERA-interim data sets (Dee et al., 2011), giving a total decrease of 365 mmol m^{-2}. Whereas nitrate is lost temporary from the system to the spring bloom and SCM production, on-shelf transport in the bottom 105 metres of the water column over the summer provides a 40 mmol m^{-2} increase to the total water column nitrate budget. Considering the change in nitrate concentration over the bottom 105 metres between March and August (1 mmol m^{-3} increase) and taking into account decreases via diapycnal mixing (-365 mmol m^{-2}) and gains due to on-shelf advection (+40 mmol m^{-2}), there remains a 430 mmol m^{-2} excess in nitrate suggesting a significant amount of organic material has been regenerated in the bottom layer. Distributed over 105 metres this equates to a concentration of 4.1 mmol m^{-3}, which would have originated from the upper 40 metres of the water column. Given the original pre-bloom concentration of 8 mmol m^{-3}, this implies that 51% of the nitrate taken up by the spring bloom had been recycled into the bottom layer by August. Note that this recycling estimate assumes that neither de-nitrification nor nitrate fluxes from sediments are significant.

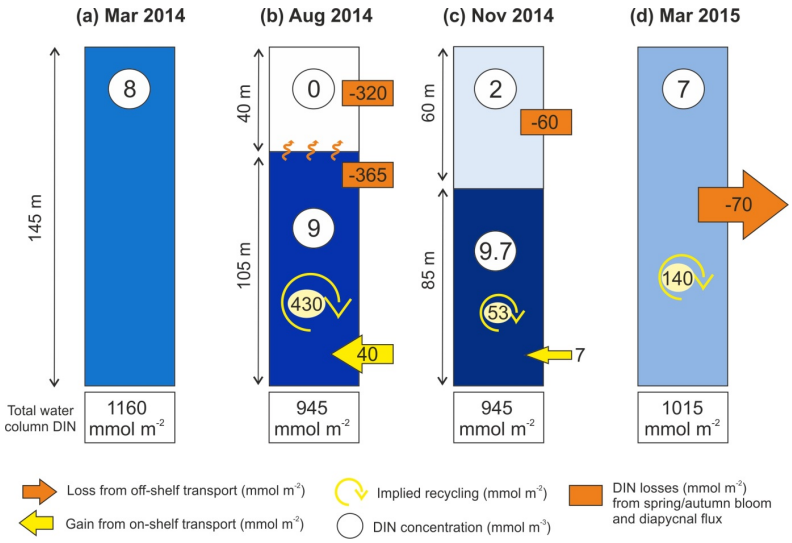

Figure 2.14: Total water column dissolved inorganic nitrogen budget at CCS between March 2014 and March 2015 based on observed nitrate concentrations (in mmol m^{-3}) and our estimates of bottom layer transport and nitrate uptake by phytoplankton. All losses (decreases in nitrate) and gains (in mmol m^{-2}) are relative to the previous date.

The total water column nitrate in November was made up of a 60 metres deep surface layer (nitrate concentration of 2 mmol m^{-3}) plus a 85 metres bottom layer (with 9.7 mmol m^{-3} nitrate), yielding 945 mmol m^{-2} (i.e. no change in total water column budget since August, Fig. 2.14c). Nitrate used by the autumn bloom is estimated by convectively mixing the August surface layer from 40 metres to 60 metres, entraining 20 metres of water with 9 mmol m^{-3} nitrate concentration. Distributing this over the 60 metres autumn mixed layer gives a concentration of 3 mmol m^{-3}. Knowing that in November only 2 mmol m^{-3} was observed in the surface layer, 1 mmol m^{-3}, or 60 mmol m^{-2}, is assumed to have been used by the autumn bloom by the time of the November survey. Between August and November there is an order of magnitude reduction in the advected bottom water supply of nitrate, estimated to be just 7 mmol m^{-2}. This is insufficient to explain the 60 mmol m^{-2} nitrate excess that accumulated between August and November (85 m $\times$ 0.7 mmol m^{-3} concentration) and 53 mmol m^{-2} nitrate is therefore assumed to have been recycled. This represents 62% of the 1 mmol m^{-3} used during the autumn bloom.

By March 2015 the total water column nitrate had increased to 1015 mmol m^{-2} (Fig. 2.14d). Over winter the 145 metres deep water column was fully mixed and nitrate concentrations pre-spring bloom in 2015 were 7 mmol m^{-3}. Off-shelf transport over the winter works to reduce the total water column nitrate at CCS. Taking into account the effect of winter rainfall, the reduction in nitrate is calculated by taking the depth-mean salinity and nitrate profiles in November 2014 and advecting them off-shelf to align with the depth-mean salinity in March 2015. This suggests that off-shelf advection reduces the total water column nitrate by 70 mmol m^{-2}. Knowing that there was a 70 mmol m^{-2} increase in total water column nitrate between November 2014 and March 2015, 140 mmol m^{-2} (approximately 1 mmol m^{-3} in 145 metres water column) must have been either recycled and/or physically re-supplied.

The closeness of our nitrate budget estimate and the observed pre-bloom nitrate suggest that a combination of on-shelf advection of nitrate (25%) from the shelf edge during the summer and 50-62% recycling of organic nitrogen are sufficient to maintain the shelf nitrate pool. River supplies also make a contribution, potentially providing some of the 140 mmol m^{-2} required to close the budget in March 2015, but we again note the significant uncertainties in our understanding of river nitrogen processing on the shelf and the transport time from the rivers to the mid and outer-shelf.

Finally, there is a 1 mmol m^{-3} difference in pre-spring nitrate concentrations across most of the shelf between 2014 and 2015. This implies significant inter-annual variability in the shelf nutrient pool, which likely arises from changes in the shelf edge and riverine boundaries as the main

sources of nutrients to the shelf. An assessment of the winter freshwater nitrogen concentration (Fig. 2.15) indicates a range in the nitrogen concentration of 200 - 450 mmol m^{-3}, so a median of 325 mmol m^{-3} with a range of $\sim$40%. At CCS this would translate into a mid-range riverine nitrate contribution of 0.8 mmol m^{-3}, with a range of 0.5 - 1.1 mmol m^{-3}. Considering the shelf edge boundary, changing the depth of the winter mixed layer will alter the nitrate concentration boundary condition adjacent to the shelf. Typical winter mixed layer depths in the Northeast Atlantic range between 212 and 476 metres (Hartman et al., 2014). Using the nitrate profile over the shelf slope in November 2014 and mixing it down to depths of 200 and 500 metres changes the mixed layer nitrate concentration from 6.4 to 8.9 mmol m^{-3}. Our tentative suggestion therefore is that variability in both riverine nutrient supplies and the depth of the ocean winter mixed layer are significant in driving inter-annual variation of shelf nutrient pools, with the oceanic mixed layer depth being the most important.

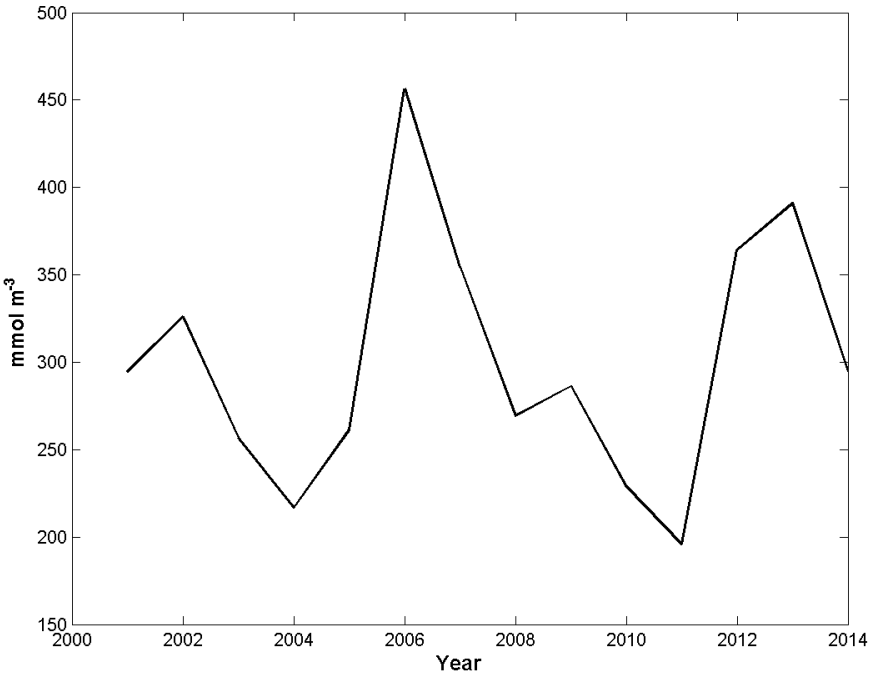

Figure 2.15: Averaged nitrate concentration input into the Bristol Channel during winter calculated from the river and nitrate time series. Each period covers the 1 of December to the 21 of March of the following year.

Acknowledgements

Sharples, Hopkins and Woodward were funded by the UK NERC-Defra Shelf Sea Biogoechmistry Programme (grant numbers NE/K002007/1, NE/K001701/1, NE/K002058/1). The Mexican National Council for Science and Technology (CONACyT) supported a scholarship to Eugenio Ruiz-Castillo. River nutrient data was kindly provided by Dr. Sonja van Leeuwen (Cefas, UK). The UK data was processed from raw data as provided from the Environment Agency, the Scottish Environment Protection Agency, the Rivers Agency (Northern Ireland) and the National River Flow Archive. Permission was granted from the Welsh Assembly to use data from the Welsh Rivers. All CTD, nutrient and mooring data is available from the British Oceanographic Data Centre. The authors thank Juliane Wihsgott for providing the CCS mooring data and Tom Hull for the Celtic Deep time series.

Chapter 3

Internal Wave and Wind-Driven Ekman transport in a Temperate Wide Shelf Sea in Summer

Abstract

In the Celtic Sea a bottom onshore flow and exchange within the pycnocline between the shelf and the North Atlantic in summer occurs. In this Chapter the mechanisms generating mean (non-tidal flows) are addressed. A 13-month time series of water column velocities and hydrographic observations from a mooring were used to calculate transport in the surface, pycnocline and bottom layers in summer. Transport within each layer was separated into the Eulerian and Stokes components, with the latter representing the transport generated by internal waves. The effects of the wind-stress on the water column were estimated from wind velocity recorded by a meteorological buoy. Variability of the velocity in the water column was assessed through an Empirical Orthogonal Function analysis. Results indicate that in the surface and bottom layers wind-driven Ekman transport was the dominant forcing agent resulting in an averaged surface offshore transport through the summer and an onshore compensatory flow in the bottom layer. In the pycnocline layer transport and exchange between the Celtic Sea and the North Atlantic

Ocean was generated by internal waves. The spatial variability of the first and second modes of the EOF analysis is consistent with the suggested mechanisms described in this Chapter.

3.1 Introduction

Evidence of net onshore advection of nutrients in the bottom layer and exchange within the pycnocline between the North Atlantic and the Celtic Sea was observed in summer (Ruiz-Castillo et al., 2018; Chapter 2 of this thesis). Whilst the mean onshore advection of bottom water was persistent and therefore well described by hydrographic observations, assessment of other components of the advection between the shelf and the ocean and quantification of the seasonal exchange required greater temporal resolution. Westerly winds are predominant in the Celtic Sea (Pingree, 1980) and in principle may explain the bottom flow as a response to wind-driven Ekman transport. However the shelf -ocean exchange within the pycnocline could result from other mechanisms. For instance, Hopkins et al. (2012) described relatively high salinity lenses intruding at least 100 km on-shelf within the pycnocline attributed to the second mode of a non-linear internal wave. Internal wave Stokes transport is also possible within the pycnocline (e.g. Henderson, 2016).

Transport across the Celtic Sea is thought to be dominated by nonlinear waves generated by the internal tide (Sharples et al., 2007; Hopkins et al. 2012), wind-driven Ekman transport (Huthnance et al., 2009) and a poleward along-slope current (Huthnance et al., 2009, Porter et al., 2016). In this Chapter, with long-term observations of temperature and salinity combined with velocity profiles recorded over a year at the Central Celtic Sea site, net advection resulting from internal waves and wind-driven Ekman transport are quantified. The main mechanisms responsible for the

bottom onshore advection in the Celtic Sea and exchange within the pycnocline between the ocean and the shelf are elucidated.

3.2 Methods

At the Central Celtic Sea site (Fig. 3.1) time series of salinity and temperature combined with current velocities from a 150 kHz ADCP seabed-mounted were used to calculate the Eulerian and Stokes transport in the surface, pycnocline and bottom layers. The effects of the wind stress on the water column were estimated using data from a meteorological buoy.

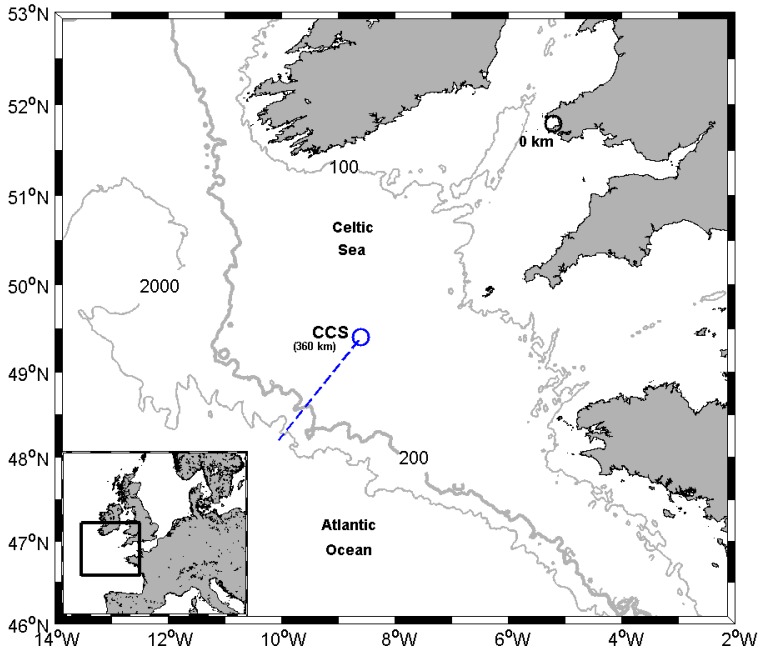

Figure 3.1: Map of the Celtic Sea. Blue circle indicate the location of the mooring at Central Celtic Sea site and meteorological buoy location and black circle indicate the zero point of the distance axis (0 km). The blue-dashed line indicates the location of hydrographic transects.

3.2.1 Mooring data

Hydrographic data

Full depth temperature and salinity time series from moorings located at the Central Celtic Sea site were available from Wihsgott et al. (2016) (Fig. 3.1). Vertical resolution of temperature ranged from 2.5 m in the pycnocline up to 5 to 20 m in the surface and bottom layers, and salinity resolution ranged from 5 m in the pycnocline up to 30 m in the bottom and surface layers, with the shallowest and deepest measurements of both time series at 10 m and 145 m, respectively. Each time series had a temporal resolution of 2.5 minutes. Temperature data were interpolated vertically every 2.5 m and spatially every 5 minutes. A scattered interpolation was used to evaluate salinity on the same grid (e.g. Hopkins et al., 2014). Further details on how data was processed can be found in Wihsgott et al. (2016). Conservative temperature and absolute salinity were calculated using TEOS-10 functions (McDougall and Barker, 2011) and potential density was calculated for each time step. Noise was removed from the time series using a low-pass Lanczos filter with a cut off frequency of 3 cycles per day (3cpd; Emery and Thompson, 2014). The periods assessed in this study include summer 2014 (22nd of June - 26th of December) and early summer 2015 (25th of April and 26th of July 2015) when the water column was stratified.

Current data

Current profile time series from moorings located at the Central Celtic Sea site were utilised to analyse velocity variability and transport in the water column throughout summer 2014 and 2015. An upward facing narrowband 150 khz FlowQuest Acoustic Current Profiler was used. Basic quality control was carried out for compass errors and sea surface echoes. Relatively high instrument noise was removed using a third-

order low pass Butterworth filter with a low pass cut-off frequency of ω=0.25^{-1} cycle m^{-1} for each profile. All velocity data were interpolated on a regular grid, with vertical and temporal resolution of 2.5 m and 5 minutes. For further details on how data were processed see Wihsgott et al.,(2018). Velocity used in this research cover from 145 m (7 metres above the seabed) up to 20 m depth (relative to mean sea level). Similarly to the hydrographic time series, a low-pass band Lanczos filter with a cut off frequency of 3 cpd was performed on each velocity time series.

3.2.2 Determination of the thicknesses of the surface, pycnocline and bottom layers

The depths of the upper and lower interfaces of the pycnocline were determined to identify the thicknesses of the surface and bottom mixed layers. There was significant seasonal variability in density, with minimum values below 25.5 kg m^{-3} in August compared to the minimum values around 27 kg m^{-3} by the end of December, so identifying the upper and lower bounds of the pycnocline based on a fixed isopycnal was not possible. Instead the upper and lower boundaries of the pycnocline were chosen based on a density increase and decrease from the mean density between 10 and 15 metres depth and the mean density between 140 and 145 metres, respectively (Table 3.1). In different regions thickness of the surface, pycnocline and bottom layers has been found to be variable throughout the year resulting in different seasonal values of density increase and decrease to estimate the thickness of each layer (e.g. Kara et al., 2000; Gomez-Valdes and Jeronimo, 2009). Vertical profiles of density were used to estimate the increase and decrease in density that best identifies the depth of the thicknesses of the surface and bottom layers in different months (Fig. 3.2). From the density time series, vertical profiles with a 10-day time step were plotted and the depths of the upper and

lower boundary of the pycnocline layer were chosen. The values used to estimate the surface and bottom mixed layer thicknesses are shown in Table 3.1. As mention before the original datasets had a greater vertical resolution in temperature than in salinity before the time series were vertically interpolated every 2.5 m. In addition, in the interior of the Celtic Sea density is controlled chiefly by temperature throughout most of the stratified period (Brown et al., 2003). Therefore, the depth of the boundaries chosen with density profiles were also evaluated for temperature profiles (Fig. 3.2). The thicknesses and depths were consistent for both variables.

Table 3.1: Values utilised for estimation of the upper and lower interface of the pycnocline.

Period	Density increase (kg m^{-3})	Density decrease (kg m^{-3})
22 Jun- 9 Jul 2014	0.04	0.05
9 Jul-27 Jul 2014	0.04	0.04
27 Jul-21 Aug 2014	0.04	0.1
22 Aug-27 Nov 2014	0.04	0.04
27 Nov-1 Dec 2014	0.028	0.032
1 Dec-27 Dec 2014	0.016	0.02
25 Apr-27 Jul 2015	0.018	0.015

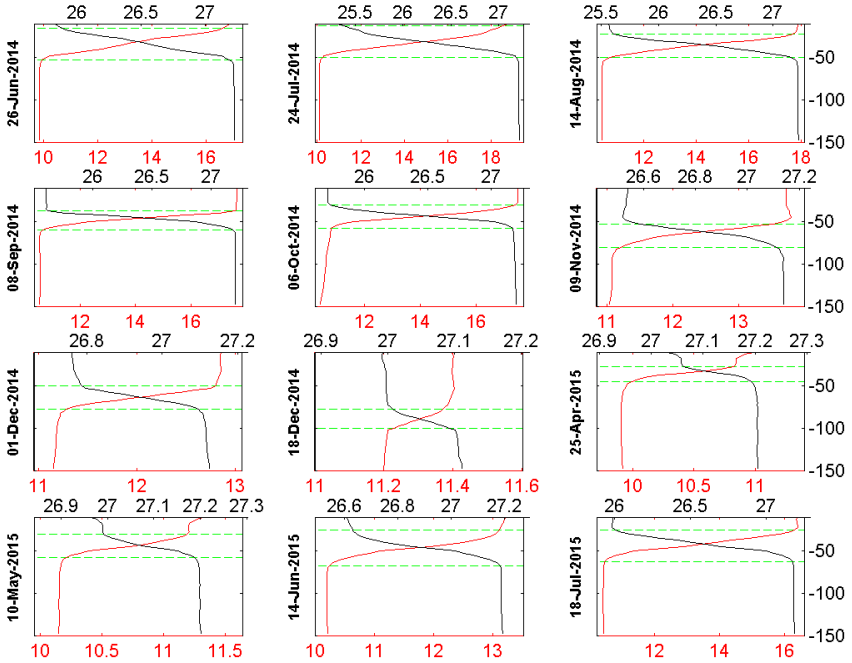

Figure 3.2: Profiles of density (black line) and temperature (red line). Scale for density and temperature are at the top and bottom of each subplot, respectively. Green dashed-lines show the depth of the upper and lower boundaries. Note the change in scale for temperature and density.

To increase confidence in the estimation of the depths of the boundaries the square BruntVäisälä frequency (N^2) was calculated:

$$N^2 = -\frac{g}{\rho_o}\frac{d\rho}{dz} \tag{3.1}$$

where $\frac{d\rho}{dz}$ represents the vertical density gradient, g=9.82 m s^{-2} is gravity and ρ_o the depth averaged density at each time step. The upper and lower boundaries of the pycnocline obtained using the values in table 3.1 were plotted on the time series of N^2 (Fig. 3.3). As expected the maximum values of N^2 in the water column corresponded to the pycnocline layer and minimum values were indicative of the surface and bottom layers. Observed vertical displacement of the interfaces was due to the passing of internal waves.

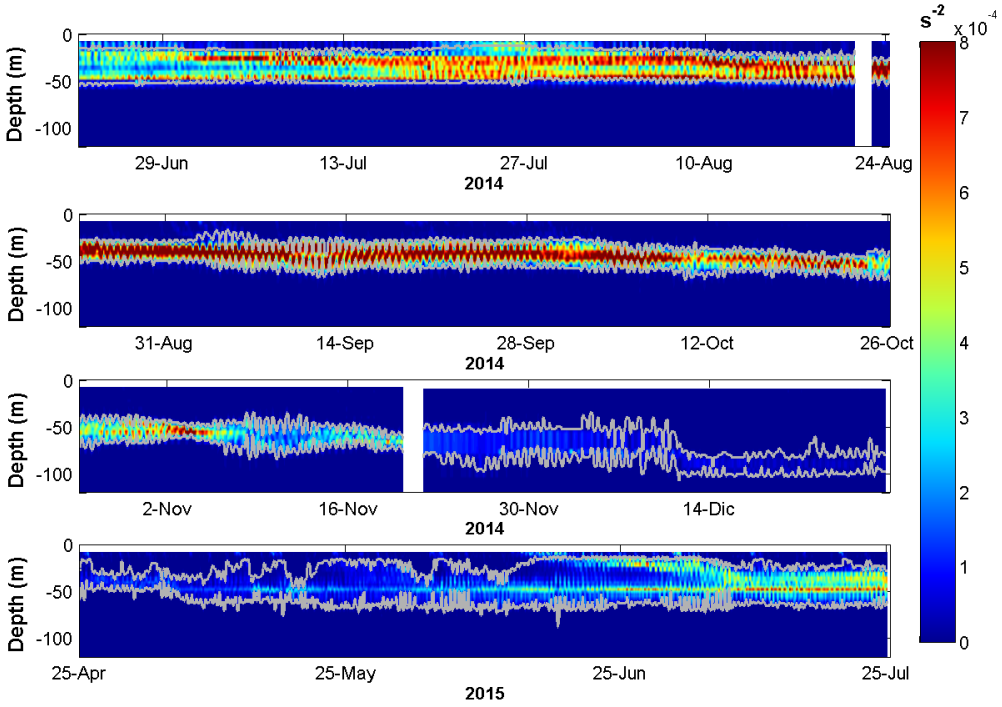

Figure 3.3: Square Brunt-Väisälä frequency at Central Celtic Sea. Grey lines indicate the upper and lower interfaces of the pycnocline based on the criteria in Table 3.1. Maximum values correspond to the pycnocline layer.

3.2.3 Non-tidal velocity anomalies and transport in surface, pycnocline and bottom layers

To assess the vertical shear in the horizontal velocities the depth-averaged flow (u_t) was calculated over the vertical span of the ADCP data, missing out the upper 20 and lower 7 metres of the water column, as follows:

$$\mathbf{u_t} = \frac{1}{H - z} \int_H^z \mathbf{u} dz \tag{3.2}$$

where $\mathbf{u}$ are the instantaneous horizontal velocities and H and z are 7 metres above the sea bed and 20 metres below the mean sea surface. The most intense velocities corresponded to an approximate 15 day periodicity resulting from the spring and neap tidal cycle (Fig. 3.4).

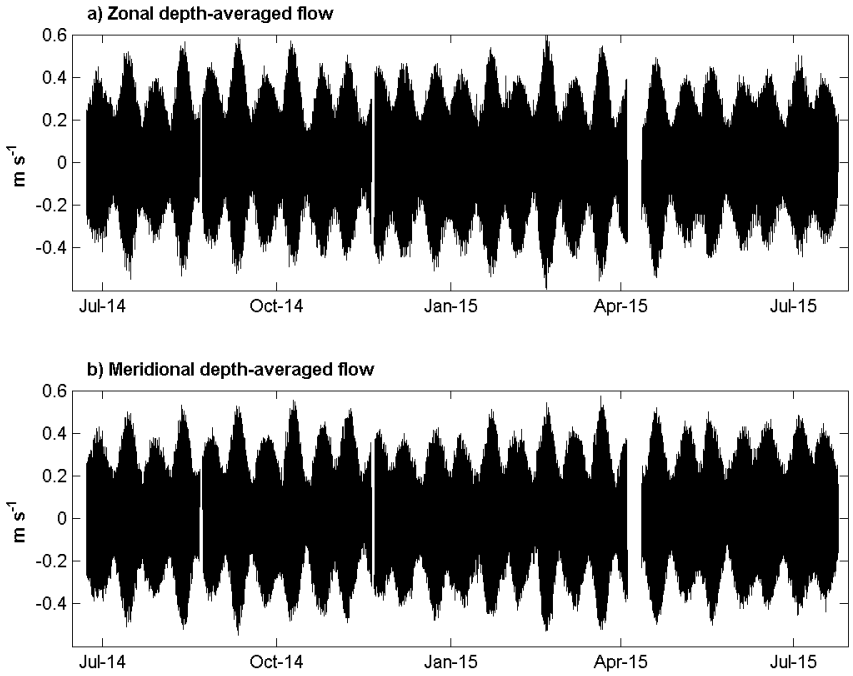

Figure 3.4: a) Zonal and b) meridional components of the depth-averaged flow

As the focus of this chapter is on the vertical variability of the horizontal velocity field, the horizontal velocity anomalies ($\mathbf{u_c}$) were calculated by removing the depth-averaged flow such that:

$$\mathbf{u_c} = \mathbf{u} - \mathbf{u_t} \tag{3.3}$$

See Figure 3.5. To obtain the corresponding transport for the surface, pycnocline and bottom layers velocity anomalies ($\mathbf{u_c}$) were vertically integrated within each layer. At each time step instantaneous transport ($\mathbf{U_{Li}}$, m^2 s^{-1}) was calculated between the upper (h_{ui}) and lower (h_{li}) boundaries as follows:

$$\mathbf{U_{Li}} = \int_{h_{li}}^{h^{ui}} \mathbf{u_c} dz \tag{3.4}$$

where the sub index i represents each layer, being 1, 2 and 3 the surface, pycnocline and bottom layer, respectively. The shallowest time series of velocity measurement was at 20 m depth, 10 m deeper than the upper

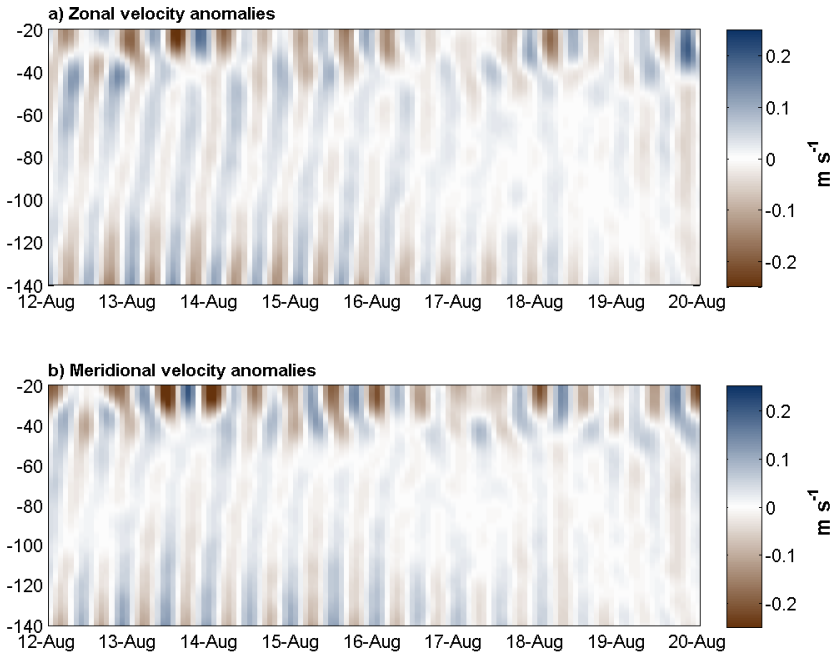

Figure 3.5: a) Zonal and b) meridional components of the velocity anomalies.

hydrographic time series. Thus, when the interface between the surface and pycnocline layers was above 20 m depth, the upper interface of the pycnocline was considered at 20 m and transport in surface layer was assumed to be 0. The net transport in the water column for each time step was zero. In the periods when transport in the surface mixed layer was above 20 m depth, the effects of surface transport on the water column, i.e. compensatory flows below the surface mixed layer, could not be quantified. Nonetheless, analysis of the filtered velocities revealed that when the surface layer was above 20 m depth the maximum variability of the flow was constrained between 40-100 m depth.

3.2.4 Spectral Density

To evaluate fluctuations of energy in transport throughout summer of 2014 and 2015, and identify potential forcing agents, a spectral density analysis was performed on transport within each layer. The dominant

tidal constituent in the Celtic Sea is M_2 (Pingree, 1980; Polton, 2015) and previous studies (e.g. Inall et al., 2013; Hopkins et al., 2014) have shown that the inertial frequency ($\sim$1.5 cpd) is significant as well suggesting that most of the energy is bounded between these two frequencies. A spectral density analysis was performed on the longest and continuous time series between the 23rd of August and 21st of November, i.e. in-between periods when the instruments were serviced. During this period the water column was stratified with the surface mixed layer extending below 20 m depth enabling calculations of the energy of transport in the surface mixed layer. Spectral density analysis confirmed that energy peaked around the semidiurnal and inertial bands and was negligible below 1.3 cpd at Central Celtic Sea (Fig. 3.6). To assess in more detail changes in transport variability within each layer the temporal resolution of the spectral density analysis was increased. Time series of transport were separated into periods of 50 hours (4 M_2 periods) and a spectral density analysis was performed for each period. The analysis was constrained to frequencies above the diurnal constituent (0.95 cpd or 25 hours) hence ruling out any potential variability introduced by low frequency signals ($<$1 cpd). However, for the whole time series there was no evidence of energy being significant below 1 cpd (Fig. 3.6). Energy obtained between two continuous periods was averaged every 100 hours to improve statistical confidence up to 4 degrees of freedom. Here, the semidiurnal and inertial frequency bands were represented between 1.9 and 2 cpd, which includes M_2, and between 1.45 and 1.55 cpd, respectively.

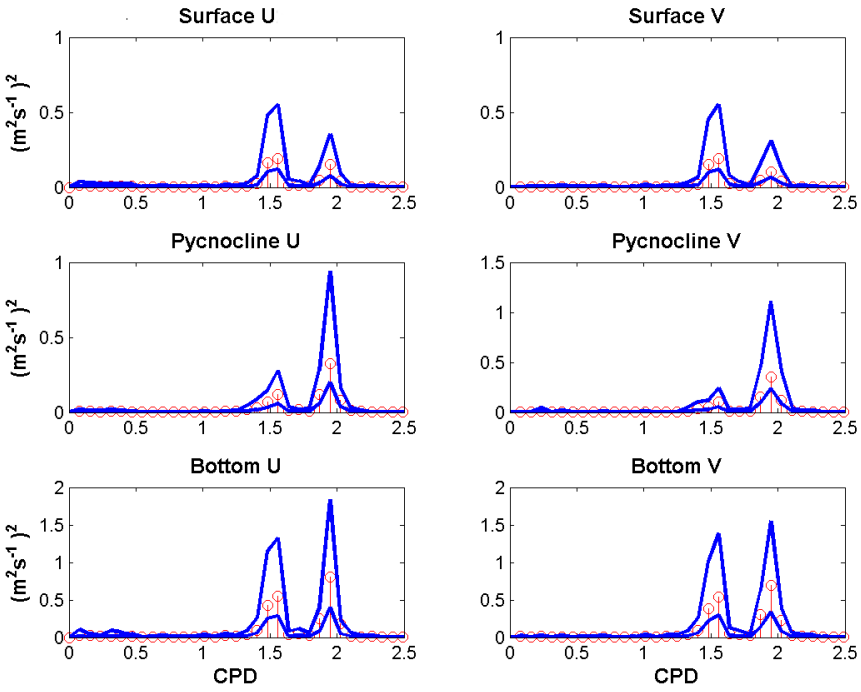

Figure 3.6: Spectral density analysis performed on surface (top), pycnocline (middle) and bottom (bottom) transport time series from the 23rd of August to the 21st of November 2014. Blue lines indicate the upper and lower intervals of confidence.

3.2.5 Stokes and Eulerian transport

Internal waves

Internal tidal waves have been reported in the Celtic Sea (Sharples et al., 2007; Green et al., 2008; Inall et al., 2011). They result from the combination of stratification of the water column and propagation of the barotropic tide from the deep ocean over the shelf and vice versa. As the tide propagates on and off the shelf the pycnocline is uplifted and depressed leading to the formation of steep waves that propagate in the tidal frequency. For infinitesimal waves the motion of a particle is symmetric and circular, moving forward and backward with the crest and the trough respectively, and returns to its original position leading to zero residual flow. In contrast, steep waves are characterized by sharp crests and flatter troughs (Simpson and Sharples, 2012). As the internal

tidal wave passes, the motion of the water particles turns asymmetric leading to a net residual flow. Associated with the passing of internal waves, advection of properties occurs due to this residual transport (Inall et al., 2001; Henderson 2016) which results from the difference between the velocity experienced by a moving particle (Lagrangian) and velocity at a fixed position (Eulerian) over a wave period; this mean transport is known as the Stokes drift (Henderson, 2016).

Calculation of Stokes and Eulerian transport in each layer

In section 3.2.3 the transports at the Central Celtic Sea site were calculated within the bottom, pycnocline and surface layers. The layer-averaged Lagrangian-mean velocities can be recovered by dividing transport ($\mathbf{U_{Li}}$) by the thickness of each layer as:

$$\mathbf{u_{Li}} = \frac{\mathbf{U_{Li}}}{h_{ui} - hli} \tag{3.5}$$

Following Henderson (2016), under the assumptions of statistically steady and weakly nonlinear waves, the velocity $\mathbf{u_{Li}}$ at the mean depth of the layer $\bar{Z}$ can be related to:

$$\langle \mathbf{u_{Li}} \rangle \approx \langle \mathbf{u_E} \rangle + \mathbf{u_S} \tag{3.6}$$

where $\langle\rangle$ indicates velocities were averaged over a wave period. The term on the left hand side is the Lagrangian velocity, or the velocity experienced by a moving particle. The first term of the right hand side is equivalent to the Eulerian mean velocity ($\mathbf{u_E}$) and the second term represents the Stokes drift ($\mathbf{u_S}$) calculated from vertical displacement ($Z^{'}$) of the interface from the mean depth of the layer ($\bar{Z}$) and has been

defined previously as (e.g., Henderson, 2016) :

$$\mathbf{u_S} = \frac{\partial}{\partial z}\langle \mathbf{u}^{'} Z^{'} \rangle \tag{3.7}$$

where $\mathbf{u}^{'} = \mathbf{u_c} - \bar{\mathbf{u}}_\mathbf{c}$, with $\bar{\mathbf{u}}_\mathbf{c}$ being the temporal mean of the velocity. Stokes drift can be separated into:

$$\mathbf{u_{nb}} = \langle Z^{'} \frac{\partial \mathbf{u}^{'}}{\partial z} \rangle \tag{3.8}$$

and

$$\mathbf{u_b} = \langle \mathbf{u}^{'} \frac{\partial Z^{'}}{\partial z} \rangle \tag{3.9}$$

The non-bolus velocity ($\mathbf{u_{nb}}$) accounts for the shear between the mean Eulerian velocity and the mean velocity at the depth of the interface, whilst the bolus velocity ($\mathbf{u_b}$) represents fluctuations of the interface and therefore fluctuations in the layer thickness. The Eulerian transport ($\mathbf{U_{Ei}}$) in each layer can be estimated by vertically integrating the velocities within the averaged layer thickness (Spingys, 2016) such that:

$$\mathbf{U_{Ei}} = \int_{\bar{h_{li}}}^{\bar{h_{ui}}} \mathbf{u_c} dz \tag{3.10}$$

where $\bar{h}$ represents the mean depth of the boundaries of each layer. Stokes transport ($\mathbf{U_{Si}}$) can be estimated by vertically integrating (3.7) leading to:

$$\mathbf{U_{Si}} = \langle \mathbf{u}^{'} Z^{'} \rangle \tag{3.11}$$

The Stokes transport ($\mathbf{U_{Si}}$) represents variations from the mean transport over a wave period. Finally, with transport averaged over wave-periods yields:

$$\langle \mathbf{U_{Li}} \rangle = \langle \mathbf{U_{Ei}} \rangle + \langle \mathbf{U_{Si}} \rangle \tag{3.12}$$

The dominant tidal constituent in the Celtic Sea is semidiurnal, predominantly M_2 (Pingree, 1980; Polton et al., 2015). In addition, spectral density analysis revealed most of the variability was bounded around the semidiurnal and f frequency bands (Fig. 3.6). Thus, transport was time averaged over 50 hours to account for variability produced by the inertial ($\sim$16 h $\times$3=$\sim$50 h) and semidiurnal ($\sim$12.5 h $\times$4=$\sim$50 h) periods (Hopkins et al., 2014). Moreover, within this time-interval deepening and/or shallowing of the interface depths due to seasonal variability can be considered negligible (e.g. Henderson et al., 2016).

Due to different hydrographic conditions Eulerian and Stokes transport were averaged over three periods (22nd June - 5th October 2014, 6th October- 26th December 2014 and 25th April - 25th July 2015). During the first period heating of the water column occurred leading to maximum stratification (Fig. 3.2, 3.3 and 3.7) and constraining transport in the surface layer above 20 m depth for most of the time, i.e. above the shallowest velocity time series. In the second period the upper interface of the pycnocline deepened below 20 m depth due to heat loss to the atmosphere leading to breaking down of stratification (Fig. 3.7). Weak stratification was persistent until early January 2015, however up to the 26 of December the maximum value of the Brunt-Väisälä frequency was greater than the inertial frequency such that the constrain for internal waves ($f < \omega < N$) was accomplished (Cushman-Roisin and Beckers, 2009). In the third period, after the winter 2014-2015, stratification was again becoming established.

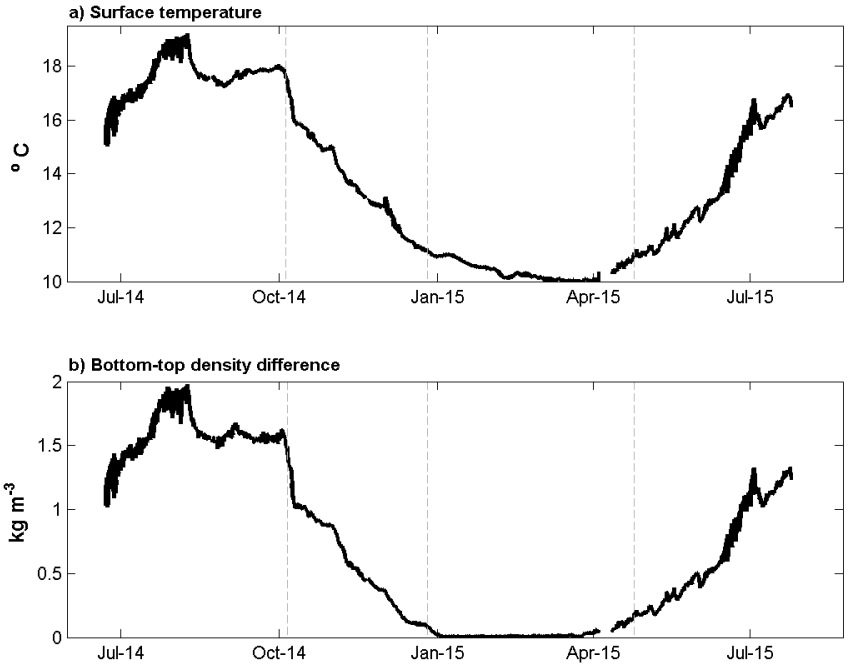

Figure 3.7: a) Temperature time series at 10 m depth and b) difference between the upper and bottom density time series indicating stratification in the water column. Dashed lines indicate the periods with different hydrographic conditions.

Ellipses of variability of the Stokes and Eulerian transport

To assess the predominant direction of variability of the Stokes and Eulerian transports the ellipses of variability were calculated for each layer and for the whole time series. An example on how the axis of variability was calculated for the Eulerian transport is described below. Through this analysis the predominant direction of variability can be obtained through the matrix of covariance (C) as follows:

$$U'_{Ei} = U_{Ei} - \bar{U_{Ei}} \tag{3.13}$$

$$V'_{Ei} = V_{Ei} - \bar{V_{Ei}} \tag{3.14}$$

$$w = [U'_{Ei}, V'_{Ei}] \tag{3.15}$$

$$C = (n-1)^{-1}(w^T w) \tag{3.16}$$

where U'_{Ei} and V'_{Ei} are the zonal and meridional anomalies of the Eulerian transport, $\bar{U}_{Ei}$ and $\bar{V}_{Ei}$ are the mean transport of each component,n is the number of elements in U'_{Ei}, and T indicates the transpose of the matrix. The size of the matrix w has n rows and 2 columns. Following Preisendorfer and Mobley (1988) the angle (θ) of maximum variability of the transport can be calculated from the covariance matrix as:

$$\theta = \frac{1}{2}\tan^{-1}[2C(2,1), C(1,1) - C(2,2)] \tag{3.17}$$

Consequently, Eulerian transports were rotated to the angle of maximum variability using a rotation matrix as follows:

$$\begin{bmatrix} U_{ri} \\ V_{ri} \end{bmatrix} = \begin{bmatrix} \cos\theta - \sin\theta \\ \sin\theta + \cos\theta \end{bmatrix} \begin{bmatrix} U_{Ei} \\ V_{Ei} \end{bmatrix} \tag{3.18}$$

where U_{ri} and V_{ri} are the zonal and meridional components of the Eulerian transports rotated to the maximum axis of variability for each layer. The major (M) and minor (m) axis of the ellipses can be estimated from the standard deviation of U_{ri} and V_{ri}, respectively, or from the covariance matrix of the rotated Eulerian transports (C_{ri}) as follows:

$$M = \sqrt{C_{ri}(1,1)} \tag{3.19}$$

$$m = \sqrt{C_{ri}(2,2)} \tag{3.20}$$

Ellipses of variability for the Stokes transport were calculated in a similar manner.

3.2.6 Wind data and Ekman transport

Wind data

At the Central Celtic Sea site wind data at 3 m above sea level was recorded every hour by a meteorological buoy. These data were used to assess the influence of the wind stress on the water column. Data were compared with the nearest time series at 10 m above sea level from ERA-interim data sets (Dee et al., 2011). High correlation coefficients (R^2) between data sets, 0.97 and 0.96 for the zonal and meridional components (Fig. 3.8), was observed. Several coefficients, such as the drag coefficient (C_d) have been calculated thoroughly in literature. Nonetheless, estimation of these coefficients is based on wind velocity at 10 m height. Therefore, the wind data at 3 m was used to calculate wind velocity at 10 m by rearranging eq. (3.21) to estimate the friction velocity of the wind ($\mathbf{w}_*$) (Cushman-Roisin and Beckers, 2009):

$$\mathbf{w_z} = \frac{\mathbf{w}_*}{k} ln \frac{z}{z_0} \tag{3.21}$$

where $\mathbf{w_z}$ is the wind velocity at height z, k is the von Karman constant (0.41) and z_0 is the roughness which was set constant at $2{\times}10^{-4}$ following Blanc et al.(1987). Spatial coverage was expanded to the whole shelf using ERA- interim data sets for each period described in section 2.5.

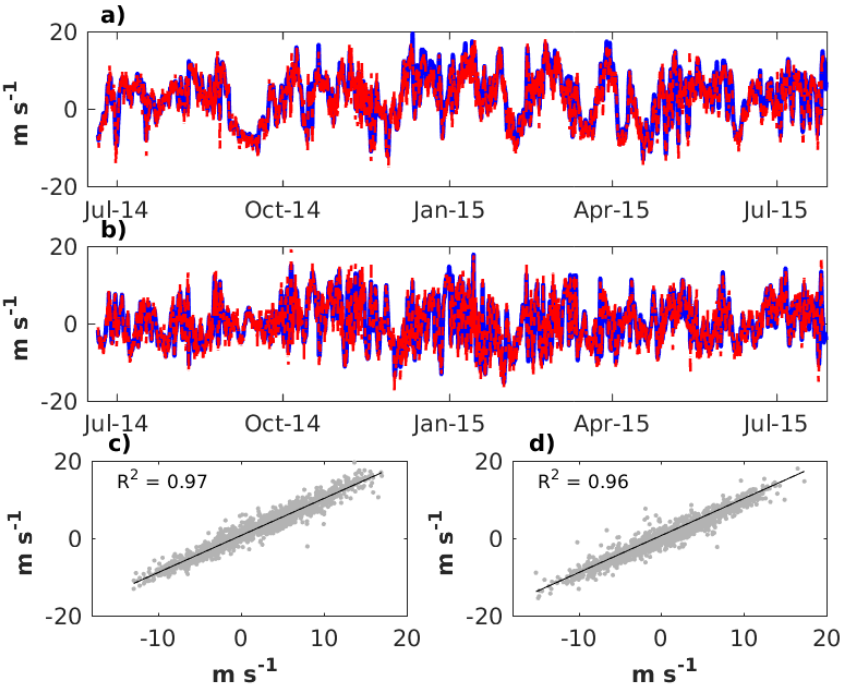

Figure 3.8: Time series of a)zonal and b)meridional components of the wind velocity of Era-interim (blue) and buoy (red) data. Correlation of the c) zonal and d)meridional components of the wind from Era-interim and buoy data

Ekman transport calculation

The effects of the wind stress on the water column are constrained within a certain depth or surface layer known as the Ekman Depth or Ekman layer (Dw). Within this layer the wind stress forcing at Central Celtic Sea can be described as:

$$\frac{\partial u_w}{\partial t} - f v_w = \frac{1}{\rho_0}\frac{\partial \tau_x}{\partial z} \tag{3.22}$$

$$\frac{\partial v_w}{\partial t} + f u_w = \frac{1}{\rho_0}\frac{\partial \tau_y}{\partial z} \tag{3.23}$$

where u_w and v_w represent the zonal and meridional velocities generated by the wind stress, respectively, referred to as the Ekman velocities, f is the Coriolis parameter, τ_x and τ_y represent the zonal and meridional components of the wind stress, respectively and ρ_0 is the mean density within the Ekman Layer. The terms on the left hand side are the local

acceleration and the effects of the Earths rotation whilst the term on the right hand side represents the wind stress forcing on the water column. The vertical coordinate was not included given that wind stress was assumed to be parallel to the sea surface. Wind-driven Ekman transport in the Ekman layer can be calculated by vertically integrating the Ekman velocities such that:

$$\mathbf{U_w} = \int_{D_w}^{0} \mathbf{u_w} dz \tag{3.24}$$

and therefore eq. (3.22) and (3.23) become:

$$\frac{\partial U_w}{\partial t} - fV_w = \frac{\tau_x}{\rho_0} \tag{3.25}$$

$$\frac{\partial V_w}{\partial t} + fU_w = \frac{\tau_y}{\rho_0} \tag{3.26}$$

In the scope of this research of particular interest were motions on timescales greater than the inertial period that may help elucidate the mechanisms generating net advection throughout the summer in the Celtic Sea. Under this scenario the resultant balance for low frequency motions is:

$$-fV_w = \frac{\tau_x}{\rho_0} \tag{3.27}$$

$$fU_w = \frac{\tau_y}{\rho_0} \tag{3.28}$$

From the latter equations it can be inferred that Ekman transport is orthogonal to the direction of the wind. In the Central Celtic Sea wind velocity ($\mathbf{u_w}$) time series from the buoy were used to calculate the wind-driven Ekman transport. From the wind time series wind stress was estimated as:

$$\tau_x = \rho_a C_d |\mathbf{u_w}| u_w \tag{3.29}$$

$$\tau_y = \rho_a C_d |\mathbf{u_w}| v_w \tag{3.30}$$

where u_w and v_w represent the zonal and meridional components of the wind velocity at 10 m above the sea surface. The air density (ρ_a) was assumed to be constant at 1.25 kg m^{-3} and the drag coefficients varied with the winds intensity following Smith and Banke (1975) such that:

$$c_d = 1 \times 10^{-3}(0.63 + 0.066(u_w, v_w)) \tag{3.31}$$

Ekman transport is expected to occur in the surface mixed layer, thus surface density (ρ_s) averaged between 10 and 15 m depth was assumed to represent the mean density of the Ekman layer. Wind stress and surface density were averaged every 50 hours (4 M_2 periods), which is a period short enough to provide a detailed analysis of the evolution of the Ekman transport and is great enough to account for low frequency motions only. Finally wind-driven Ekman transport was calculated as:

$$V_w = -\frac{\tau_x}{f\rho_s} \tag{3.32}$$

$$U_w = \frac{\tau_y}{f\rho_s} \tag{3.33}$$

where $f = 1.043 \times 10^{-4}$, s^{-1} was evaluated at Central Celtic Sea site.

Variability of the surface Ekman transport was quantified using the ellipses of variability as in section 3.2.5. Time series of Eulerian, Stokes and wind-driven transport were compared through a Pearson correlation analysis. An example on how correlation was calculated between the zonal components of wind-driven transport and Eulerian transport is provided below:

$$R^2 = \frac{cov(U_w^{'}, U_{Ei}^{'})}{std(U_w^{'})std(_{Ei}^{'})} \tag{3.34}$$

where *cov* represents the covariance matrix and *std* the standard deviation.

3.2.7 Empirical Orthogonal Functions

To identify spatial and temporal patterns within the time series and compare with the physical mechanisms presented here, an independent statistical assessment of the variability in the time series was carried out. An Empirical Orthogonal Function analysis using singular value decomposition (Venegas, 2001) was performed on the velocity ($\mathbf{u_c}$) and salinity (s_c) anomalies. The latter were calculated by removing the depth average salinity from the instantaneous salinity (s) obtained from the mooring as follows:

$$s_c = s - \frac{1}{H - z} \int_H^z \; s dz \tag{3.35}$$

The empirical orthogonal analysis was performed to assess the temporal and spatial variability of each field; therefore the temporal mean was removed from each series:

$$u^{'} = u_c - \bar{u_c} \tag{3.36}$$

$$v^{'} = v_c - \bar{v_c} \tag{3.37}$$

$$s_c^{'} = s_c - \bar{s} \tag{3.38}$$

and the matrix $W^{'}$ was created as follows:

$$W^{'} = u^{'} + iv^{'} \tag{3.39}$$

where $\bar{}$ represents the temporal mean and $^{'}$ anomalies from the temporal mean.

The singular value decomposition was performed on $W^{'}$ and $s_c^{'}$. Salinity was chosen given that signals corresponding to seasonal cycles are negligible compared to temperature or density, i.e. changes in temperature

due to seasonal heating and cooling of the water column. Secondly salinity is able to identify waters from different origins such as fresher waters from the Celtic Sea and relatively high salinity waters from the North Atlantic (Ruiz-Castillo et al., 2018; Chapter 2). Due to the horizontal salinity gradient, with salinity increasing towards the North Atlantic Ocean, positive and negative values indicate oceanic and fresher waters, respectively, revealing transport patterns in Central Celtic Sea. Time series of the averaged salinity within each layer were compared with the temporal modes or principal components of the EOF analysis.

3.3 Results

3.3.1 Internal waves and Stokes transport

During the stratified period the surface, pycnocline and bottom layers were identified (Fig. 3.9). Maximum seasonal heat input into the surface layers hinders the capacity of winds to vertically mix the water column leading to the minimum thickness of the surface layer (<15 metres) between the 20th of July and the 10th of August 2014 and 15th of June to 10th of July 2015. After August 2014 surface density gradually increased and stratification broke down leading to a deepening of the surface mixed layer, reaching maximum depths of 70 m by the end of December 2014. In contrast, the thickness of the bottom mixed layer remained constant at around 90 m from June to September 2014 and from April 2015 until the end of the record. From the 25th of April 2015 to mid-June 2015 enhanced vertical displacement occurred in the upper boundary of the pycnocline layer and can be attributed to a competition between atmospheric heat input and wind stress mixing. The mean thickness of the pycnocline was 26 m from June to December 2014 and 40 m from April to July 2015. The averaged depth of the pycnocline layer deepened from

late June 2014 to late December 2014, from 30 m to 80 m, respectively.

Throughout the stratified period internal waves were identified in the density time series by the vertical displacement of the upper and lower boundaries of the pycnocline layer (Fig. 3.9). Between mid-June and September 2014 vertical fluctuations, i.e. small amplitude of the vertical displacements, were relatively low for the pycnocline layer. From September to mid-December fluctuations were intensified to up to 25 m. From the 25th of April 2015 to the 25th of July vertical displacement due to internal waves was greater in the lower interface than in the upper interface of the pycnocline.

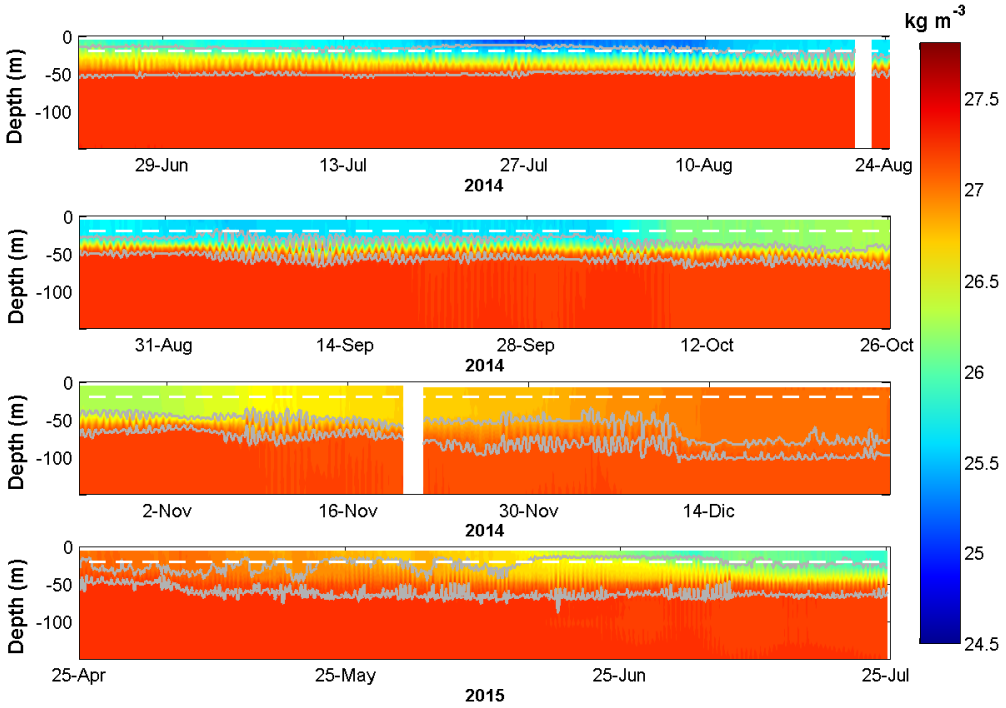

Figure 3.9: Density time series. White gaps indicate periods when instruments were removed from the water. White dashed line shows the upper extent of the ADCP measurements. Grey lines represent the upper and bottom boundaries of the pycnocline layer.

The temporal changes of the energy in transport in each layer are shown in Figure 3.10. Variability within the inertial frequency band intensified in the period October - late-December 2014 and late-April-

June 2015, being occasionally greater than the semidiurnal band particularly between October and late-December 2014. In contrast, in the pycnocline layer (Fig. 3.10b) maximum variability of the transport was bounded by the semidiurnal band and decreased from October 2014 onwards consistent with the period when stratification was breaking down (Fig. 3.7). Energy of the vertical displacement of the upper and lower interfaces of the pycnocline peaked in the semidiurnal frequency band mainly throughout the stratified period, revealing the passing of internal waves (Fig.3.10d). However, from November to late-December 2014 and between April and May 2015, events when the inertial frequency and the diurnal frequency bands were considerable occurred. Apart from mid-May, energy within the semidiurnal band was greater in the upper boundary.

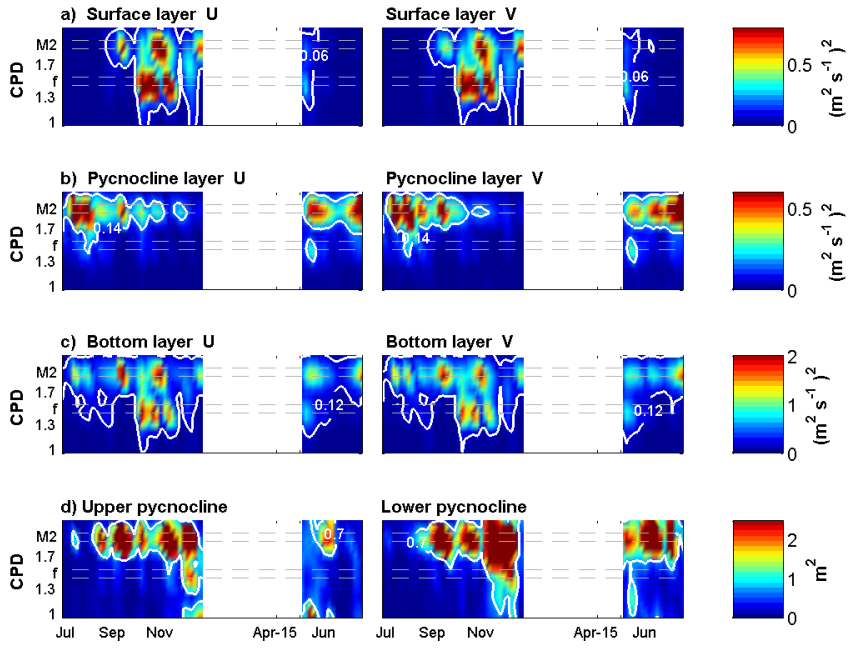

Figure 3.10: Spectral density analysis of the zonal (left column) and meridional (right column) components of total transport within the a) surface, b) pycnocline and c) bottom layers and d) upper (left) and lower (right) interface of the pycnocline layer.

The maximum averaged Stokes transport (∼0.08 - 0.1 m^2 s^{-1}) in the pe-

riods mid-June - 5th October and 6th October - 26th December 2014 occurred at the pycnocline and was off-shelf in the first period and on-shelf in the second (Fig. 3.11a-b). Stokes transport in the pycnocline layer for both periods was compensated in the surface and bottom layers by flow in the opposite direction. From late-April 2015 until the end of the record, minimum averaged Stokes transport occurred for the three layers being maximum ($\sim$0.025 m^2 s^{-1}) in the bottom layer in the on-shelf direction (Fig. 3.11c). For the whole time series the greatest variability occurred within the pycnocline layer with the ellipses of variability aligned perpendicularly to the 200 m isobath (Fig. 3.11d). Surface Stokes transport variability was also orientated perpendicular to the 200 m isobath whilst bottom Stokes transport was lined up in the south-north axis. Overall, throughout the record (Fig. 3.11d) Stokes transport was a maximum in the pycnocline heading off-shelf and was compensated in the surface and bottom layers in the on-shelf direction.

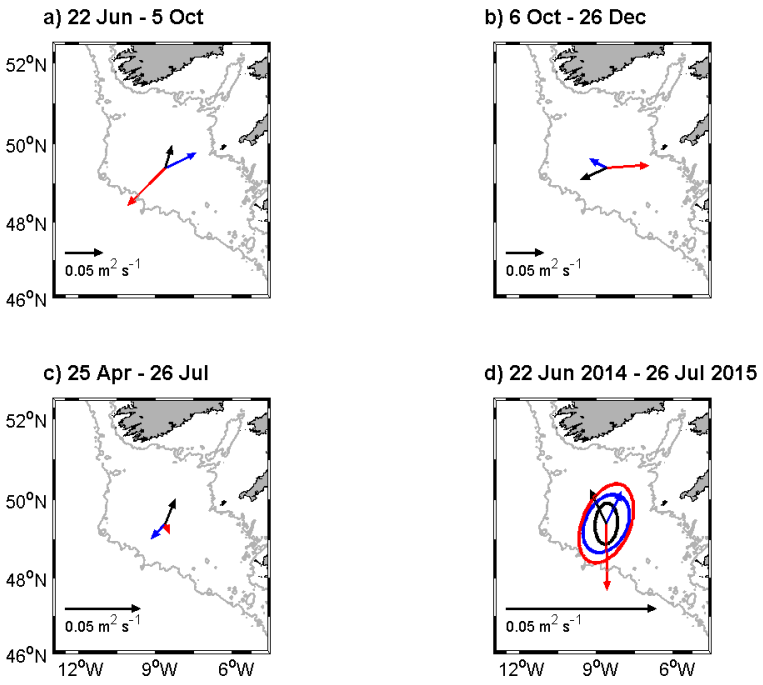

Figure 3.11: Averaged Stokes transport for the periods a) 22nd June to 5th October 2014, b) 6th October to 26th December 2014, c) 25th April to 26th July 2015 and d) Ellipses of variability and averaged Stokes transport for the whole record. Blue, red and black represent the surface, pycnocline and bottom layer, respectively.

3.3.2 Eulerian and Ekman transport

At Central Celtic Sea site the predominant winds were westerly south-westerly with mean velocities between 4 and 8 m s^{-1} (Fig. 3.12). Events when northeasterly winds occurred were observed. However in the long term north easterly winds may be considered negligible compared to the westerly wind events. Overall, for the whole shelf westerly winds prevailed throughout the summer of 2014 and 2015 (Fig. 3.13). Similarity between the averaged winds in Central Celtic Sea and the whole shelf indicates wind-driven dynamics described at the mooring location can be considered representative of the whole shelf.

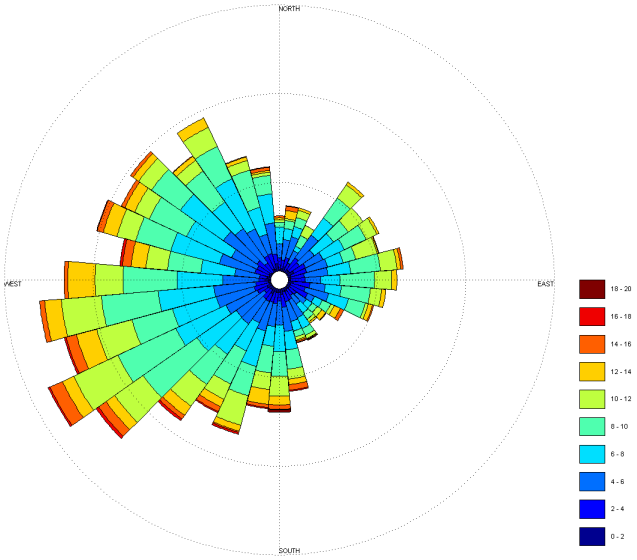

Figure 3.12: Histogram of winds direction and velocity (m s^{-1}), from their origin, and intensity at Central Celtic Sea at 10 m above sea level for the periods 22nd June to 29th December 2014 and from 25th April to 26th July 2015.

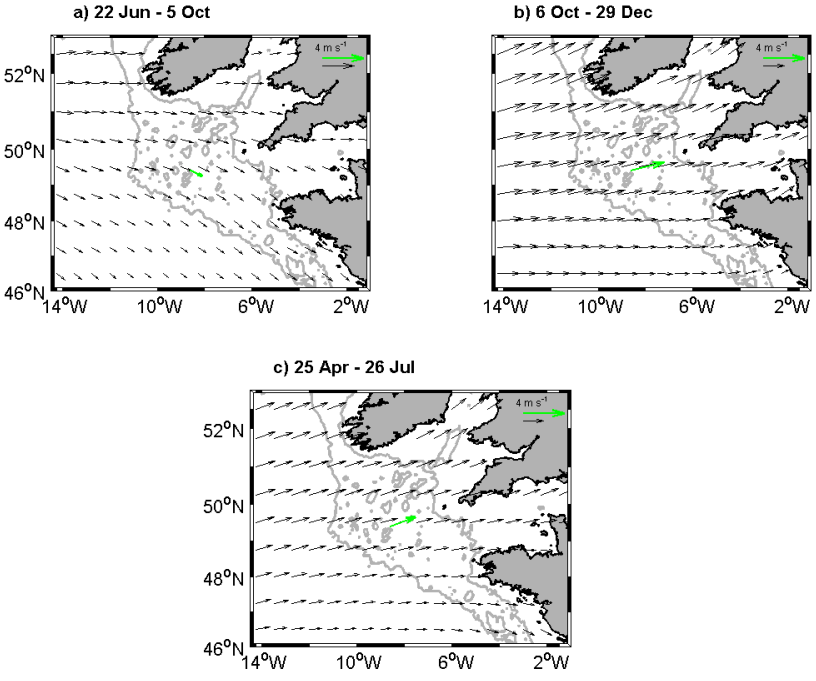

Figure 3.13: Average wind field for the periods a) 22nd June - 5th October 2014, b) 6th October - 29th December 2014 and c) 25th April - 26th July 2015. The green vector represents the averaged wind calculated at Central Celtic Sea.

During summer 2014 and 2015 the averaged wind-driven Ekman trans-

port was offshore (Fig. 3.14), south-south eastward and coincided with the direction of surface Eulerian transport from 6th October 2014 to late-July 2015 (Fig. 3.14b-c). Eulerian transport in the surface layer and Ekman transports were a maximum, $\sim$ 0.5 m^2 s^{-1} and 0.45 m^2 s^{-1}, respectively, between October and late-December 2014 (Fig. 3.14b). Variability for both transports was orientated along the south-south eastward direction throughout the record (Fig. 3.14d), being more intense for the Ekman transport. Between October and late-December 2014 bottom Eulerian transport was a maximum with values around $\sim$0.5 m^2 s^{-1} and was in the opposite direction to the surface Eulerian and Ekman transports (Fig. 3.14b), although its variability was predominately aligned with the ellipses of variability of the Ekman and surface Eulerian transport (Fig. 3.14d). In the pycnocline layer Eulerian transport was of the same order of magnitude for the three periods ($\sim$0.07 m^2 s^{-1}), and was onshore in the first and third periods and offshore in the second one. Most of the variability was aligned with the north-south axis (Fig. 3.14d), nonetheless, low eccentricity of the ellipse indicates variability of the Eulerian transport within the pycnocline was more disorganised compared to Eulerian transport in the surface and bottom layers. In the first and third periods, bottom transport was off-shelf similarly to surface Ekman transport.

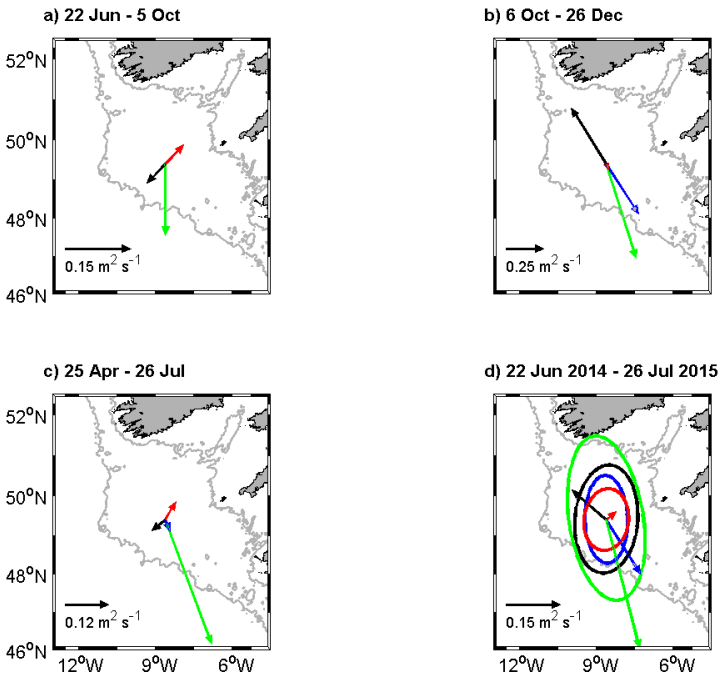

Figure 3.14: Averaged Eulerian and Ekman transports for the periods a) 22nd June to 5th October 2014, b) 6th October to 26th December 2014, c) 25th April to 26th July 2015 and d) Ellipses of variability and averaged Eulerian transport for the 3 periods (a-c). Blue, red and black represent the surface, pycnocline and bottom layer. The green vector indicates the surface and Ekman transport.

Time series of the Ekman and surface and bottom Eulerian transport are shown in Figure 3.15. Surface Eulerian transport was negligible from mid-June to mid-August 2014 when stratification was a maximum for the zonal and meridional components. The shallowest velocity time series was below the surface layer leading to a relatively low correlation coefficient ($R^2 < 0.5$) between the Ekman and the surface Eulerian transports (Table 3.2). From mid-August to late-December 2014 the zonal and meridional components of the surface and bottom transports responded to variations in the Ekman transport time series. Intensification and relaxation of the Ekman transport were reflected in increases and decreases of the surface transport, respectively. Particularly, the meridional component of the Eulerian surface and Ekman transports was highly correlated (R^2 between 0.73 and 0.82). In contrast, strong negative correlation

between the Ekman and Eulerian bottom transports occurred (R^2 of -0.71 and -0.7) indicating bottom transport responded to wind-driven Ekman flow in the opposite direction. From the 26th of April 2015 onwards, despite periods when surface Eulerian transport was negligible, events when maxima and minima coincided were observed and reflected in a relatively high correlation (R^2) between Ekman and surface Eulerian transport of 0.64 and 0.71 for the zonal and meridional components, respectively. For this period in the bottom layer negative correlation coefficients (R^2= -0.54 and -0.46) were observed. Low correlation in the period 23rd of June - 18th of August 2014 and events between mid-June and July 2015 when bottom transport was aligned to surface Ekman transport indicate cross-shelf transport was not governed by wind driven Ekman dynamics.

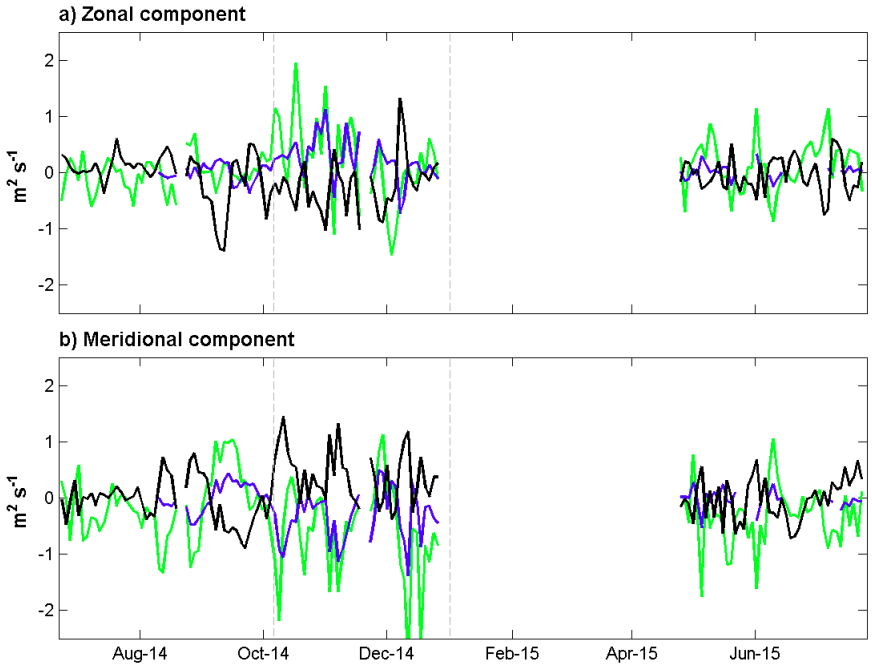

Figure 3.15: a) Zonal and b) meridional component of Ekman transport (green), surface (blue) and bottom (black) Eulerian transport. Discontinuity in the time series corresponds to winter and the periods when the mooring was serviced.

Table 3.2: Correlation R^2 between Ekman and surface, pycnocline and bottom Eulerian transport.

	23 Jun-18 Aug 2014	23 Aug-17 Nov 2014	22 Nov-26 Dec 2014	25 Apr-3 Jul 2015
Meridional surface transport	0.43	0.74	0.83	0.71
Meridional Pycnocline transport	0.11	-0.29	0.12	-0.28
Meridional bottom transport	-0.47	-0.71	0.70	-0.46
Zonal surface transport	0.41	0.53	0.06	0.64
Zonal pycnocline transport	0.18	-0.29	-0.17	0.38
Zonal bottom transport	-0.23	-0.15	-0.049	-0.54

3.3.3 Empirical Orthogonal Functions

The first mode of the velocity anomalies explains between 61 and 79% of the total variability (Fig. 3.16, top). Similarly, the first mode of the salinity anomalies explains between 63 and 71% of the total variability except for the 4^{th} period where it accounts for 91% (Fig. 3.16 2^{nd} row). The spatial modes of velocity and salinity anomaly indicate that variability can be represented in a three layer system except in the period between 22nd June and 21st August 2014 for the velocities. In this interval the shallowest velocity time series was below the surface layer throughout most of the time, therefore, variability in this period is represented by a two layer system. Seasonal deepening of the layers was observed in the spatial mode and consistent with density time series. Variability of the velocities indicates flows in the bottom layer were opposite to flows in the surface layer. Similarly, salinity anomalies indicate that events where fresher water was in the surface layer, relatively high salinity occurred in the bottom layer and vice versa which is consistent with the variability

described for the velocity anomalies.

The patterns observed in the principal component of the first mode of salinity anomalies described the evolution of the time series of averaged salinity within each layer (Fig. 3.16 5^{th} and 6^{th} row). In the period mid-July - mid-September the principal component increased to maximum positive values indicating intensification of the spatial structure (Fig. 3.16 2^{nd} row), thus freshening of waters in the surface layer and increases in salinity in the bottom. Depth-averaged salinity within each layer showed that salinity in surface and pycnocline layer decreased to 35.4 g kg^{-1} whilst bottom salinity remained around 35.62 g kg^{-1} fitting with the principal and spatial component of the first mode (Fig. 3.16 6^{th} row). Afterwards, the principal component decreased and turned negative between mid-September and mid-October and fitted with shortening of the difference between surface-pycnocline and bottom salinity being salinity in the pycnocline and surface layer higher than salinity in the bottom. From mid-October until December the vertical difference in salinity increased, with higher salinity in the bottom layer as described by the positive values of the principal component in this period. In early December an event of greater salinity in surface and pycnocline layers than in the bottom layer occurred and was consistent with the negative values of the principal component. The spatial mode changed direction between mid-June 2015 and the end of the record, the principal component was negative indicating relatively high salinities occurred in the surface and pycnocline layers.

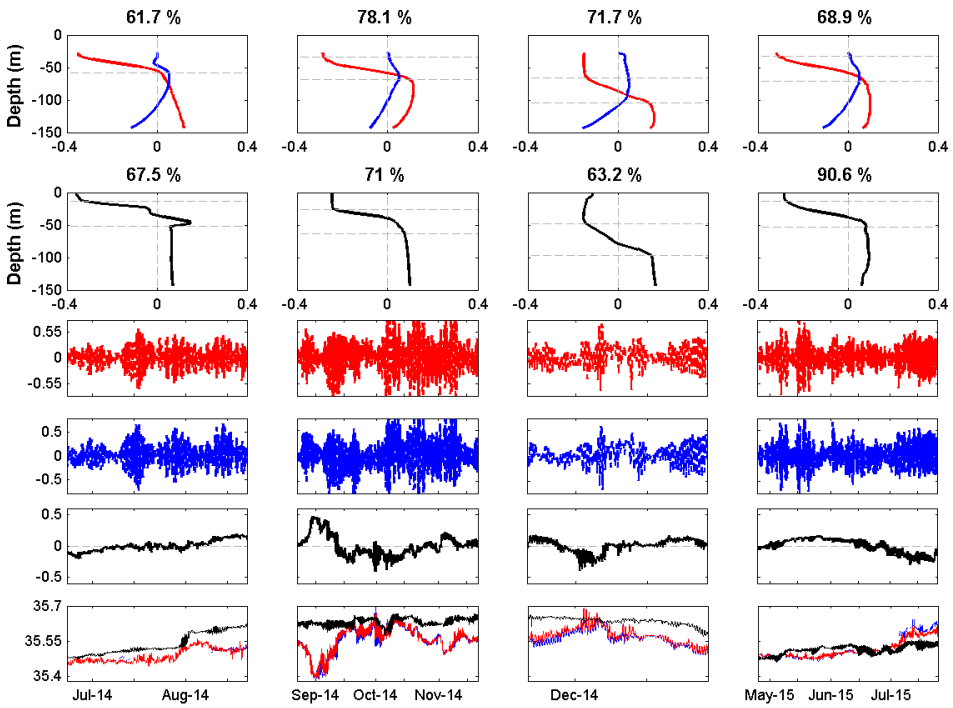

Figure 3.16: Spatial first mode of the zonal (red) and meridional (blue) components of the velocity anomalies (top) and anomaly of salinity (black) (2^{nd} row). Principal component of the zonal (3^{rd} row) and meridional (4^{th} row) velocity anomalies, salinity anomalies (5^{th} row) and averaged time series of salinity (g kg^{-1}) in surface, pycnocline and bottom layers (bottom).

Similarly, the second spatial mode of the velocity and salinity anomalies can be expressed in a three-layer system, with the same exception in the first period of the velocities (Fig. 3.17 1^{st} and 2^{nd} row). The second mode expressed between 19 and 33 % of the total variability except for the 4^{th} period of the salinity anomalies where the variability accounts for 4.9%. Seasonal deepening of the layers was observed. The spatial mode of the velocities indicates that the more intense velocities occurred at mid-depths within a layer coinciding with the location of the pycnocline. Velocities in this layer were opposite to velocities in the surface and bottom layers. Similarly, the highest variability of the spatial mode of salinity anomalies occurred at mid-depths. When relatively high salinity occurs at mid-depths, fresher salinity was found in the surface and bottom layers and vice versa.

The principal component indicates two different regimes in the period June-December 2014 (Fig. 3.17, 5^{th} row). Overall, between June and mid-October positive values were more predominant in the principal component. In contrast, from mid-October until the end of the year negatives values were more common. From mid-May 2015 until the end of the record values of the principal component fluctuated around zero suggesting variability due to the second mode was negligible in this period, consistent with the relatively low percentage of the variability explained by this mode (4.9%).

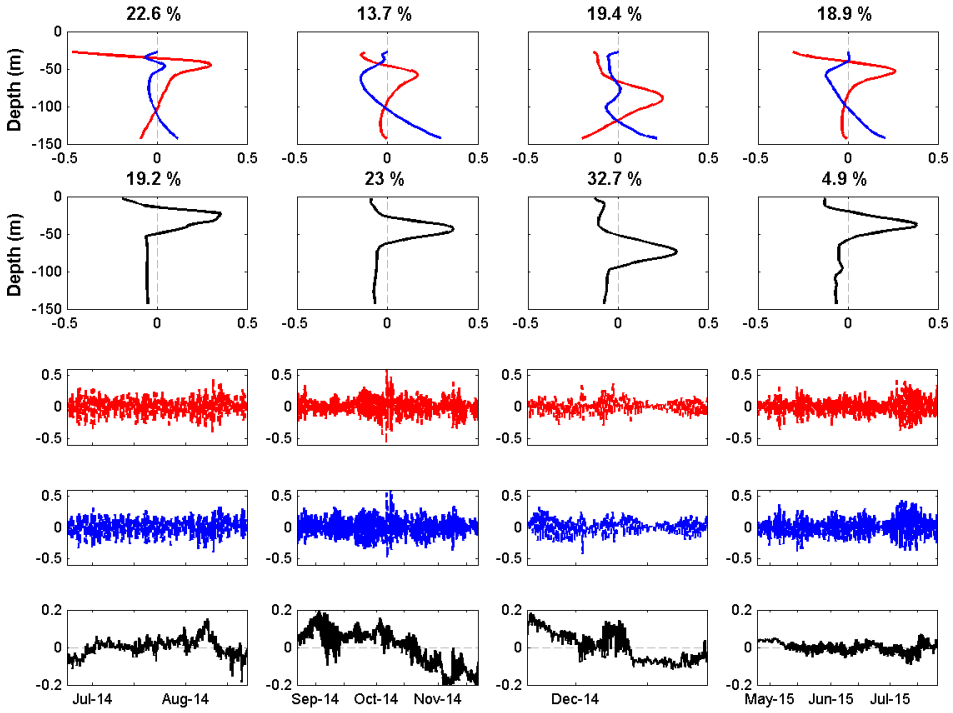

Figure 3.17: Spatial second mode of the zonal (red) and meridional (blue) components of the baroclinic velocities (top) and anomaly of salinity (black) (2^{nd} row). Principal component of the zonal (3^{rd} row), meridional (4^{th} row) velocity anomalies and salinity anomalies (bottom).

3.4 Discussion

3.4.1 Internal waves and Stokes transport

During the summer of 2014 and 2015 in the Central Celtic Sea internal waves were identified by the vertical displacements of the upper and lower boundaries of the pycnocline layer. Previous studies have shown that internal tides generated at the shelf break can propagate on-shelf (Sharples et al., 2007; Vlasenko et al., 2012) at least up to 170 km in the Celtic Sea (Inall et al., 2011) well beyond the Central Celtic Sea site. Nonetheless, internal tides can also be generated on the Celtic Sea (e.g. Palmer et al., 2013) due to sharp changes in topography (e.g. Jones Bank) and propagate off the shelf. Overall, spectral density analysis showed that variability of the vertical movement of the boundaries was greater within the semidiurnal frequency band in summer 2014 and 2015 indicating internal waves oscillated in a semidiurnal period fitting with previous observations in the Celtic Sea (Pingree and New, 1995; Inall et al., 2013; Hopkins et al., 2014). In the upper boundary of the pycnocline only, intensified vertical displacement was found between the 25th of April and mid-June 2015 suggesting a combination of processes occurred simultaneously. Potentially, this could arise from competition between atmospheric heat input and strong wind stress events, stratifying the water column and redistributing the heat vertically between the surface and pycnocline layers. The enhanced variability is linked to the meteorological forcing. This competition caused maxima fluctuations of the upper boundary within the diurnal frequency band. However, when compared to transport in the surface and pycnocline layers (Fig. 3.10), there was no evidence of transport fluctuations bounded by the diurnal band. In fact, transport peaked on the inertial and semidiurnal frequency bands throughout the record for the surface, pycnocline and bottom lay-

ers. Therefore, transport in each layer resulted from a combination of internal tides and wind-stress forcing.

Associated with the internal waves, Stokes transport was calculated for each layer. In the surface and bottom layers variability introduced by wind stress was reflected in energy peaking in the inertial frequency band and being occasionally greater than energy bounded by the semidiurnal band as seen in Inall et al. (2013). However, in the pycnocline maxima variability of transport and the vertical displacements of the interfaces were bounded by the semidiurnal frequency band indicating most of its variability resulted from internal tides and not from the wind stress. Therefore, Stokes transport is expected to govern dynamics within the pycnocline whilst Eulerian transport due to wind stress can be considered minimum. Maximum Stokes transport associated to the passing of internal waves occurred in the pycnocline and was off-shelf and on-shelf between mid-June and the 5th of October and between the 6th of October and late-December 2014, respectively, with opposite flows in the surface and bottom layers. In these periods, within the pycnocline layer averaged Stokes transport (0.10 - 0.08 m^2 s^{-1}) was greater than the averaged Eulerian transport (0.067 - 0.049 m^2 s^{-1}) and in the opposite direction (Fig. 3.11). Even though, averaged over periods of 50 hours, the magnitude of the Eulerian transport in the pycnocline layer was more intense its variability was disorganised compared to Stokes transport variability which was clearly aligned perpendicularly to the shelf break (Fig. 3.11). Therefore, transport within the pycnocline was governed by Stokes transport generated by internal tides.

Through internal tides exchange between the Celtic Sea and North Atlantic Ocean is enabled due to the semi diurnal time-scale and therefore

the Taylor-Proudman theorem beaks down (Huthnance, 1995; Inall et al., 2001). Hydrographic sections carried out in summer 2014 and 2015 (Fig. 3.18), which were orientated in the same direction of the ellipses of variability, illustrate exchange within the pycnocline layer between the Celtic Sea and the North Atlantic Ocean. The 35.7 g kg^{-1} isohaline separates the relatively high salinity waters from the Atlantic and the fresher waters of the Celtic Sea (Ruiz-Castillo et al., 2018; Chapter 2). In August 2014 (Fig. 3.18a), relatively high salinity waters intruded at least a 100 km into the Celtic Sea. This fits with previous studies in the Celtic Sea (Hopkins et al., 2012) and other shelf seas (e.g. Lentz, 2003) where high salinity waters within the pycnocline are advected on-shelf. In contrast in July and August 2015 fresher waters were exported off-shelf (Fig. 3.18b-c).

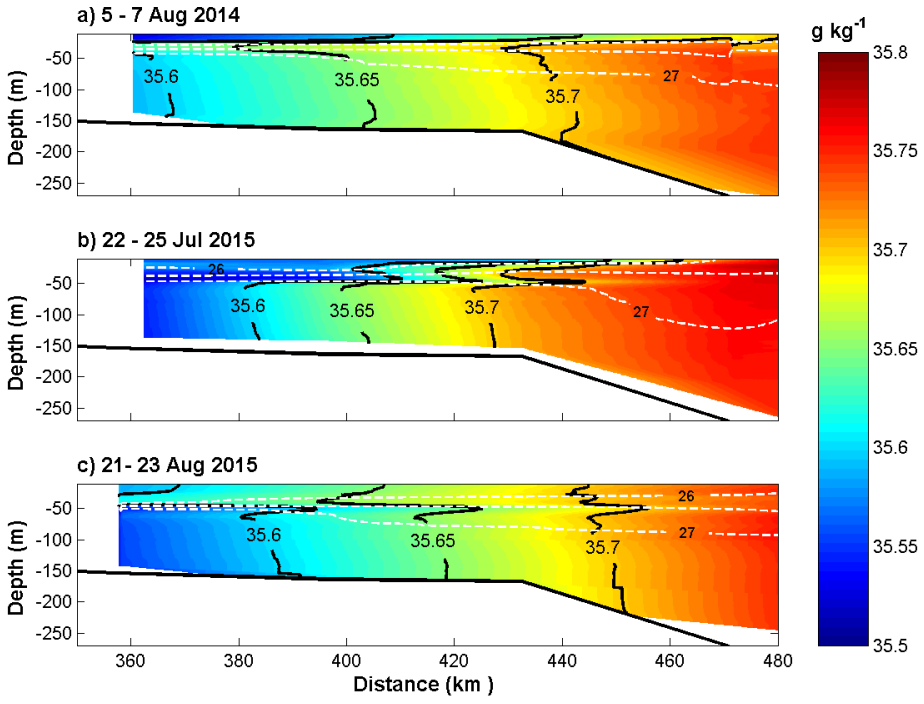

Figure 3.18: Absolute Salinity sections. Each section was carried out between a) 5-7 of August 2014, b) 22-25 of July 2015 and c) 21-23 August 2015. Distance is referenced to the coast and CCS is located at 360 km. White dashed lines indicate the 26, 26.5 and 27 kg m^{-3} contours representing the location of the pycnocline.

3.4.2 Eulerian and Ekman transport

In the Celtic Sea westerly winds were predominant in the summer of 2014 and 2015 generating favourable conditions for an averaged offshore Ekman transport and a compensatory onshore flow in the surface and bottom layers, respectively. At Central Celtic Sea evidence of Ekman transport occurring was identified. For instance, transport variability in surface layer peaked in the inertial frequency band, indicative of wind stress forcing. In addition, averaged Ekman and Eulerian transport in the surface layer was off-shelf, south-south eastward, with both of their ellipses of variability aligned in the same direction. Eulerian transport in the surface layer was less than wind-driven Ekman transport given that Eulerian transport was not quantified in the upper 20 metres of the water column. Finally, high correlation coefficients, particularly from mid-August onward (R^2 of 0.71 - 0.82), indicated that wind stress, in the form of wind-driven Ekman transport, was the main forcing agent in the surface layer. However, low correlation between the 23rd of June and the 18th of August 2014 and events between mid-June and July 2015 revealed dynamics at Central Celtic Sea were generated by another mechanism. In the periods when transport was not controlled by Ekman dynamics, stratification was a maximum, i.e. the surface layer was above 20 m depth and above the shallowest velocity time series. The wind headed towards the east (Fig. 3.19a) and the velocity anomalies were stronger along the zonal component describing a more intense eastward flow between 40 and 100 m depth (Fig. 3.19b). Time series of magnitude (Fig. 3.19c) of the low frequency flow (¡1 cpd) and averaged raw velocities with its ellipses of variability (Fig. 3.19d) indicate the flow was more intense between 40 and 100 m depth and was aligned zonally from 40 to 140 m depth. The enhanced eastward current probably resulted from the density cross-shelf gradient within the bottom mixed

layer. The background horizontal density gradient set in the previous winter combined with bottom onshore transport results in a cross-shelf density gradient with denser waters north of CCS as will be described in the following chapter. Under this scenario an eastward geostrophic flow would be generated. After mid-August deepening of the upper boundary of the pycnocline allowed measurement of transport in the surface layer, i.e. weakening of stratification, and variability in surface Eulerian transport responded to intensification and relaxation of the wind-driven Ekman transport.

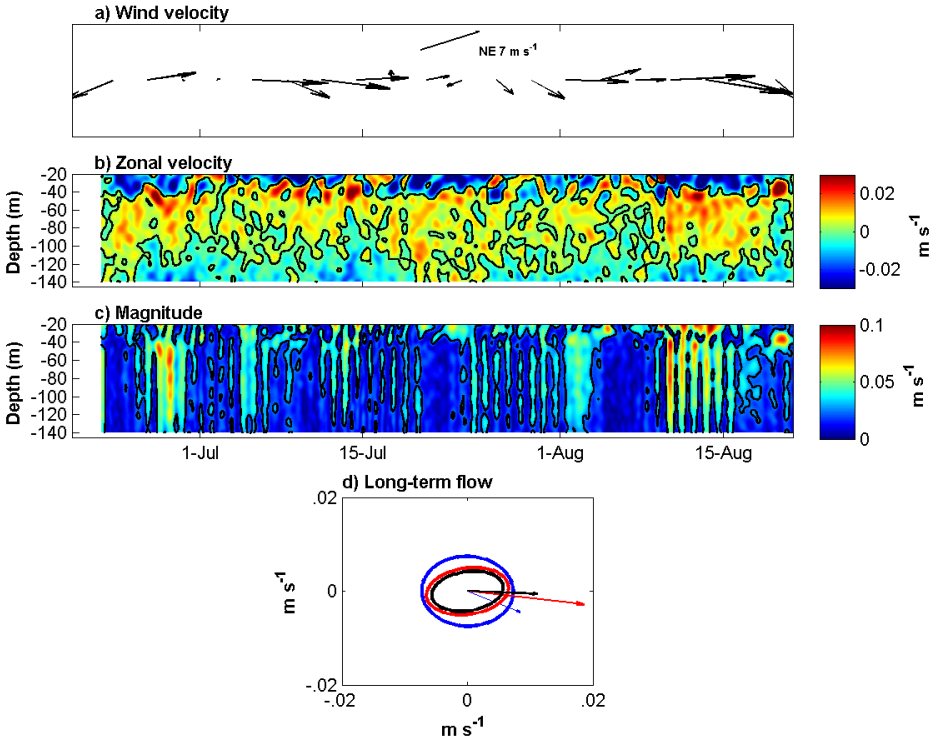

Figure 3.19: Time series at the Central Celtic Sea of a) wind velocity, b) zonal velocity anomalies, c) time series of the magnitude of the filtered and raw (anomalies plus the depth averaged flow) velocity and d) averaged velocity and ellipses of variability between 20 and 40 m depth (blue), 40 and 100 m depth (red), 100 and 140 m depth (black) in the period 22nd of June - 18th of August. High frequencies above 1 cpd were removed from b), c) and d). In b) positive values indicate eastward.

Variability in bottom transport peaking in the inertial frequency band indicated wind stress forcing occurred in the bottom layer in the form of a compensatory flow. This compensatory flow ($\mathbf{U_{wb}}$) was assumed to be

in the form:

$$\mathbf{U_{wb}} = -\mathbf{U_w} \tag{3.40}$$

Ekman and bottom Eulerian transport time series were negatively correlated indicating bottom transport responded to Ekman transport variability in the opposite direction fitting with a compensatory onshore flow as described in equation (3.40). Furthermore, the ellipse of variability in the bottom layer was aligned in the south-south westward direction coinciding with most of the ellipse of variability of the Ekman transport (Fig. 3.14). For the surface and bottom transports, stronger correlation was found along the meridional components due to the predominant westerly winds that generate transport mainly in the north-south direction.

In the Celtic Sea relatively high salinity waters intruding coastward in the bottom layer occurred following the onset of stratification in the summer of 2014 and 2015 (Ruiz-Castillo et al., 2018; Chapter 2). The maximum northward intrusion was between November and December 2014 consistently with the greatest (negative) correlation between the Ekman and Eulerian bottom transports (R^2=0.71), which suggests that this bottom onshore flow can be explained mainly as the result of a compensatory flow of off-shelf wind-driven Ekman transport. Ekman and bottom flow between October and late-December 2015 was 0.5 m^2 s^{-1} and taking the bottom layer thickness to be 70 m on average leads to a mean-layer velocity of 0.6 km day^{-1}, which is well aligned to the velocities described in Ruiz-Castillo et al. (2018) based on the salinity displacement across the Celtic Sea.

Previous studies indicate westerly winds prevail in the Celtic Sea (Pingree 1980; Pingree et al., 1999) creating favourable conditions for wind-driven upwelling events throughout the year, i.e. wind-driven Ekman

dynamics. Nonetheless, no clear evidence has been observed such as cold water creeping up on-shelf or a band of cold water along the coast (e.g. Ruiz-Castillo et al., 2016). Due to the Ekman transport relatively high salinity waters were advected to the inner shelf (depth <100 metres). Stratification prevailed throughout summer in the relatively deep inner shelf hindering mixing so that high salinity waters from the bottom were not seen in the surface. In addition, waters would be advected across the inner shelf by a cyclonic jet (Horsbourgh et al., 1998; Brown et al., 2003, Young et al., 2004). Far from the inner shelf, dynamics may be governed by the poleward along-slope current at the shelf edge (Pingree et al., 1999; Huthnance et al., 2001; Holt et al., 2009). Nonetheless, events where the along-slope generated upwelling in the bottom layer due to reversal of the along-slope current had been documented (Porter et al., 2016). However, on average, this current is thought to be in the poleward direction and therefore export shelf waters to the deep ocean through an Ekman drain mechanism at the bottom boundary layer (Souza et al., 2001; Holt et al., 2009; Simpson and McCandliss, 2013). Thus the wind-driven Ekman dynamics would oppose Ekman drain dynamics and the along-slope current may inhibit wind-driven upwelling (e.g. Roughan and Middleton, 2002; Marchesiello and Estrade, 2010; Rossi et al., 2013). Therefore, despite favourable conditions, wind-driven Ekman dynamics might be clearly identifiable in the Central Celtic Sea, but be masked by other processes towards the shelf edge, such as the poleward along-slope current. Further evidence of these two processes occurring simultaneously and the implications for oceanic waters supply onto the Celtic Sea are described in the following chapter.

3.4.3 Empirical Orthogonal Functions

At the Central Celtic Sea site an independent statistical assessment of the variability of the velocity and salinity anomalies was performed through an empirical orthogonal function analysis. The first and second modes explain between 83 and 95% of the total variability throughout the record with the variability patterns consistent with the dynamics observed in the Central Celtic Sea. For instance, the first and second spatial modes of the velocity and salinity anomalies describe a three-layer system and deepening of each layer is consistent with seasonal deepening observed in density time series. In addition, spatial mode 1 of the velocity anomalies indicates transport across the shelf in the surface layer was opposite to the bottom layer. Related to this transport as seen in mode 1 of the salinity anomalies when relatively high salinity waters were found in the surface layer, fresher waters occur in the bottom layer, and vice versa. The evolution of the first principal component was consistent with the fluctuations of the averaged salinity within each layer and fitted with the spatial mode. Finally, the second mode of variability indicated waters were transported across the shelf at mid-depths, advecting either fresher waters offshore or relatively high salinity waters onshore. Thus, both mechanisms governing transport in the Celtic Sea coincide with the spatial variability patterns described by the Empirical orthogonal function analysis.

3.5 Summary

Hydrography and transport at the Central Celtic Sea site were assessed using a three layer system approach. The thickness of the layers changed throughout the stratified period. In each layer transport was separated into Stokes and Eulerian components.

Stokes transport was a maximum in the pycnocline, being greater on average than the Eulerian transport. Variability of the Stokes transport was aligned perpendicular to the shelf edge.

Eulerian transport in surface and bottom layers was mainly generated by wind-driven Ekman dynamics. Westerly wind-stress generate offshore surface transport and a compensatory bottom onshore flow.

Bottom onshore advection in the Celtic Sea and exchange between the shelf and the North Atlantic in the pycnocline layer can be explained by wind-driven Ekman transport and Stokes transport generated by internal tides.

Chapter 4

Cross-shelf exchange between a temperate shelf sea and the North Atlantic Ocean in autumn and winter

Abstract

In the interior of the Celtic Sea wind stress forcing from predominantly westerly winds governs cross-shelf flow leading to the potential for off-shelf surface transport and onshore advection in the bottom layer. This process could potentially extend to the shelf edge enabling exchange between shelf waters and the deep-ocean region. However at the shelf edge a poleward along-slope current occurs and generates off-shelf transport in the bottom layer through an Ekman drain mechanism opposing wind-driven exchange. In this chapter exchange between the Celtic Sea and the North Atlantic Ocean is elucidated. The mechanism on how oceanic properties, particularly nutrients, from the North Atlantic are transported onto the Celtic Sea is explained. Time series recorded at Celtic Deep and Central Celtic Sea from the 1st of November 2014 to the 15th of March, of surface wind-stress, hydrography and horizontal velocities in the water column were combined with hydrographic data obtained from glider and CTD casts to assess transport and exchange between the Celtic Sea and the North Atlantic Ocean. Nutrient data

was utilised to quantify advection of nutrients from oceanic origin. Results indicate that North Atlantic waters are transported 80 km onto the Celtic Sea in the bottom layer due to wind-driven transport in a 7-8 month period. In the bottom layer of the Celtic Sea about 50% of the nutrients observed were advected from the North Atlantic Ocean. In December, evidence of Ekman drain and wind-driven transport were found to occur simultaneously in the cross-shelf direction. Interaction of both processes resulted in convergence at the shelf edge and prevented cross-slope exchange. Surface waters from the shelf and ocean were forced to recirculate onshore and off-shelf in the bottom layer, respectively. Velocities in the bottom layer due to the Ekman drain process were estimated around 0.06 - 0.1 m s^{-1} fitting with previous observations. Associated with the convergence of surface waters, a geostrophic eastward flow is expected to occur at the shelf edge of the Celtic Sea. Due to recirculation of fresher waters the stratified period was extended beyond that expected despite heat loss and surface cooling. There was no evidence of cross-shelf exchange throughout winter.

4.1 Introduction

In the interior of the Celtic Sea relatively high salinity and nutrient-rich waters originating from the North Atlantic Ocean are transported across the shelf (Ruiz-Castillo et al., 2018). However, exchange of salinity and nutrients, as well as other water properties, between shelf seas and oceans is limited by geostrophic currents flowing along isobaths (Allen et al., 2009), i.e. the along-slope current. When geostrophy fails cross-slope transport at the shelf edge of the Celtic Sea is enabled and is thought to be governed by wind-driven flow (0.85 m^2 s^{-1}), Ekman drain (0.5 m^2 s^{-1}) and internal waves (1 m^2 s^{-1}) (Huthnance et al., 2009). This Chapter elucidates how relatively high salinity and nutrient-rich waters from the

North Atlantic are supplied onto the Celtic Sea.

Observations at the shelf break of the North-western European shelf have identified a poleward along-slope current centred on the 500 m depth contour from September-October to March-April (Pingree and Le Cann, 1989; Souza et al., 2001; van Aken, 2002; Simpson and McCandliss, 2013) with mean velocities of 0.05 m s^{-1} (Pingree and Le Cann 1989; van Aken, 2002). In contrast, in summer the along slope current weakens/ or appears to be absent (van Aken 2002) and even reverses flowing equatorward with velocities of 0.015 m s^{-1} (Pingree and Le Cann, 1989; Porter et al., 2016). Associated with the along-slope poleward current, off-shelf export in the bottom layer has been observed through an Ekman drain mechanism (Souza et al., 2001; Holt et al., 2009; Simpson and McCandliss, 2013).

The Ekman drain mechanism can be explained by considering a poleward geostrophic flow in the water column and the frictional forces in the bottom boundary layer. Away from the seabed friction is negligible. However within the bottom boundary layer the flow gradually decreases up to zero at the seafloor. The total velocities (u,v) in the water column can be expressed as:

$$u = u_g + u_{Ekb} \tag{4.1}$$

$$v = v_g + v_{Ekb} \tag{4.2}$$

where u_g and v_g represent the geostrophic flow, u_{Ekb} and v_{Ekb} are the Ekman velocities which are only important within the bottom boundary layer (D). Therefore the resulting blance is:

$$-fv = -\frac{1}{\rho_0}\frac{\partial P}{\partial x} + Az\frac{\partial^2 u}{\partial z^2} \tag{4.3}$$

$$fu = -\frac{1}{\rho_0}\frac{\partial P}{\partial y} + Az\frac{\partial^2 v}{\partial z^2} \tag{4.4}$$

where f is the Coriolis parameter and A_z is the vertical viscosity coefficient. The first term on the right hand side in eq. (4.3) and (4.4) is the pressure gradient force governing the flow far from the seabed. The frictional forces are represented by the second term and are only important within the bottom boundary layer. If we orientate the along-slope current along the x-axis, as it would be aligned at the shelf edge of the Celtic Sea, we get:

$$-fv = Az\frac{\partial^2 u}{\partial z^2} \tag{4.5}$$

$$fu - fu_g = Az\frac{\partial^2 v}{\partial z^2} \tag{4.6}$$

where $fu_g = -\frac{1}{\rho_0}\frac{\partial P}{\partial y}$. At the seabed zonal ($u$) and meridional ($v$) velocities are zero whilst above the Ekman depth $u = u_g$ and $v = 0$. With the previous boundary conditions the solutions to eq. 4.5 and 4.6 are (Cushman-Roisin and Beckers, 2009; Simpson and Sharples, 2012):

$$u = u_g\left(1 - e^{\left(\frac{-\pi z}{D}\right)}\cos\left(\frac{\pi z}{D}\right)\right) \tag{4.7}$$

$$v = u_g e^{-\left(\frac{\pi z}{D}\right)}\sin\left(\frac{\pi z}{D}\right) \tag{4.8}$$

Eqs. (4.7) and (4.8) describe a flow within the bottom boundary layer deflected to the left of the geostrophic current (Fig. 4.1).

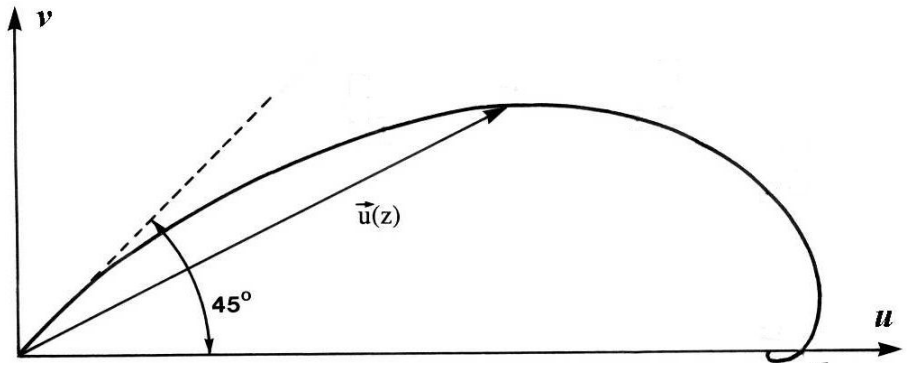

Figure 4.1: Schematic of the flow within the bottom boundary layer. Geostrophic flow above the Ekman layer is in the eastward direction. The flow within the bottom boundary layer deflects to the left. Adapted from Cushman-Roisin and Beckers (2009).

Cross-shelf transport (V) within the Ekman depth can be estimated in the form (Cushman-Roisin and Beckers, 2009; Simpson and Sharples, 2012):

$$V = \int_H^D v dz = \frac{u_g D}{2} \tag{4.9}$$

Transport within the bottom boundary layer is proportional to the intensity of the geostrophic current and the thickness of the Ekman depth. For the northwest European shelf deflection is off-shelf due to the poleward along-slope current. The transport in the bottom boundary layer must be replenished leading to a compensatory flow above the bottom Ekman depth (e.g. Souza et al., 2001).

In the interior of the Celtic Sea bottom onshore advection results mainly from wind-driven transport (Chapter 3). The dynamics of how wind stress generates transport in the water column are described in detail in the previous chapter. At the shelf edge surface currents have been observed to be deflected to the right of the wind-stress (Pingree and Le Cann, 1990) and westerly winds prevail in the Celtic Sea (Pingree, 1980; Pingree et al., 1999) and are favourable for cross-slope exchange. In principle, nutrient-rich, cold and relatively high salinity waters would be advected on-shelf in the bottom layer. However, the Ekman drain mech-

anism generated by the poleward along-slope current exports shelf waters off-shelf in the bottom layer (Souza et al., 2001; Holt et al., 2009; Simpson and McCandliss, 2013) and would oppose wind-driven exchange. In this Chapter the mechanisms driving cross-shelf exchange and how waters from the North Atlantic Ocean are supplied onto the Celtic Sea are described. In addition, the interaction between wind-driven flow and Ekman drain at the shelf edge and its effects on cross-slope exchange are analysed during autumn and winter.

4.2 Method

Time series recorded in the Celtic Sea (Fig. 4.2), from the 1st of November 2014 to the 15th of March 2015, of surface wind-stress, hydrography and horizontal velocities in the water column were combined with hydrographic data obtained from glider and CTD casts to assess transport and exchange between the Celtic Sea and the North Atlantic Ocean.

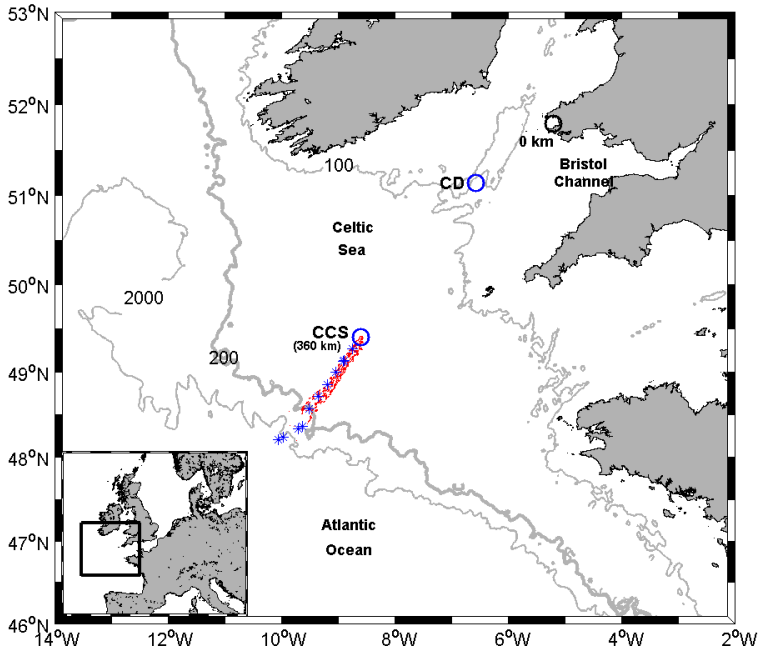

Figure 4.2: Map of the Celtic Sea. Blue circles indicate the locations of the Central Celtic Sea and Celtic Deep moorings and the black circle indicates the reference point. Red points show the track of the glider. Blue points indicate where CTD casts were carried out in November 2014.

4.2.1 Time series of hydrographic data

At the Celtic Deep (Fig. 4.2) surface time series of salinity and temperature with a temporal resolution of 30 min and 1 hour, respectively, (Hull et al., 2017), were used to assess the influence of fresher waters and changes in water column temperature from the 1st of January to the 15th of April 2015. There was a gap between the 31st of January and 10th of March in the salinity time series. At the Central Celtic Sea site near full depth time series of temperature and salinity were recorded from March 2014 to August 2015. Data utilised in this chapter covers the period from the 1st of November 2014 to the 15th of March 2015. Each time series had a temporal resolution of 5 minutes and was vertically interpolated every 2.5 m. A detailed description on how data were

processed is provided in the previous chapter and Wihsgott et al. (2016). This Chapter describes long-term fluctuations, slower than the tidal and inertial motions. Therefore high frequency fluctuations from time series at the Celtic Deep and Central Celtic Sea were removed using a low-pass Lanczos filter (Thompson and Emery, 2014) with a cut off frequency of 24^{-1} h^{-1} (Fig. 4.3). Conservative temperature, absolute salinity and potential density were calculated (McDougall and Barker, 2011). Relatively high salinity and fresher waters were considered to represent waters from the shelf edge and interior of the Celtic Sea, respectively. In winter intensified wind stress and heat loss ensure the water column is fully mixed (Wihsgott et al., 2019) (Fig. 4.3b-d). Therefore, for the period covering winter the analysis was carried out on the depth-averaged time series at Central Celtic Sea whilst at Celtic Deep surface measurements of salinity and temperature were representative of the whole water column.

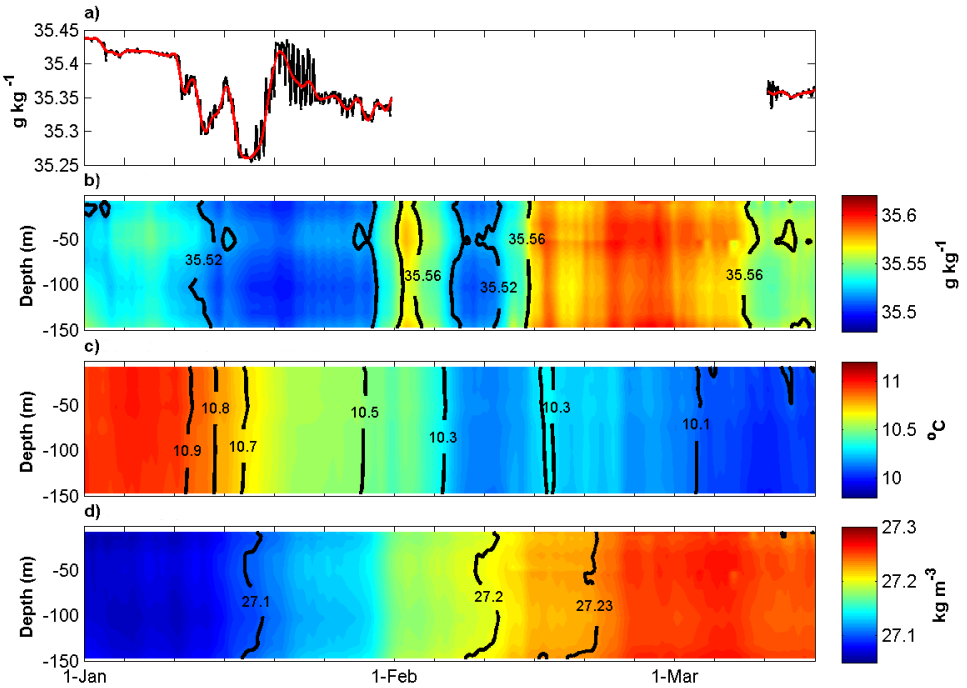

Figure 4.3: a) Filtered (red) and raw (black) time series of surface absolute salinity at Celtic Deep and Hovmöller of diagram of filtered b) absolute salinity c) conservative temperature and d) density at Central Celtic Sea.

4.2.2 Time series of current data

Current measurements at the Central Celtic Sea and the Celtic Deep were used to evaluate cross-shelf flow. At the Central Celtic Sea time series of horizontal velocities from near the bottom (150 m) up to 20 m depth were recorded using an ADCP from March 2014 to August 2015. Each time series was interpolated on a regular grid with a temporal and spatial resolution of 5 minutes and 2.5 m respectively (Wihsgott et al., 2018). At the Celtic Deep a time series was recorded every hour in the bottom 40 m with a vertical resolution of 0.5 m (Thompson et al., 2017; Thompson et al., 2018) using an ADCP from mid-November 2014 to the 1st of April 2015 with a gap in the period 21st of February-13th of March. For the Celtic Deep site only data between the 1st of January and 13th of March, when the water column was mixed was analysed. For the Central Celtic Sea only data in the period 1st of November -15th of March were analysed in this Chapter. As with the hydrographic time series a low-pass Lanczos filter was used with a cut off frequency of 24^{-1} h^{-1} (Thompson and Emery, 2014).

To assess the net cross-shelf flow depth-mean transport was estimated at the Celtic Deep and Central Celtic Sea. The depth-averaged velocity ($\bar{\mathbf{u}}$) was calculated from the filtered velocities ($\mathbf{u}$) in the form:

$$\bar{\mathbf{u}} = \frac{1}{H}\int_{H}^{0} \mathbf{u} dz \tag{4.10}$$

Subsequently, full water column transport ($\mathbf{U}$) was quantified at each time step as follows:

$$\mathbf{U} = \bar{\mathbf{u}} H \tag{4.11}$$

where depth of the water column (H) was set at 100 and 145 m for Celtic Deep and Central Celtic Sea, respectively.

To assess the vertical variability of the flow in the water column at Central Celtic Sea the horizontal velocity anomalies ($\mathbf{u_c}$) were calculated. As in the previous chapters, the depth-averaged flow ($\bar{\mathbf{u}}$) was removed at each time step from the filtered velocities ($\mathbf{u}$) as follows (Fig. 4.4) (e.g. Chapter 3):

$$\mathbf{u_c} = \mathbf{u} - \bar{\mathbf{u}} \tag{4.12}$$

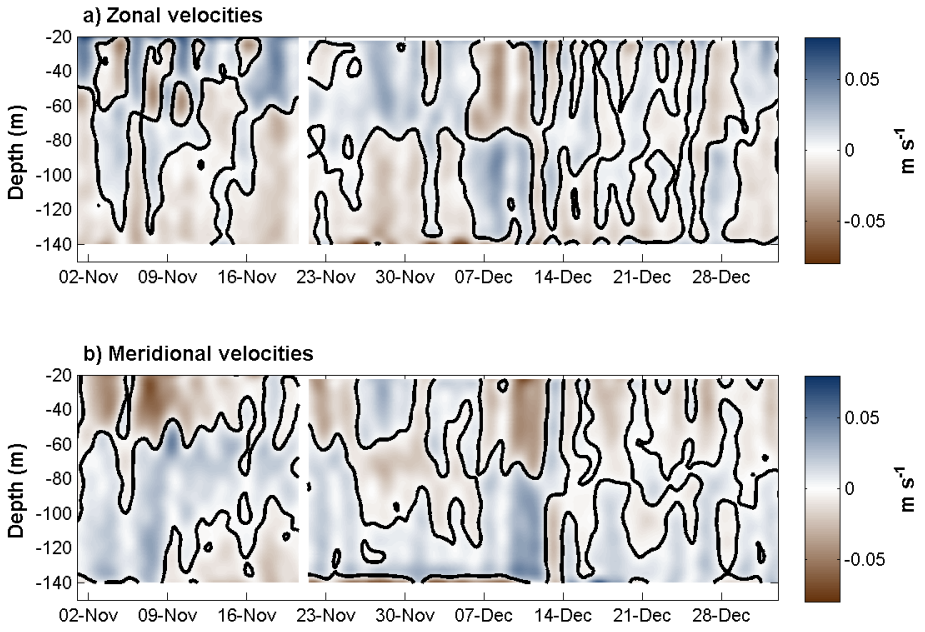

Figure 4.4: a) Zonal and b) meridional components of the velocity anomalies at the Central Celtic Sea. Black contours indicate zero velocity separating positive (northward and eastward) from negative (southward and westward) velocities.

4.2.3 Wind data

At the Central Celtic Sea wind data recorded every hour by a meteorological buoy were used to assess the influence of the wind stress on the water column in the form of wind-driven Ekman transport. As in

Chapter 3 Ekman transport was calculated in the form:

$$V_w = -\frac{\tau_x}{f\rho_s} \tag{4.13}$$

$$U_w = \frac{\tau_y}{f\rho_s} \tag{4.14}$$

where the meridional (τ_y) and zonal (τ_x) components of the wind stress were estimated as:

$$\tau_x = \rho_a C_d |\mathbf{u_w}| u_w \tag{4.15}$$

$$\tau_y = \rho_a C_d |\mathbf{u_w}| v_w \tag{4.16}$$

with u_w and v_w representing the zonal and meridional components of the wind. Surface density (ρ_s) was averaged between 10 and 15 m depth and the air density (ρ_a) was set constant at 1.25 kg m^{-3}. The zonal and meridional components of the wind-stress were averaged every 24 hours to account for low frequency motions. The drag coefficients varied with the winds intensity following Smith and Banke (1975) such that:

$$C_d = 1 \times 10^{-3} \left(0.63 + 0.066 \left(u_w, v_w\right)\right) \tag{4.17}$$

Transport in the surface layer

Before the water column was fully mixed at Central Celtic Sea (e.g. before the 1st of January 2015) the thickness of the surface layer was determined using the same criteria as in Chapter 3 (Table 3.1). Examples of the surface and bottom layers in salinity and temperature profiles are shown in Figure 4.5. Transport in the surface layer was estimated by vertically integrating the horizontal velocity anomalies at each time step from the upper boundary of the pycnocline to the shallowest velocity time series. The Influence of the wind-driven Ekman transport on the water column was evaluated through Pearson correlation coefficients.

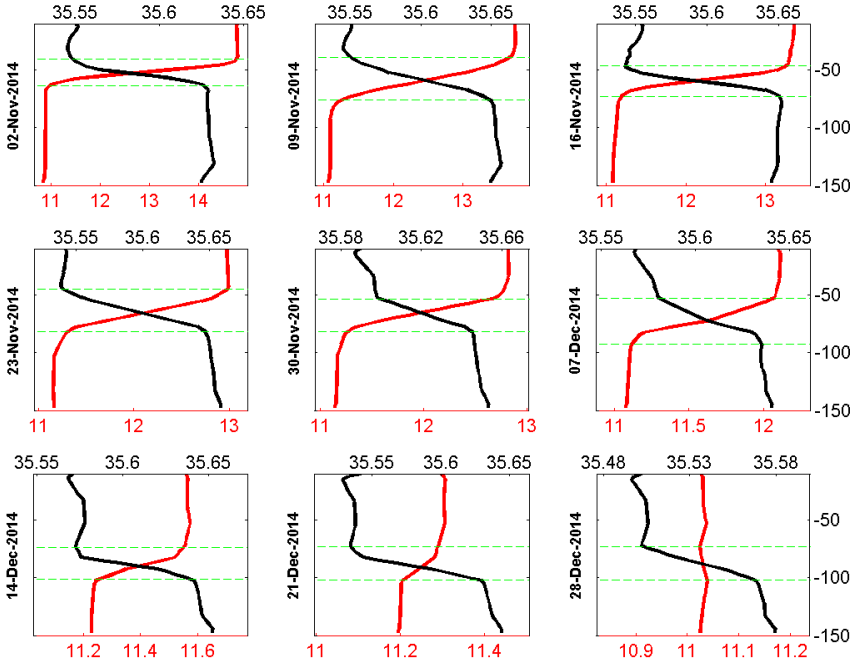

Figure 4.5: Examples of temperature and salinity profiles used to estimate depth of the surface layer at Central Celtic Sea. Salinity and temperature axis are at the top and bottom of each panel. Green lines indicate the upper and lower interface of the pycnocline layers.

4.2.4 Hydrographic transects

CTD casts

Hydrographic data (CTD) were collected in November 2014 on board the RRS Discovery (blue dots in Fig. 4.2). Data quality control is detailed in Chapter 2. Conservative temperature, absolute salinity and potential density were calculated (McDougall and Barker, 2011) and cross-shelf transects were constructed. Due to the specific dynamics described in wind time series, only data collected between the 13th and 16th of November from the Central Celtic Sea site to the shelf edge were considered. The distance is referred to the eastern side of St. Georges Channel. As with the mooring data, absolute salinity is used to determine horizontal displacement from waters adjacent to the shelf edge and on the Celtic Sea.

Glider data

A glider was deployed in the Celtic Sea between the 18th of November 2014 and 22nd of March 2015 and measured sea water properties from the Central Celtic Sea site to the shelf edge. The effect of thermal inertia on the conductivity cell was corrected using NOCL glider thermal inertia toolbox developed by Dr Matthew Palmer. The average upward and downward velocity was assumed to be constant at 0.65 m s^{-1} and the relaxation time of thermal anomaly was estimated to be 25 s. Pressure, temperature and the corrected conductivity were filtered using a low-pass band Butterworth filter with a sample rate every 0.2 s^{-1} and utilised to estimate practical salinity (Fig. 4.6) using the UNESCO polynomial (1983). Two consecutive upward and downward salinity profiles are shown in Figure 4.6. Black and red profiles show practical salinity before and after the thermal inertia correction applied on conductivity, respectively. Data was bin averaged every metre. The TEOS-10 functions were used to derive absolute salinity, conservative temperature and potential density (McDougall and Barker, 2011).Glider salinity and temperature were calibrated with CTD casts from the cruise carried out in November 2014. Only data obtained in the periods 26th of November-16th of December and 17th of January- 28th of February were analysed due to glider malfunction. Cross-shelf transects were constructed to analyse hydrographic evolution from the Central Celtic Sea to the shelf edge.

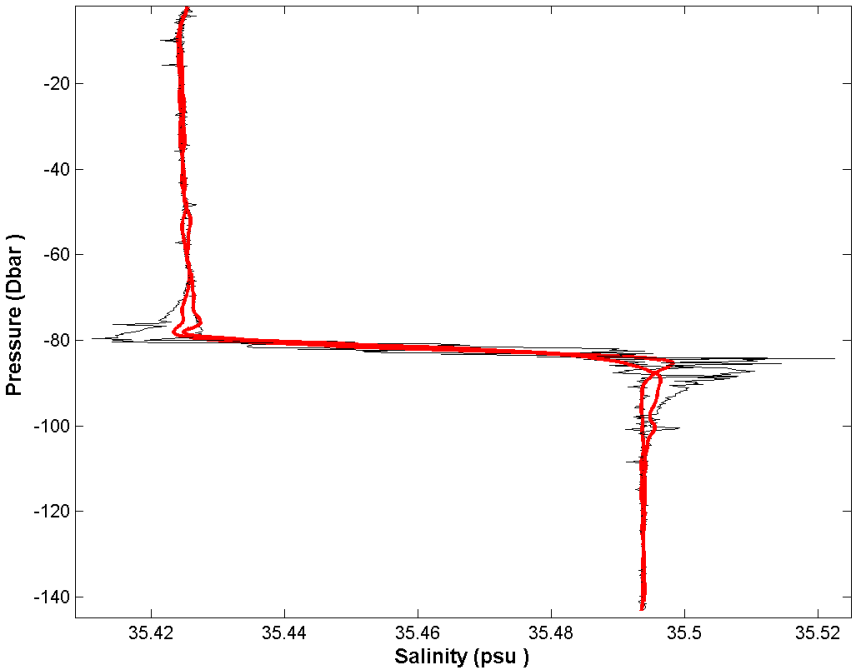

Figure 4.6: Raw salinity profiles (black lines) and salinity after the thermal inertia correction on conductivity (red lines).

Nutrients

To analyse advection of nutrients from the North Atlantic onto the Celtic Sea dissolved inorganic nutrients (NO_2 and NO_3) sampled between March and November 2014 were used. Further details on how nutrients were processed are described in detail in Ruiz-Castillo et al. (2018), Woodward (2016) and Poulton et al. (2018). This Chapter aims to understand exchange processes between the shelf and oceanic waters therefore only nutrients sampled between the Central Celtic Sea and the North Atlantic Ocean were utilised.

4.3 Results

4.3.1 Autumn

Wind stress forcing of transport and hydrography in the Central Celtic Sea

In the Celtic Sea between the 2nd of November and 30th of December 2014 two sustained westerly-wind events occurred in the periods 2-18 of November and 7-28 of December generating favourable conditions for surface off-shelf wind-driven Ekman transport (Fig. 4.7a). In contrast, easterly winds favourable for onshore Ekman flow in the surface layer occurred between the 25th and 30th of November. Northerly winds were observed in the period 1-7 of December. Throughout the record surface transport responded to wind-stress forcing (Fig. 4.7b and c). During the first westerly wind event, between the 2nd and 18th of November, in Central Celtic Sea surface and wind-driven transport were strongly correlated $R^2 = 0.84$ and 0.85 for the zonal and meridional components, respectively. In this period off-shelf transport occurred and was a maximum, above 2 $m^2\ s^{-1}$ on the 8th of November. Ekman transport gradually decreased to $\sim$0.1 $m^2\ s^{-1}$ on the 18th of November due to relaxation of the westerly wind stress and surface transport reversed and headed onshore with values below 0.2 $m^2\ s^{-1}$. Between the 25th and 30th of November onshore transport of 0.4 $m^2\ s^{-1}$ occurred in the surface layer and was consistent with easterly wind stress. Both time series were correlated with R^2 values of 0.85 and 0.58, for the meridional and zonal components, respectively. During the northerly wind-event surface and Ekman transport correlation was greater in the zonal (R^2 =0.66) component than in the meridional (R^2= 0.23). During the second event of westerly winds, between the 7th and 28th of December, surface and Ekman time series were strongly correlated, R^2= 0.84 and 0.68 for the

meridional and zonal components, respectively. Maximum off-shelf surface (2 m^2 s^{-1}) and Ekman (3.1 m^2 s^{-1}) transport occurred on the 10th of December and were the greatest off-shelf transport for the whole time series. Reversals of the surface flow were consistent to decreases in Ekman transport on the 13th and 21st of December with on-shelf transport of 0.6 m^2 s^{-1} and below 0.2 m^2 s^{-1}, respectively.

Variability in salinity time series was consistent with off and on-shelf transport in the surface layer (Fig. 4.7d). The freshest waters ($<$ 35.55 g kg^{-1}) occurred in the periods where westerly wind events generate off-shelf wind-driven flow (8th of November and from the 19th of December onwards). In contrast, throughout the record increases in surface salinity coincided with easterly wind events and/or relaxation of the off-shelf Ekman flow. In the bottom layer relatively high salinities (>35.6 g kg^{-1}), indicative of waters originating from the ocean, were observed from the 1 of November until the 26 of December. However, from the 7th until the 19th of December, during westerly wind events, fresher waters between 35.55 and 35.6 g kg^{-1} occurred in the surface layer and were subsequently found in the bottom layer in the period 24th - 31st of December. Between the 1st and 7th of December, salinity above 35.6 g kg^{-1} was located in the surface and bottom layers given that northerly winds (Fig. 4.7a) generated alongshelf Ekman transport.

In the period 1st of November - 28th of December seasonal heat loss to the atmosphere from the surface layer was observed at Central Celtic Sea. Maximum surface temperature above 14^{o}C decreased to values below 11^{o}C (Fig. 4.7e). In contrast, in the bottom layer minimum values below 11^{o}C were observed on the 2nd of November and between the 27th and 30th of December. From the 28th to the 30th of December colder

waters with temperature below 11^{o}C in the surface layer overlaid warmer waters (>11^{o}C) in the bottom.

The water column was stratified between the 1st of November and the 31st of December with relatively low-density waters in the surface layer (Fig. 4.7f). Increases in density in the surface layer were consistent to temperature decreases up to the 28th of December. Between the 28th and 30th of December despite colder waters overlaying warmer waters a stable water column was maintained by the vertical distribution of salinity, with relatively high salinity waters occupying the bottom layer.

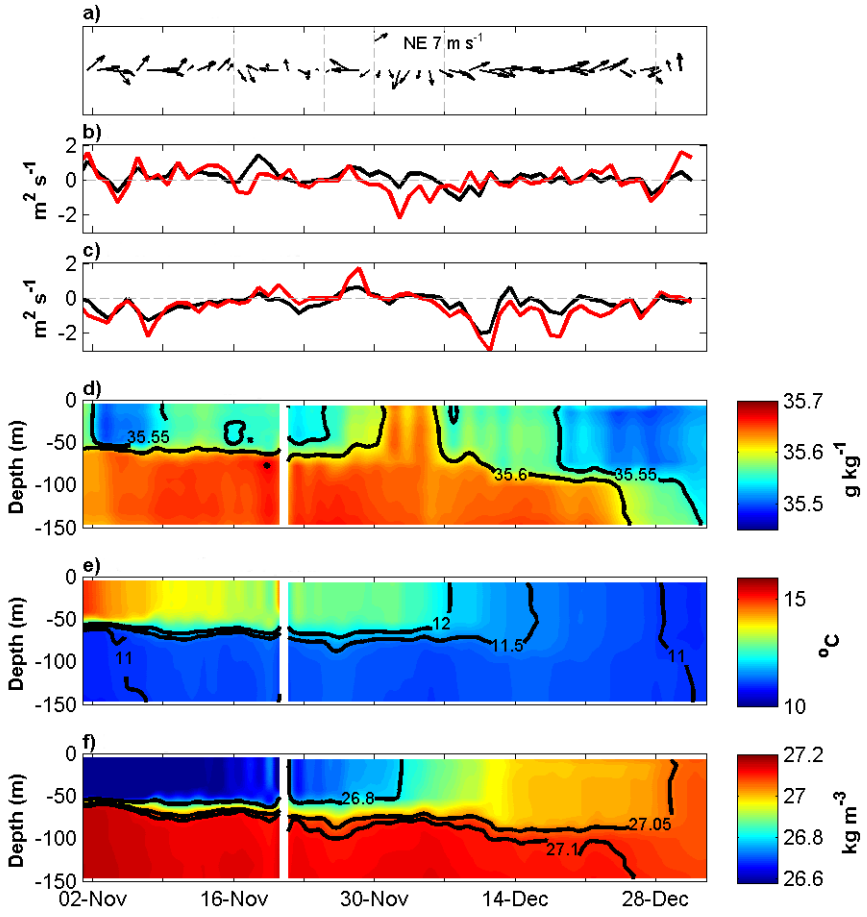

Figure 4.7: Time series of a) winds velocity, b) zonal and c) meridional components of surface (black) and Ekman (red) transport, d) absolute salinity, e) conservative temperature and f) density at Central Celtic Sea. In a) the scale is in the northeast direction.

Shelf-Ocean interaction

Salinity sections at the shelf edge in the period 13th-16th of November were consistent with wind-driven transport caused by westerly wind stress (Fig.4.8a). Above 70 m depth relatively low salinity waters (below 35.75 g kg^{-1}) seemed to be transported in the seaward direction. Waters with salinity greater than 35.7 g kg^{-1} were advected on-shelf below 70 m depth intruding up to a 400 km distance from the coast. At the shelf edge, salinity above 35.75 g kg^{-1} was observed in the water column between 460 and 480 km. The breaking of an internal wave over the shelf break could have, vertically distributed higher salinity from below the pycnocline and increased salinity in the surface layer (New, 1988; New and Pingree, 1990; Sharples et al., 2007). Between the 20th and 26th of November in the upper 80 m relatively low salinity waters below 35.64 g kg^{-1} extended from Central Celtic Sea ($\sim$360 km) to near 400 km off the coast and shear in the 35.7 g kg^{-1} salinity contour remained at 410 km (Fig. 4.8b). Below 80 m depth relatively high salinity waters above 35.75 g kg^{-1}, characteristic of the North Atlantic Ocean, were found at the shelf break between 450 km and 500 km.

In the following periods oceanward intrusion and retreat of fresher waters can be attributed to wind-stress forcing (Fig. 4.8c, d and e). For instance, between the 26th of November and the 3rd of December (Fig. 4.8c) retreat of fresher waters ($<$35.64 g kg^{-1}) occurred and was consistent with easterly winds in the period 25th-30th of November. Between the 4th and 11th of December (Fig. 4.8d) the fresher waters were located at 360 km and were advected up to 390 km from the coast in the period 11th-16th of December (Fig. 4.8e) fitting with surface off-shelf Ekman transport from the 7th of December onwards (Fig.4.7a). Whilst the low salinity surface water responded to wind-stress forcing, evidence of another mechanism

governing the dynamics at the shelf edge and the adjacent ocean region was found. The 35.72 g kg^{-1} contours were distributed vertically from the bottom up to the surface at 420 km in the period 20th - 26th November (Fig. 4.8b). Afterwards shear of this isohaline around 420 km (Fig. 4.8c, d and e), with relatively high salinity waters overlying fresher ones, is indicative of relatively low salinity waters from the Celtic Sea being exported off-shelf in the bottom layer below 90 m depth. Interaction of the wind-driven dynamics and off-shelf export in the bottom layer can be followed via the 35.7 g kg^{-1} contour. Between the 20th of November and 3rd of December (Fig. 4.8c and d) shear of the 35.7 g kg^{-1} isohaline resulted in relatively high salinity waters in the bottom at 410 km. In the following period (Fig. 4.8d) the shear of the 35.7 g kg^{-1} contour fitted with off-shelf export dynamics up to 380 km from the coast when wind-driven off-shelf surface flow was a minimum. Afterwards, between the 11th and 16th of December (Fig. 4.8e) displacement of the 35.7 g kg^{-1} isohaline indicates retreat of the off-shelf export mechanism beyond 400 km from the coast consistent with the oceanward export of fresher surface waters. In the deep-ocean region salinity increased above 35.75 g kg^{-1} in the upper 150 m suggesting oceanic water encroached towards the shelf.

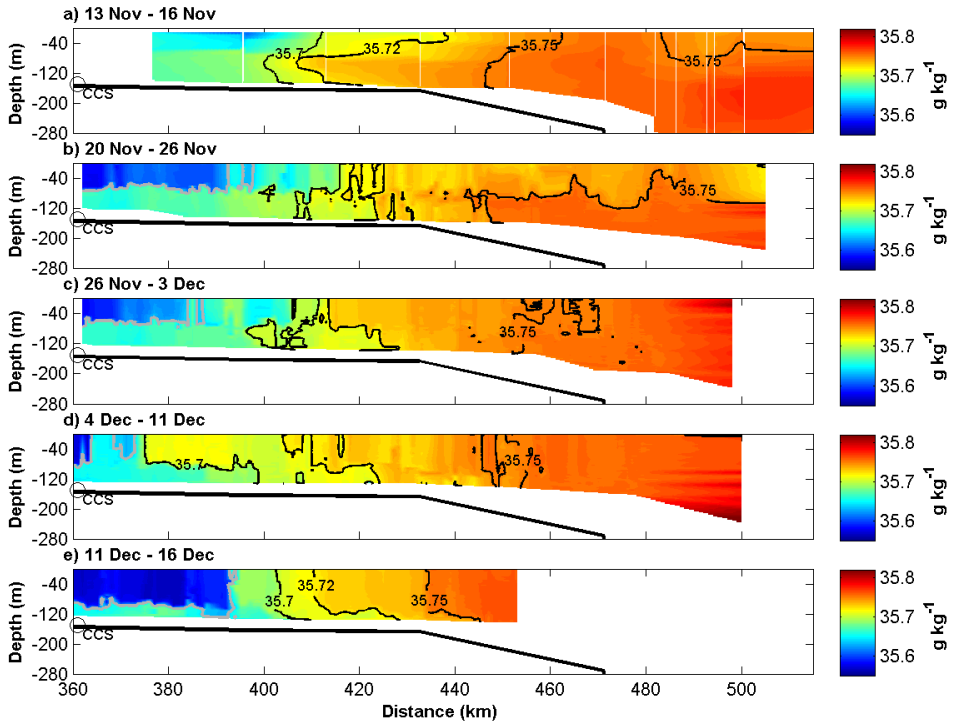

Figure 4.8: Cross-shelf sections of absolute salinity from a) CTD casts, and b-e)glider data. Contours represent the 35.64, 35.7, 35.72 and 35.75 g kg^{-1} isohalines.

Relatively warm waters above 13^{o}C were found in the upper 70 m at the shelf edge and North Atlantic Ocean indicating a two layer system on and off the shelf in the period 13th -16th of November (Fig. 4.9a). Waters <12^{o}C were observed over the Celtic Sea below 70 m depth between 380 and 415 km and off the shelf below 150 m depth. At the shelf edge, minimum temperatures above 12^{o}C and discontinuity in the 14.1^{o}C contour suggests mixing between bottom and surface waters. As observed in the salinity section, relatively cold waters at the shelf edge may be explained by the breaking of an internal wave that distributed heat vertically increasing and decreasing temperature in the bottom and surface layers, respectively. The two layer system on and off the shelf prevailed until the 11th of December (Fig. 4.9b, c and d). Below the thermocline waters with minimum temperature of ∼11 ^{o}C occurred in the Celtic Sea (<400 km distance) and were colder than waters at the same depth in the deep-ocean region. Nonetheless, despite discontinuity of the data at

the shelf edge, waters off shelf seemed to be colder than waters at the bottom of the shelf slope at the same depth (440 and 480 km). In the Celtic Sea and off the shelf temperature decreased in the surface layer due to seasonal atmospheric heat loss, with temperature decreases more rapid on the shelf. Between the 11th and 16th of December (Fig. 4.9e) the surface mixed layer deepened on the shelf and shelf break leading to a horizontal gradient with warmer waters at the shelf edge. Shear in the 12 and 12.5^{o}C isotherm, with relatively cold waters at the bottom corresponds to the off-shelf export mechanism observed in the salinity sections.

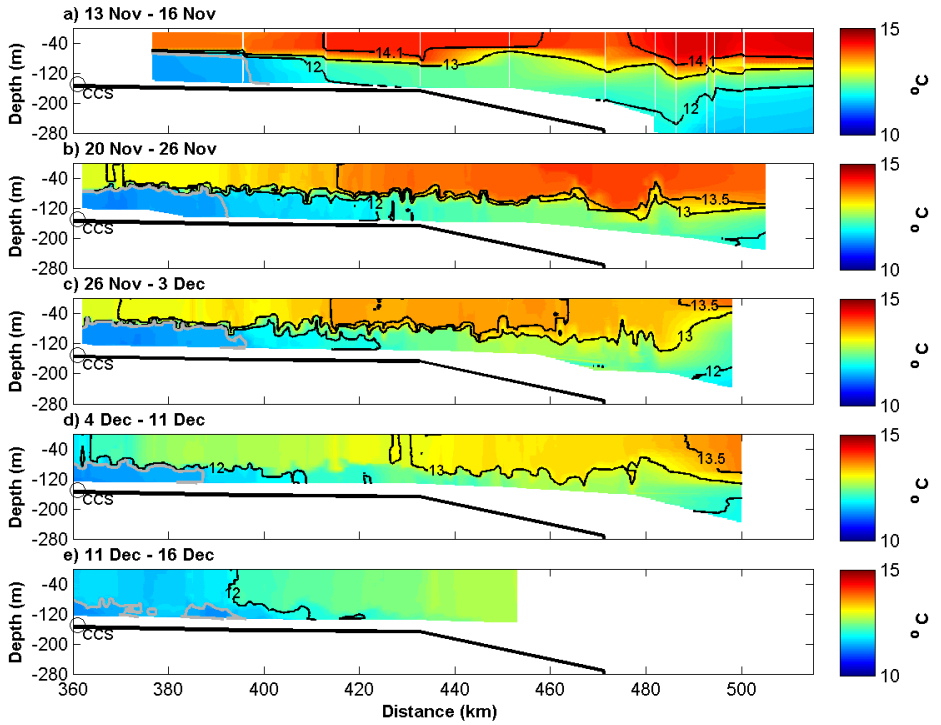

Figure 4.9: Cross-shelf sections of conservative temperature from a) CTD casts, and b-e) glider data. The minimum isotherm displayed in the sections is the 11.5^{o}C (gray contour).

As with temperature, a two layer system was observed in the density sections over the Celtic Sea and the deep ocean region from the 13th of November to the 11th of December (Fig. 4.10a to d). In the bottom layer relatively high density waters above 27 kg m^{-3} were found on the shelf between 70 and 160 m and in the North Atlantic from 480 km and

beyond below 200 m depth. Despite discontinuity in the data across the shelf break, bottom density on the shelf seemed to be greater than density at the shelf edge. Similarly, water off the shelf seemed to be denser than waters at the shelf break at the same depth. In the surface layer minimum densities below 26.8 kg m^{-3} reflected the warmest waters above 80 m depth from 360 km up to 500 km and were greater on the shelf and deep-ocean (>480 km) than at the shelf break. In the period 11th-16th of December (Fig. 4.10e) the horizontal thermal and salinity gradients between waters from the Celtic Sea and the North Atlantic Ocean were reflected on density transects generating shear of the 26.95 kg m^{-3}. The 27 kg m^{-3} contours suggest denser water (>27 kg m^{-3}) from the shelf were exported to the shelf break.

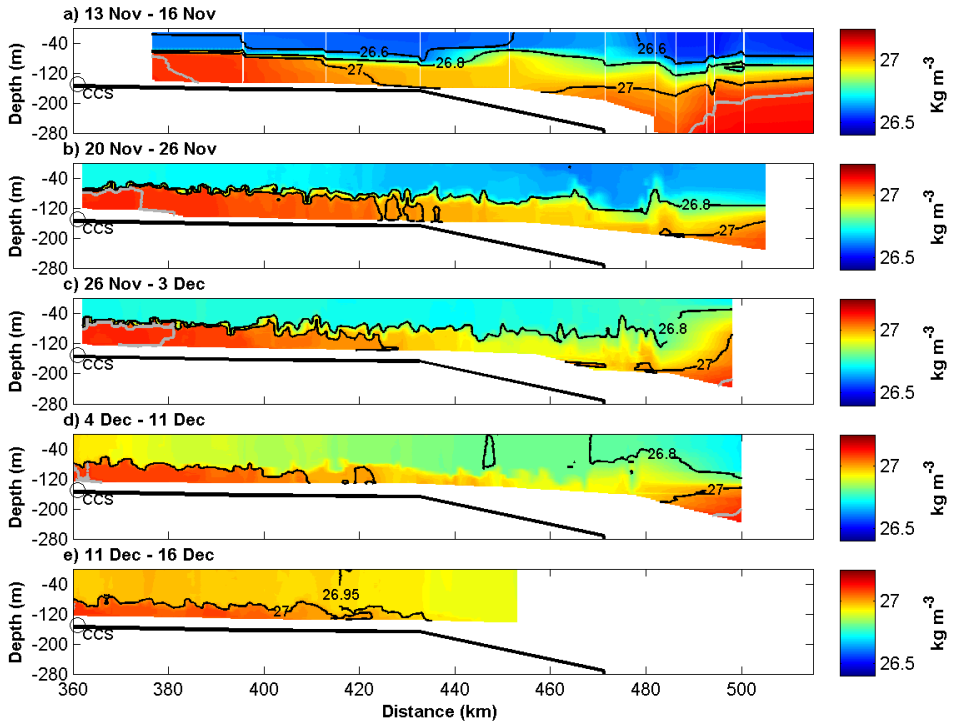

Figure 4.10: Cross-shelf sections of density from a) CTD casts and b-e) glider data. The maximum density contour is 27.1 kg m^{-3} (gray contour).

4.3.2 Winter

Cross-shelf depth-averaged transport

In winter, overall, depth-averaged transport at the Celtic Deep was south-westward in the periods 1st - 17th of January, 23rd -30th of January and 18th -21st of February (Fig. 4.11a). South-eastward transport occurred in the periods 18th - 24th of January and 31st of January - 6th of February. On average, between the 1st and 30th of January transport was south westward (2.4 m^2 s^{-1}) and then eastward from the 31st of January until the 21st of February (1 m^2 s^{-1}). At the Central Celtic Sea southward barotropic transport prevailed between January and mid-February (Fig. 4.11b) and was on average 2.2 m^2 s^{-1} between the 1st and 30th of January. Two anomalous northward transport events, lasting 4 and 5 days respectively, occurred on the 1st and 15th of February reaching maximum magnitudes around 8.5 m^2 s^{-1}. Between the 31st of January and the 1st of March averaged transport was in the north-eastward direction with values of 1.5 m^2 s^{-1}. Between the 1st and 15th of March an average westward transport occurred (2 m^2 s^{-1}).

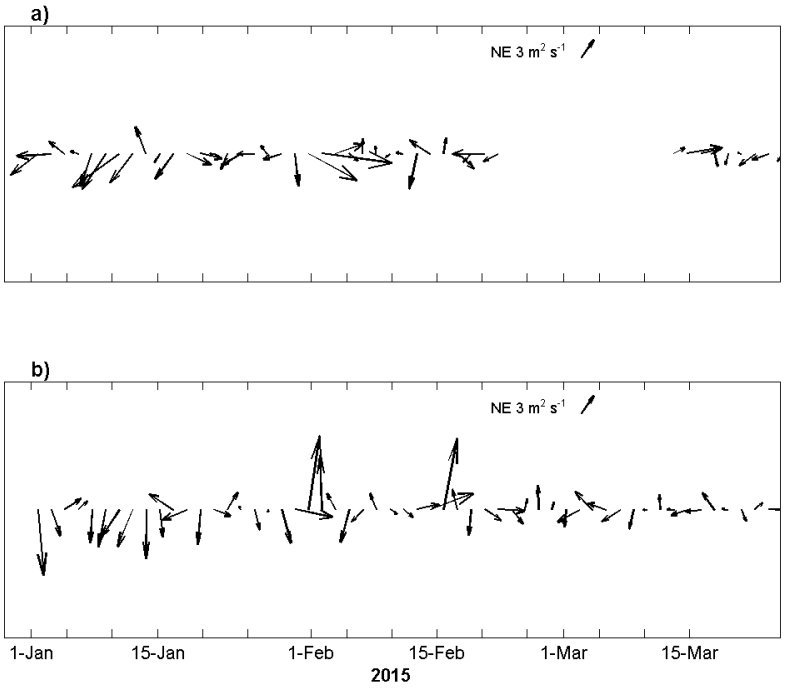

Figure 4.11: Depth-averaged transport at a) Celtic Deep and b) Central Celtic Sea.

At Central Celtic Sea westerly wind events were more frequent throughout winter and occurred in the periods January-February and mid-February - early March (Fig. 4.12a). The effects of the wind stress were observed in the vertical variability of the horizontal flow time series (Fig. 4.12b-c). Despite the water column being vertically mixed throughout winter, vertical structure of the flow was observed, particularly in the meridional component (Fig. 4.12c). Southward surface velocities were persistent in the upper 70 m in the periods January- February, mid-February and 22nd February - 5th of March. In contrast, northward velocities were consistent with westward wind events in the periods 31st of January - 13th of February. The compensatory flows occurred in a bottom layer with a thickness of 70-80 m.

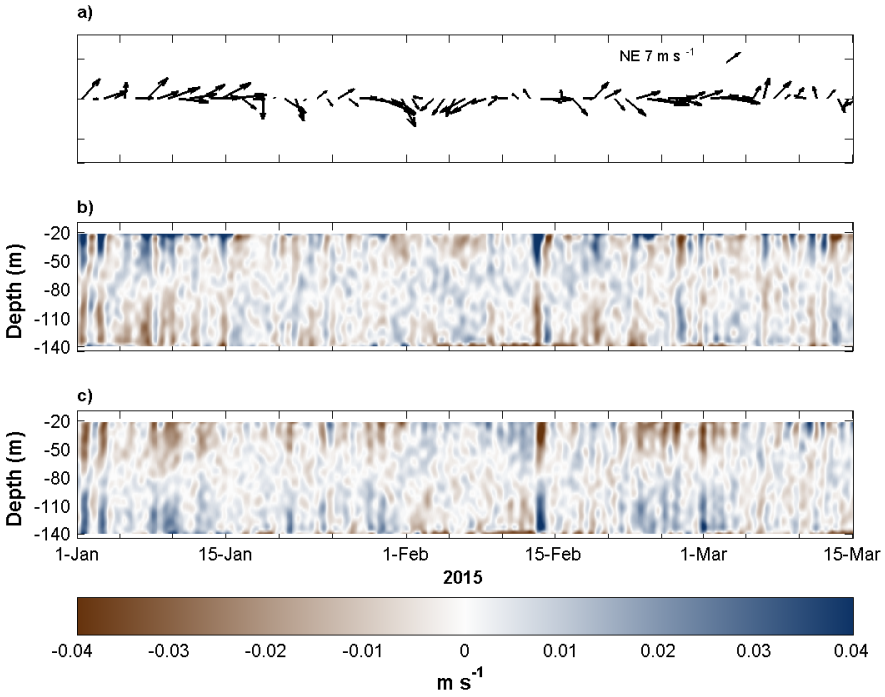

Figure 4.12: a) Wind velocity at 10 m, b) zonal and c) meridional horizontal velocity anomalies at Central Celtic Sea. Positive values indicate eastward and northward flow.

Relatively low salinity waters occurred in the Celtic Sea (Fig. 4.13). Consistent with south-westward flow at the Celtic Deep salinity dropped from 35.45 g kg^{-1} on the 1st of January to 35.25 g kg^{-1} on the 17th of January (Fig. 4.12a and 13a). Salinity increased in the period 18th - 23rd of January when the transport was south-eastward. In Central Celtic Sea salinity gradually decreased from 35.54 g kg^{-1} to <35.52 g kg^{-1} between the 1st and 30th of January coinciding with southward transport. A sharp increase in salinity (>35.56 g kg^{-1}) was observed between the 1st and 5th of February as a result of an anomalous northward transport event and was followed by a dropped in salinity to 35.52 g kg^{-1}. Increases in salinity occurred on the 11th of February being consistent again with northward transport (Fig. 4.11b). Salinity gradually increased from 35.52 to >35.56 g kg^{-1} on the 1st of March and dropped to 35.55 g kg^{-1} on the 8th of March.

Temperature decreased at the Celtic Deep and the Central Celtic Sea throughout the winter (Fig. 4.13b). Maximum temperature occurred in the early winter, being greater at the Celtic Deep (11.6^{o}C) than at the Central Celtic Sea (11^{o}C). Temperature gradually decreased and by the end of winter reached minimum values around 9.2^{o}C and 10^{o}C at the Celtic Deep and the Central Celtic Sea respectively. Between the 16th and 30th of January a similar temperature was observed at the Celtic Deep and the Central Celtic Sea ($\sim$10.6^{o}C) indicating a negligible horizontal thermal gradient between both sites. At Central Celtic Sea two increases in temperature were observed on the 1st and 15th of February consistent with periods of northward flow.

The influence of low salinity waters and heat loss in the Celtic Sea was reflected in the density time series (Fig. 4.13c). Density was greater at the Central Celtic Sea than at the Celtic Deep throughout the winter. Although temperature was similar at both sites between the 16th and 30th of January, density at Celtic Deep was lower due to relatively low salinity waters. At the Central Celtic Sea, despite decreases in salinity, density gradually increased and indicated variations in temperature, particularly heat loss, were dominant in controlling density.

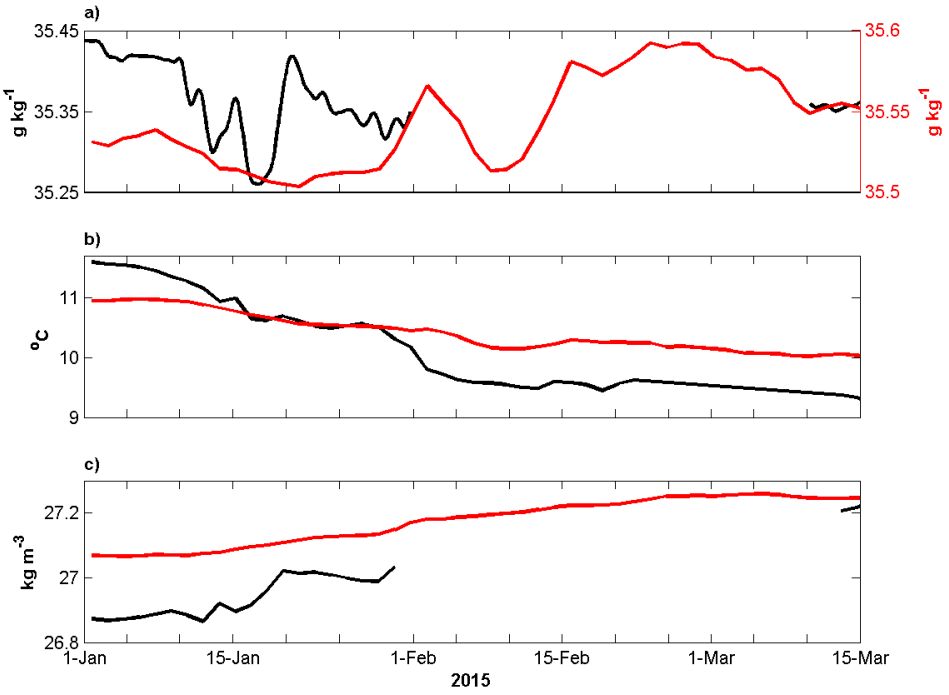

Figure 4.13: Surface time series at the Celtic Deep (black) and depth-averaged at the Central Celtic Sea (red) of a) absolute salinity, b) conservative temperature and c) potential density.

Shelf-Ocean interaction

Throughout winter the water column was vertically mixed and a horizontal thermal gradient occurred between the Central Celtic Sea and the North Atlantic Ocean, with temperatures increasing towards the shelf edge (Fig. 4.14). Near the shelf edge, at 440 km temperature decreased from 11.5^{o}C to 11^{o}C between the 17th of January and 28th of February. On the shelf, at 390 km, a lesser decrease in temperature was observed. Temperature was ∼11.7^{o}C in the period 17th of January - 8th of February and in the period 16th - 28th of February temperature decreased to 10.5^{o}C.

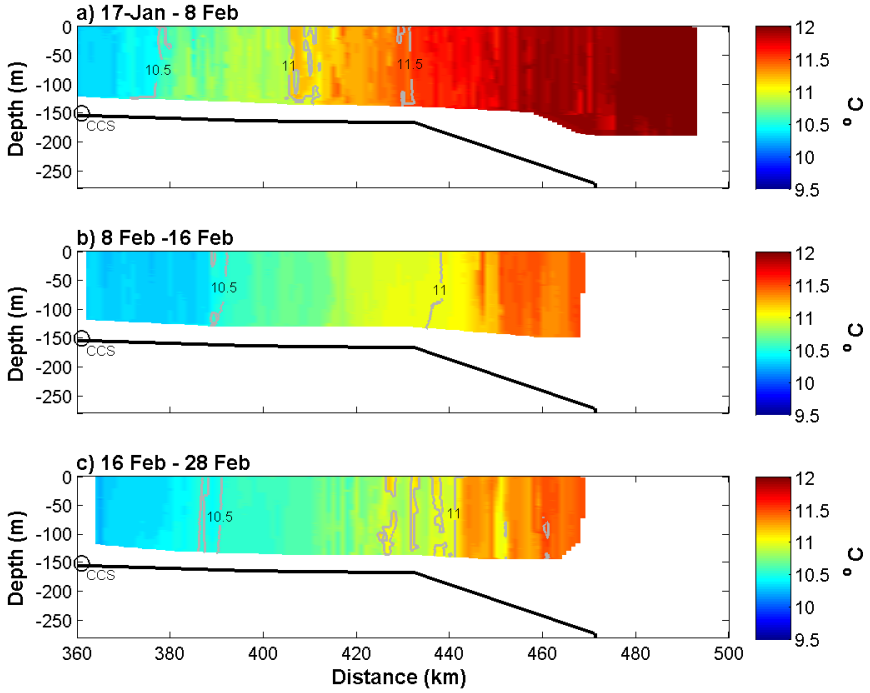

Figure 4.14: Cross-shelf section of conservative temperature. The Central Celtic Sea site is located at 360 km.

Similarly to the horizontal distribution of temperature, a horizontal salinity gradient prevailed in winter with fresher waters (<35.6 g kg^{-1}) on the shelf and relatively high salinity waters (35.7 g kg^{-1}) at the shelf edge (Fig. 4.15). Low salinity waters below 36.5 g kg^{-1} were observed up to 380 km in the period 17th of January -8th of February. Between the 8th and 16th of February these low salinity waters occurred 10 km further offshore at 390 km and in the period 16th-28th of February were found at 365 km. The horizontal displacement of salinity was consistent with the variations in salinity time series at Central Celtic Sea. At the shelf edge, between 420 km and 500 km, waters with salinity (>35.7 g kg^{-1}) typical of North Atlantic Ocean waters occurred. Despite off-shelf and onshore movement of relatively low salinity waters, oceanic waters with a consistent salinity above 35.7 g kg^{-1} remained from 420 km and further into the North Atlantic Ocean throughout winter (Fig. 4.14).

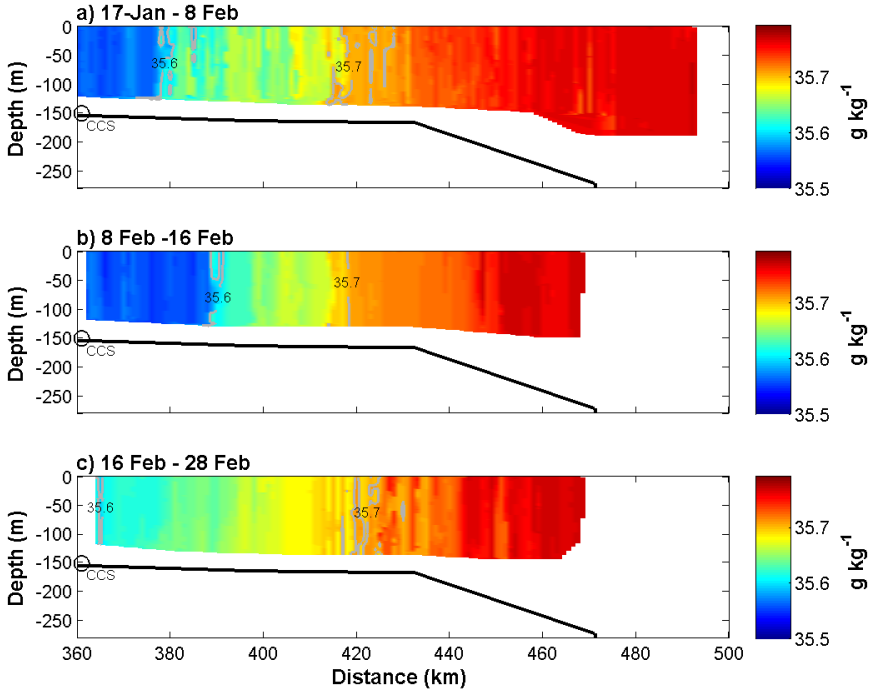

Figure 4.15: Cross-shelf sections of absolute salinity. The Central Celtic Sea site is located at 360 km.

The horizontal distribution of temperature and salinity were reflected in the density sections (Fig. 4.16). At the shelf edge density augmented from 27.1 kg m^{-3} to 27.21 kg m^{-3}. Salinity remained constant at 35.7 g kg^{-1} and therefore increases in density resulted from heat loss. In contrast, near Central Celtic Sea temperature remained around $\sim$10.3^{o}C. Nonetheless, density augmented from$\sim$27.19 kg m^{-3} in the period 17th January-8th February to >27.21 kg m^{-3} between the 16th and 28th of February suggesting salinity was more important on controlling density.

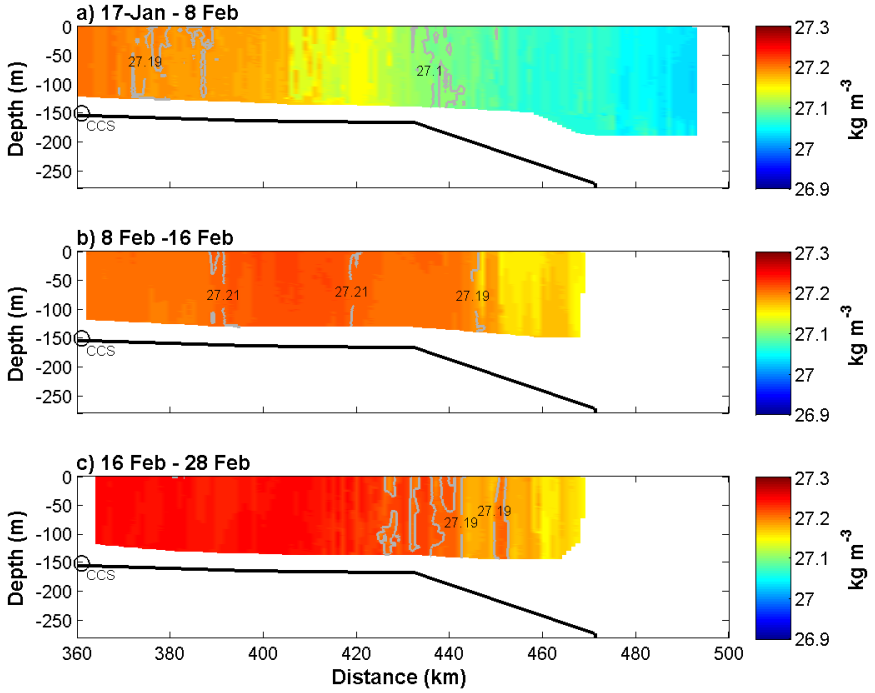

Figure 4.16: Cross-shelf section of potential density. The Central Celtic Sea site is located at 360 km.

4.4 Discussion

Based on the results described before, three different regimes were observed in the Celtic Sea between the 1st of November and 15th of March. During the first event, wind-driven exchange between the Celtic Sea and the North Atlantic Ocean occurred in the period 2nd-18th of November. Secondly, interaction at the shelf edge of surface wind-driven transport and off-shelf export in the bottom layer took place between the 7th and 28th of December whilst the water column remained stratified. In the third event low salinity waters from the north of the Celtic Sea were advected oceanward in winter between the 1st and 30th of January. The implications on transport and exchange between the Celtic Sea and the North Atlantic Ocean are discussed below for each event.

4.4.1 Wind-driven exchange in the period 2-18 of November 2014

Between the 2nd and 18th of November 2014 westerly winds occurred in the Celtic Sea generating off-shelf wind-driven surface Ekman transport and a compensatory onshore flow in the bottom layer (Fig. 4.7). Maximum off-shelf transport in the surface was on the 8th of November causing fresher waters with salinity below 35.55 g kg^{-1} to reach the Central Celtic Sea site (Fig. 4.7d). Hydrographic sections provide evidence that exchange between the Celtic Sea and the North Atlantic Ocean occurred between the 13th and 16th of November (Fig. 4.8a). Oceanic waters, identified by their relatively high salinity (>35.7 g kg^{-1}), intruded on-shelf in the bottom layer whilst fresher waters were advected off-shelf in the upper 70 m.

On the shelf, waters with temperatures of 11 - 11.5^{o}C and densities above 27.1 kg m^{-3} were located between 370 and 400 km from the coast in the bottom layer reaching maximum depths of 160 m (Fig. 4.9a). In contrast, waters with similar properties occurred at least further off the shelf at ∼470 km from the coast below 250 m. We can identify the origin of the relatively cold waters and discern whether they were transported onto the shelf during the westerly wind event in the period 2nd - 18th of November by calculating the horizontal and vertical wind-driven velocities. For instance, in this period averaged off-shelf Ekman transport was 0.5 m^2 s^{-1} in the surface layer of the Central Celtic Sea. Assuming a similar and opposite transport in the bottom layer with a 60 m thickness leads to onshore velocities of 0.72 km day^{-1} indicating oceanic waters intruded ∼11.5 km on-shelf during this 16 day-long event. Vertical velocities of the displacement of the pycnocline can be calculated by accounting for

the horizontal Ekman flow from the continuity equation as follows:

$$\frac{\partial u_{Ek}}{\partial x} + \frac{\partial v_{Ek}}{\partial y} + \frac{\partial w_{Ek}}{\partial z} = 0 \tag{4.18}$$

where u_{Ek}, v_{Ek} and w_{Ek} are the zonal, meridional and vertical components of the Ekman velocity. Integrating vertically within the surface Ekman layer and applying eq. (4.18) to a westerly wind stress leads to:

$$-w_{Ek} = \frac{\partial V_{Ek}}{\partial y} \tag{4.19}$$

On narrow shelves (<50 km) surface divergence caused by wind-stress generates vertical and surface outcropping of the pycnocline at the shelf break (e.g. Torres and Gomez-Valdes, 2015) as described by eq. (4.19). However, for a wide shelf sea such as the Celtic Sea (∼500 km), surface off-shelf transport at the shelf break was replenished by waters from further on the shelf and therefore vertical velocities and/or upwelling of deeper waters at the shelf break are negligible. Thus relatively cold waters off the shelf from 250 m depth and at 470 km from the coast were not advected 100 km on-shelf in this period only. The origin of the relatively cold waters (11-11.5^{o}C) located between 360-390 km from the coast is explained below with available data throughout the year.

In the previous winter (March 2014) waters in the Celtic Sea were vertically mixed with a horizontal gradient in temperature increasing towards the North Atlantic Ocean. During the onset of stratification a two layer system was observed across the shelf and extended into the deep-ocean region (Ruiz-Castillo et al., 2018; Chapter 2). Surface temperatures eventually were similar between the Celtic Sea and North Atlantic as heating of the water column occurred. However, in the bottom layer the horizontal temperature gradient remained, with warmer waters off the shelf

(11- 11.5^{o}C at 470 km) than over the Celtic Sea (<10^{o}C). Temperature in the bottom layer gradually increased from ∼9.4^{o}C in April 2014 to maximum values around 11.3^{o}C by mid-November 2014 in Central Celtic Sea (∼360 km) (Fig. 4.17a). On-shelf intrusion of relatively warm waters from the North Atlantic onto the Celtic Sea occurred between April and mid-November. Waters between 11 and 11.5 ^{o}C located at ∼ 470 km in March 2014 seemed to be advected to distances of 360 - 400 km (Fig. 4.17b). Westerly winds prevailed in summer and wind-driven Ekman dynamics govern cross-shelf transport in the surface and bottom layer (Chapter 3) and extended further into the deep-ocean (Fig. 4.8a). We can utilise transport of the onshore compensatory bottom flow between the 2nd and 18th of November (0.5 m^2 s^{-1}) to calculate velocities throughout the stratified period of 2014. If we assume a bottom layer with a thickness of 90 m and the 1st of April 2014 to be the onset of stratification, by mid-November (229 days) waters off the shelf would have been advected 70 - 110 km on-shelf due to net Ekman transport. This distance fits with the horizontal displacement of waters suggested by the 11 and 11.5^{o}C (Fig. 4.17b) and indicate increases in bottom temperature resulted mainly from warmer water off the shelf being horizontally advected to the Celtic Sea in a 7-8 month period. The same analysis can be applied to waters between 35.65 and 35.7 g kg^{-1} (white contours in Fig. 4.17b). In March 2014, these waters were located between 440 and 450 km and by mid-November the waters had been advected between 50 and 90 km on-shelf due to wind-driven transport. Differences in the displacement observed in salinity and temperature contours may be caused by the breaking of internal waves at the shelf edge (New, 1988; New and Pingree, 1990; Sharples et al., 2007). The internal waves at the shelf edge generate mixing and redistribute fresher and warmer waters from the surface layer below the pycnocline, increasing and decreasing tem-

perature and salinity in the bottom layer. These features confirm that cross-shelf wind-driven transport expanded further into the deep-ocean region enabling cross-shelf exchange.

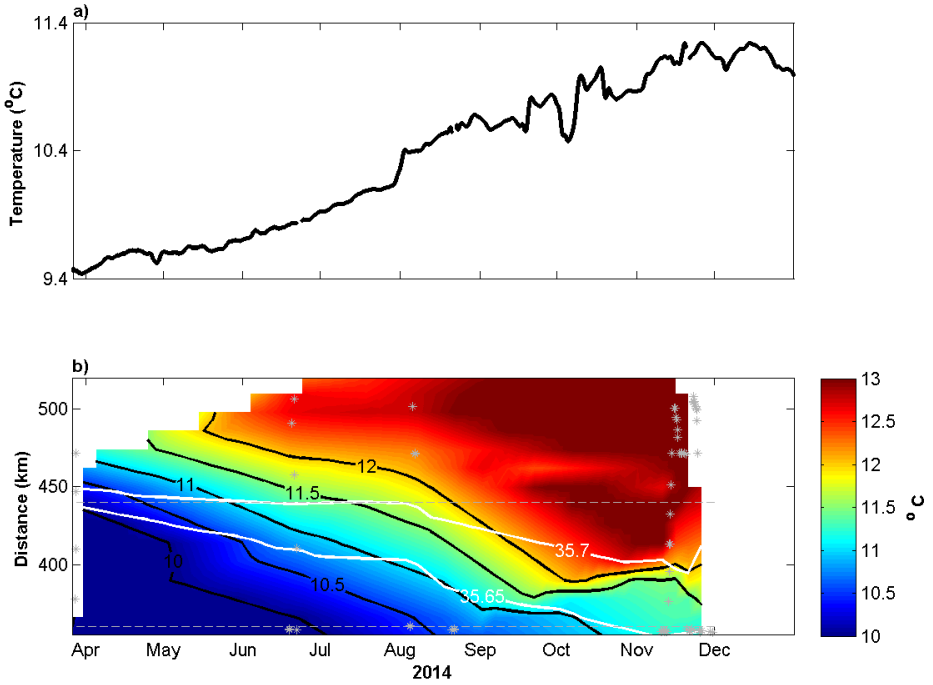

Figure 4.17: a)Time series of conservative temperature at 130 m depth at Central Celtic Sea and b) Hövmöller diagram of conservative temperature (map in colour and black contours) and absolute salinity (white contours) at 80 m depth. In b) grey lines indicate the location of the Central Celtic Sea site (360 km) and the shelf edge (440 km).

Implications for nutrient supply to the Celtic Sea

Wind-driven transport across the shelf edge has further implications for nutrient supply to the Celtic Sea. Based on advection of temperature and salinity, waters from ~470 km in March 2014 with a nutrient concentration of 8.9 mmol m^{-3} (Fig. 4.18) would reach distances of 360-400 km from the coast by mid-November 2014. Averaged wind-driven Ekman transport was 0.5 m^2 s^{-1} and in a 90 m bottom layer thickness would result in onshore velocities of 0.5 km day^{-1}. By mid-June, 90 days after nutrients were quantified at the shelf edge, waters would have been advected ~ 45 km on-shelf. Nutrients sampled at 410 km indicate nutri-

ents in the surface layer were depleted (Fig. 4.18) (Poulton et al., 2018). By mid-November the nutrient concentration in the bottom layer was 10.28 mmol m^{-3} (Fig. 4.18) and greater than expected if only Ekman transport was accounted for (8.9 mmol $^{-3}$). To further investigate the relative importance of wind-driven advection, an estimation of the total amount of nutrients was assessed at 376 km from the coast in a water column of 160 m. We can assume three layers with an averaged nutrient concentration of 2.76, 6.34 and 10.28 mmol m^{-3} in the surface, pycnocline and bottom, respectively. In November an autumn bloom event occurred in the Celtic Sea (Garcia-Martin et al., 2017; Carr et al., 2018; Wihsgott et al., 2019) and resupplied nutrients to the surface layer leading to a decrease in the nutrient concentration below the pycnocline. By the time the water was sampled in November, 1 mmol m^{-3} had already been consumed in the surface layer (Ruiz-Castillo et al., 2018; Chapter 2) therefore the expected nutrient concentration would be ∼3.76 mmol m^{-3}. If we multiply by each layer thickness 50, 10 and 100 m, integrated water column nutrient concentration is ∼1279.4 mmol m^{-2}. In addition, in late April enhanced wind stress and a short heat loss event deepened the pycnocline 20 m (Wihsgott et al., 2019; chapter 5) and entrained ∼166 mmol m^{-2}, from the bottom layer (chapter 5). We can ignore the intensified wind stress event in April hence ∼166 mmol m^{-2} remained in the bottom layer. Moreover, throughout summer dyapicnal fluxes from the bottom layer to the pycnocline were estimated to be 365 mmol m^2 (Ruiz-Castillo et al., 2018). If we neglect dyapicnal mixing the nitrate concentration in the bottom layer would be ∼1810.4 mmol m^{-2}. Nutrient concentrations in the surface layer preceding the bloom were negligible due to consumption (Pingree et al., 1976) and therefore nutrients are expected to be within the bottom layer (90-100 m thickness), resulting in a concentration of 18.1-20.1 mmol m^{-3}. This estimation suggests that

44-50% of the nutrient concentration available for the autumn bloom in the outer shelf were advected from the North Atlantic due to wind-driven Ekman transport. Therefore between 50-56% of the nutrients were recycled in the water column between March and mid-November.

Background nutrient concentrations off shelf in spring are set by the variation in the depth of the winter mixed layer (Ruiz-Castillo et al., 2018; Chapter 2). During the stratified period nutrients are advected ~70-110 km on-shelf due to wind-driven dynamics in a 7-8 month period before winter mixing. Therefore, nutrients from the North Atlantic would cover the whole shelf (500 km) in at least a two year-time period, consistent with previous estimates (Hydes et al., 2004).

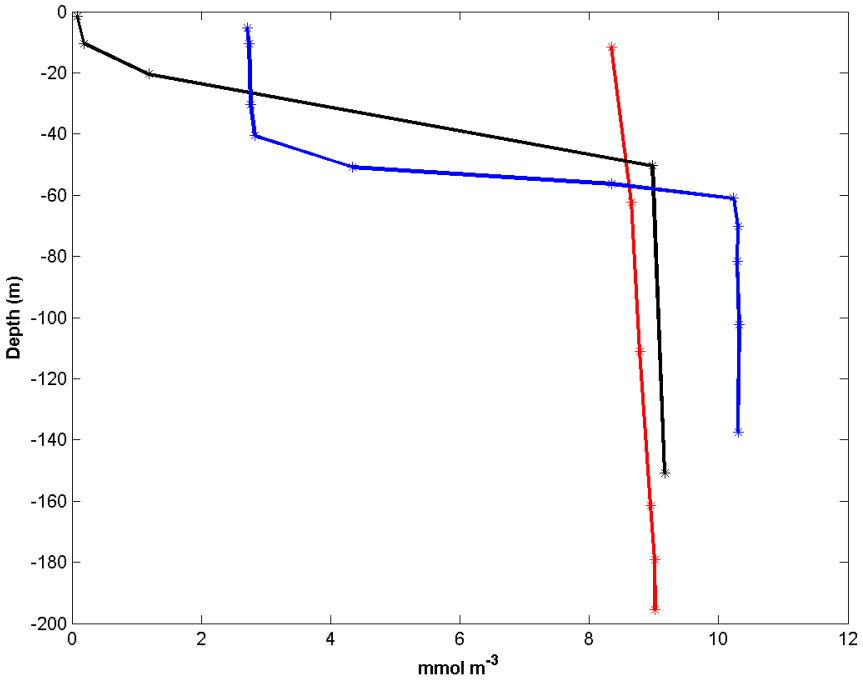

Figure 4.18: Nitrate (NO_3+NO_2) profiles for March 2014 at 470 km (red), June 2014 at 410 km (black) and November 2014 at 376 km (blue).

4.4.2 Interaction between bottom off-shelf and surface wind driven transport in the period 7-28 of December

In the second event westerly winds occurred between the 7th and 28th of December 2014. At the Central Celtic Sea site surface and Ekman transport were highly correlated (R^2 >0.8) with oceanward surface and onshore bottom water displacement (Fig. 4.7). Overall, in the Celtic Sea fresher waters were advected towards the shelf edge above the pycnocline. However, at the shelf edge there was no hydrographic evidence that supported wind-driven exchange between the Celtic Sea and the North Atlantic. In contrast, salinity sections obtained between the 26th of November and the 16th of December indicate shelf waters were exported off-shelf in the bottom 60-80 m (Fig 4.8 c-e). The off-shelf export of Celtic Sea waters can be explained by two mechanisms. In the North-western European shelf cascading (e.g. Hill et al., 1998) and Ekman drain (Souza et al., 2001, Simpson and Mcandliss, 2013) have been documented before. Based on the hydrographic conditions we can assess the likely occurrence of each process. Despite discontinuity in the data across the shelf break (430 -470 km) bottom density seemed to decrease as moving from the ocean towards the shelf break below 160 m depth (Fig. 4.10). Thus, cascading seems unlikely along the shelf break and the adjacent North Atlantic between the 13th of November and the 16th of December. However, on the Celtic Sea between 400 and 440 km favourable conditions such as denser waters on the shelf than at the shelf edge were observed. Following Shapiro and Hill (1997) the relative influence of cascading (U_{cas}) and Ekman drain (U_{Ekdr}) can be calculated as:

$$\frac{U_{cas}}{U_{Ekdr}} = \frac{2g'S}{fv_0} \tag{4.20}$$

where g' is the reduced gravity, S the bottom slope, f the Coriolis parameter and $v_0$is the velocity of the along-slope current. Using a density difference of 0.1 kg m^{-3}, of 1026.5 kg m^{-3}, slope of 6.6×10^{-5} (2 m/ 30 km) and setting the along slope current at 0.05 m s^{-1} (Pingree and LeCann, 1989; van Aken, 2002) results in a ratio of 0.02 indicating Ekman drain is more important on the shelf. Therefore, it is suggested that between the 7th and 28th of December Ekman drain and wind-driven transport occurred simultaneously at the shelf edge. The poleward along-slope current has been reported to be centred along the 500 m isobath (Pingree and Le Cann, 1989; Souza et al., 2001), however on-shelf displacement of the 35.75 g kg^{-1} isohaline between the 26th of November and 16th of December (Fig. 4.8c and d) indicates encroachment upon the shelf of oceanic waters and potentially enhanced cross-shelf flow in the bottom boundary layer (e.g. Roughan and Middleton, 2004; Schaeffer and Roughan, 2015).

The interaction of the Ekman drain and wind-driven transport at the shelf edge was reflected in the hydrographic time series at Central Celtic Sea. For instance, waters with salinity between 35.55 and 35.6 g kg^{-1} occurred in the surface layer between the 7th and 18th of December and were advected towards the shelf edge (Fig. 4.7 and 4.8). However, the along-slope current and the Ekman drain process appears to have inhibited export into the North Atlantic Ocean, impeding intrusion of oceanic waters onto the Celtic Sea in the bottom layer, and forced onshore recirculation of surface shelf waters, i.e. slope current acts as a boundary. Salinity time series indicate these waters returned to the Central Celtic Sea site between the 24th and 28th of December in the bottom layer and earlier in the period 10th-24th of December between 70 and 90 m depth within the pycnocline (Fig. 4.7). Between the 7th and 24th of

December, when these waters were first seen in the surface and bottom layers, the averaged transport in a ∼70 m thick surface layer was 1.14 m^2 s^{-1} suggesting waters were displaced 12 km towards the shelf edge around the 15th of December and subsequently returned in the bottom. It is probable that only Celtic Sea waters within a 10 km distance from the Ekman drain forcing were exported off-shelf.

A spatial analysis of wind driven transport and Ekman drain interacting simultaneously can be assessed through the salinity sections (Fig. 4.8). At the shelf edge the Ekman drain mechanism was identified by the shear of the 35.7 and 35.72 g kg^{-1} isohalines from the 26th of November onwards with maximum intrusion (370 km) of the 35.7 g kg^{-1} contour in the period 4th-11th December. Afterwards, between the 11th and 16th of December the 35.7 g kg^{-1} contour retreated 20 - 30 km oceanward consistent with the distance that fresher waters were advected due to wind-stress forcing (Fig. 4.8e). Nonetheless, the oceanward displacement of the 35.7 g kg^{-1} isohaline indicates the Ekman drain mechanism remained whilst waters were advected towards the shelf edge by the wind-driven flow. Off shelf, oceanic waters with salinities greater than 35.75 g kg^{-1}, encroached upon the shelf from 450 km from the coast during the period 26th of November- 3rd of December to 420-430 km between the 11th and 16th of December. Although shelf and oceanic waters were advected off- and onshore, respectively, the 35.72 g kg^{-1} isohaline remained at 410 km from the 26th of November until the 16th of December. Hence, exchange due to Ekman drain was inhibited by the wind-driven mechanism resulting in convergence of oceanic and fresher waters between 390 and 440 km. Thus, given that there is no net exchange at the shelf edge, oceanic waters encroaching on the shelf recirculated off-shelf in the bottom as a result of the Ekman drain mechanism. Similarly waters on the Celtic Sea

side recirculated onshore in the bottom (Fig. 4.7d).

Transport generated by the Ekman drain mechanism can be estimated by neglecting mixing and assuming motions at the shelf edge are constrained to two dimensions, horizontal distance and depth. In this highly ideal scenario, the net off-shelf export can be assessed by evaluating the difference in the area covered by the waters with salinity between 35.7 and 35.75 g kg^{-1} on the periods 4th - 11th December and 11th - 16th December. The deepest hydrographic observations were on average at 137 m from 400 to 440 km which will be considered the bottom. The difference in the area covered was 3.652×10^6 m^2 which in a 7-day period leads to an off-shelf export of 6 m^2 s^{-1}. Based on the salinity sections, transport was carried out in a 60-80 m thick bottom layer resulting in off-shelf velocities of 0.06 - 0.1 m s^{-1} being of the same order of magnitude as the velocities reported previously for the Hebridean shelf of 0.026 - 0.05 m s^{-1} (Simpson and Mcandliss, 2013).

Convergence at the shelf edge has further implications on the dynamics in the along-shelf direction on and off the shelf. Using long-term (2 months) current measurements, evidence of an eastward flow with velocities of 0.02 m s^{-1} has been identified previously at the shelf edge of the Celtic Sea (Pingree and Le Cann, 1989). Nonetheless, no dynamical explanation has supported this eastward flow. As mentioned before, wind-driven offshore transport was obstructed at the shelf edge causing recirculation similar to a wind-driven downwelling type mechanism. The slope current behaves like a wall at the upper slope and associated with downwelling events, waters converge in the coastal region and increase the height of the sea surface (e.g. Tilburg, 2003). Thus, during this westerly wind-stress event the sea surface at the shelf edge is expected

to increase reaching maximum height at the shelf edge and gradually decrease in the onshore direction generating a northward pressure gradient. The eastward flow observed in Pingree and Le Cann (1989) can be explained by assuming geostrophic balance in the cross-shelf direction, flat topography and hydrostatic balance in the vertical as follows:

$$fu = -\frac{1}{\rho_0}\frac{\partial P}{\partial y} \tag{4.21}$$

$$P = -\rho_0 g H \tag{4.22}$$

where H represents the mean depth of the water column. Following Winant (1980) along-shelf transport can be obtained by vertically integrating and combining eq. (4.21) and (4.22) resulting in:

$$U = -\frac{g\,(H+\eta)}{f}\frac{\partial \eta}{\partial y} \tag{4.23}$$

where η stands for the sea level anomalies. Eq. (4.23) describes a flow in geostrophic balance and due to convergence of waters at the shelf edge the sea level is tilted in the form $\left(\frac{\partial \eta}{\partial y} < 0\right)$ producing an eastward flow. The balance presented here may explain the eastward velocities observed in Pingree and Le Cann (1989) as a result of the interaction of off-shelf surface wind-driven transport with the along-slope current. Off shelf, convergence at the shelf edge results in a similar balance as described in eq. (4.23) with sea level decreasing southward enhancing the along-slope current in the poleward direction.

Finally, in the Celtic Sea recirculation of surface waters in the bottom layer had further implications for stratification of the water column. For instance, between the 28th and 31st of December relatively warm waters ($>11^oC$) occurred in the bottom layer underlying colder waters ($<11^oC$) (Fig. 4.7e). Heat loss to the atmosphere occurred gradually and de-

creased the temperature of the surface waters whilst being advected towards the shelf edge. Waters in the surface layer were colder than in the bottom (Fig. 4.7e), however a stable water column was maintained (Fig. 4.19) by the vertical distribution of salinity with relatively high salinity occupying the bottom layer (Fig. 4.7d). The horizontal salinity gradient, with salinity decreasing onshore, combined with westerly wind stress ensured fresher waters from the interior of the Celtic Sea flowed over waters with greater salinity from near the shelf edge and prolonged the stratified period until the 1st of January. Salinity combined with westerly winds have further implications in the onset of stratification in spring, after the mixing period, as will be described in Chapter 5.

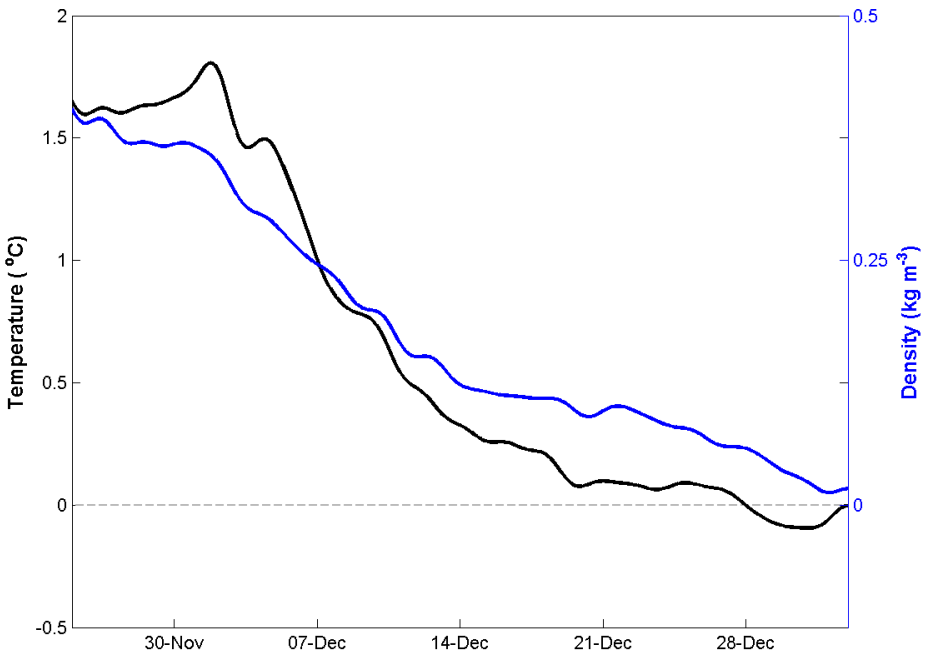

Figure 4.19: Differences between surface and bottom temperature (black) and bottom and surface density (blue).

4.4.3 Cross-shelf transport in winter in the period 1-30 of January

In winter, at the Celtic Deep and Central Celtic Sea sites decreases in salinity were observed between the 1st and 30th of January. The horizontal distribution of salinity prior to winter mixing generates a cross-shelf salinity gradient in winter with relatively low salinity waters in the north (Ruiz-Castillo et al., 2018; Chapter 2). At Celtic Deep decreases in salinity were consistent with south-westward flow suggesting waters off the mouth of the Bristol Channel were advected towards the Celtic Deep site. For instance, on the 10th of January salinity was 35.44 g kg^{-1} and reached a minimum ($\sim$35.25 g kg^{-1}) on the 17th of January whilst transport was south-westward (Fig. 4.11a and 13a), i.e. heading off the Bristol Channel. Afterwards salinity gradually increased up to $\sim$35.42 g kg^{-1} on the 20th of January coinciding with the period when the flow turned south-eastward (Fig. 4.11a and 13a), i.e. towards the mouth of the Bristol Channel. At the Central Celtic Sea decreases in salinity were consistent with southward advection suggesting transport of relatively low salinity waters from the north of the shelf. Nonetheless, winter is the wettest season in the region (Pingree, 1980) and therefore precipitation may also contribute to decreases in salinity across the shelf.

The relative influence of the fresher waters off the Bristol Channel and the effects of precipitation on the salinity in Celtic Deep and Central Celtic Sea can be estimated using rainfall time series from Era-interim data sets (Dee et al., 2011). At the Celtic Deep total precipitation between the 10th and 17th of January was 3 cm, and in a 100 m water column implied a change of 0.01 g kg^{-1}. Therefore only 5% of the salinity decrease can be attributed to precipitation indicating advection governed salinity variations off the Bristol Channel mouth. Further in the interior

of the shelf, in Central Celtic Sea salinity dropped from 35.54 g kg^{-1} to 35.51 g kg^{-1} in the period 8th -21st of January (Fig. 4.13a) and total precipitation was 4 cm. In a 150 m water column rainfall input resulted in a change of 0.01 g kg^{-1} or 33% of the salinity difference. Hence, averaged south-westward and southward advection dominated dynamics at the Celtic Deep and the Central Celtic Sea.

Cross-shelf advection was governed by wind-driven Ekman dynamics in summer and autumn (Fig. 4.7). Whilst the water column was stratified, fresher and relatively high salinity waters were transported in the surface and bottom layers, respectively (Fig. 4.8a). In winter, even though the water column was fully mixed the effects of wind-stress were reflected in the vertical structure of the horizontal flow and were coherent with wind-driven Ekman dynamics in Central Celtic Sea (Fig. 4.12). The vertical variability of the horizontal velocities indicates surface and bottom flow occupied a 70-80 m thickness in a $\sim$150 m depth water column. Therefore advection of salinity in the upper half of the water column would be compensated in the bottom half leading to a negligible net salinity change once mixing occurred. Thus cross-shelf southward advection of fresher waters from the north resulted from another mechanism.

Assessment of the mechanism driving this southward cross-shelf transport across the Celtic Sea can be carried out if we assume that the Bristol Channel is the only source of fresher water for the shelf (Uncles, 1984; Brown et al., 2003; Hydes et al., 2004). Whilst it is difficult to describe transport with only measurements at two sites, a plausible explanation can be suggested. Events of freshwater discharge into the Bristol Channel occurred since the previous October (Fig. 8 in Ruiz-Castillo et al., 2018), being a maximum in winter (Uncles and Radford, 1980; Uncles,

2010), and strengthened the salinity gradient between waters from the north of the Celtic Sea and the Bristol Channel. Decreases in salinity at Celtic Deep indicate relatively low salinity waters were introduced into the north of the shelf from the Bristol Channel (Fig.4.13) in an averaged south-westward transport of 2.4 m^2 s^{-1} (Fig. 4.20). A greater decrease in salinity in Celtic Deep than in Central Celtic Sea may result from the enhanced salinity gradient off the Bristol Channel mouth. In Central Celtic Sea southward transport of ∼2.2 m^2 s^{-1} was observed suggesting 0.2 m^2 s^{-1} of the transport at Celtic Deep recirculated in the north of the shelf and/or left the Celtic Sea through the St. Georges Channel. Waters from Central Celtic Sea headed southward (2.2 m^2 s^{-1}) and were advected ∼40 km towards the shelf edge. Nonetheless, at the shelf edge oceanic waters (>35.7 g kg^{-1}) remained at 420 km since December (Fig. 4.8d-e) and throughout winter (Fig. 4.15) suggesting negligible net exchange between the North Atlantic Ocean and the Celtic Sea. Following southward transport, after the 30th of January, salinity increased in the Central Celtic Sea to values of 35.55 g kg^{-1} (Fig. 4.13a), above the salinity observed on the 1st of January, indicating relatively high salinity waters from regions closer to the shelf edge were transported into the Central Celtic Sea site, even though there was no evidence of oceanic waters (>35.7 g kg^{-1}) intruding further into the interior of the Celtic Sea (Fig. 4.15). Potentially the relatively low salinity waters from Central Celtic Sea were advected southward and recirculated within the shelf leading to the northward flow (∼1.5 m^2 s^{-1}) in the periods 31st January - 1st March (Fig. 4.20). Results suggest that there was no exchange between the Celtic Sea and the North Atlantic Ocean in the winter 2014-2015.

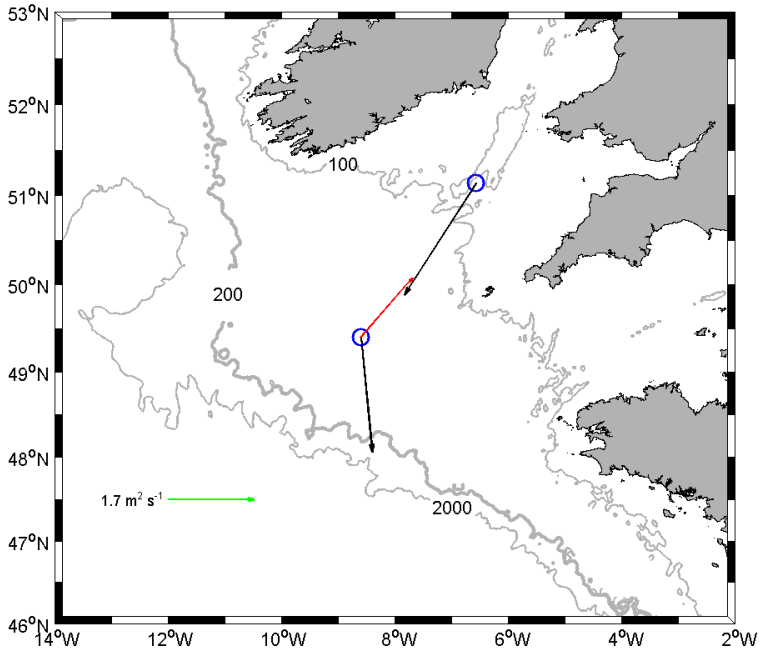

Figure 4.20: Transport at the Celtic Deep and Central Celtic Sea sites. Black vectors represent the averaged transport between the 1 and 30 of January at Celtic Deep (2.4 m^2 s^{-1}) and Central Celtic Sea (2.2 m^2 s^{-1}). Red vector represents transport in the period 31 of January and 1 of March (1.5 m^2 s^{-1}).

4.5 Summary

Cross-shelf exchange between the Celtic Sea and the North Atlantic Ocean was assessed between the 1st of November 2014 and 15th of March 2015.

Wind-driven dynamics govern exchange between the North Atlantic Ocean and the Celtic Sea between April and mid-November. Relatively high salinity, nutrient-rich and relatively warm water from the North Atlantic was advected onto the Celtic Sea. The bottom on-shelf advection occurred in a 7-8 month period and oceanic waters intruded 70-110 km on-shelf. About 44-50% of the nutrients observed on the shelf were advected from the North Atlantic Ocean.

In late autumn, between the 7th and 28th of December Ekman drain and wind-driven transport occurred simultaneously preventing cross-slope exchange between the North Atlantic and the Celtic Sea. Convergence of waters resulted at the shelf edge and forced surface shelf and oceanic waters to recirculate onshore and off-shelf in the bottom layer. In the Celtic Sea, stratification was extended despite of relatively warm waters occupying the bottom layer. Onshore recirculation of relatively high salinity waters in the bottom, below fresher waters from the interior of the Celtic Sea, prolonged the stratified period. The convergence of waters at the shelf edge may generate a geostrophic eastward flow.

In winter relatively low salinity waters were supplied into the north of the Celtic Sea from the Bristol Channel. Transport towards the shelf edge occurred between the 1st and 30th of January. Despite southward transport there was no evidence of exchange between the Celtic Sea and the North Atlantic Ocean during the winter 2014-2015.

Chapter 5

Onset and evolution of stratification in a temperate shelf sea; implications for phytoplankton growth

Abstract

Many key biological processes in shelf seas, including phytoplankton growth, depend on stabilisation of the water column. Therefore understanding the driving mechanisms responsible for the onset of stratification is essential to better comprehend the biology of shelf seas. This chapter describes the dynamics responsible for the onset and evolution of the stratified period in spring 2014 and spring 2015 and the implications for phytoplankton growth. Meteorological data, measured by an instrumented buoy, combined with remote sensing datasets from Era-interim, were used to assess the effects of wind stress, wind-driven transport and net heat flux on stratification at the Central Celtic Sea site. In the water column, horizontal velocities obtained from an ADCP were utilised to calculate cross-shelf advection in the surface layer. The onset and evolution of stratification was analysed with full-depth time series of conservative temperature, absolute salinity and potential density. Surface chlorophyll-a time series were analysed and used as an indicator of phytoplnakton biomass. The analysis was complemented with in situ nutrient data. Re-

sults for spring 2014 indicate stratification strengthened due to positive (into the sea) net heat flux after the 31st of March, leading to a relatively weak spring bloom until the 12th of April when surface chlorophyll-a fluorescence decreased. On the 25th of April intensified wind stress and an event of heat loss eroded stratification in the upper 60 m. Nutrients below the pycnocline were introduced into the surface mixed layer and resulted in a second bloom event which was greater than the first. During spring 2015 the onset of stratification was triggered by positive net heat flux on the 26th of March. However, in the early stages of the stratified period, despite the positive net heat flux, temperature above and below the pycnocline decreased and increased, respectively and led to colder waters occupying the upper 70 m. Wind-driven transport introduced colder and fresher waters above the pycnocline. Thus stability of the water column was maintained by the vertical distribution of salinity triggering phytoplankton growth in the absence of stable thermal stratification.

5.1 Introduction

The onset and maintenance of stratification of the water column is vital for biological processes in shelf seas, such as phytoplankton growth (Pingree et al., 1977). In winter the Celtic Sea is mixed due to heat loss combined with tidal and wind stress (Simpson, 1981; Wihsgott et al., 2019) resulting in a homogeneous distribution of nutrients in the water column (Pingree et al., 1976; Ruiz-Castillo et al., 2018; Chapter 2). The general view is that during spring positive net heat flux overcomes mixing leading to stratification of the water column and therefore controlled by temperature (Pingree et al., 1976 and 1977; Wihsgott et al., 2019). However, stratification may be maintained by the vertical distribution of salinity, with relatively high salinity waters in the bottom, as seen in Chapter 4 and later on in this chapter. Once the water col-

umn stabilises primary productivity is enabled within the euphotic zone (Pingree et al., 1977; Garcia-Martin et al., 2017; Carr et al., 2018) until nutrients are depleted in the surface mixed layer (Pemberton et al., 2004; Davis et al., 2014; Poulton et al., 2018). Following nutrient depletion phytoplankton biomass decreases (Pingree et al., 1976; Fasham et al., 1983). This event of sudden growth of phytoplankton in spring is known as the spring bloom and indicates the onset of primary productivity (Rees et al., 1999). It is thought that secondary production of higher trophic levels depends upon the duration and timing of these relatively short spring bloom events (Townsend et al., 1994). Following the spring bloom, throughout summer relatively weak but sustained primary productivity occurs within the pycnocline or nitracline (Hickman et al., 2012; Carr et al., 2018). Nutrients are supplied from the bottom layer by diapycnal flux as a response to variations in internal tidal (Sharples et al., 2001) and wind stress (Williams et al., 2013) forcing. Furthermore, during enhanced wind stress events, surface mixing may reach and deepen the pycnocline and entrain nutrients from the bottom mixed layer and promote primary productivity (e.g. Davis et al., 2014). In autumn, heat loss and intensified winds deepen the pycnocline (Wihsgott et al., 2019) and resupply surface waters with nutrients from the bottom layer (Ruiz-Castillo et al., 2018) leading to autumn bloom events (Pingree et al., 1976; Garcia-Martin et al., 2017; Carr et al., 2018; Wihsgott et al., 2019).

The Celtic Sea is a highly productive region (Seguro et al., 2017). Therefore understanding the driving mechanisms controlling the onset and evolution of stratification is essential to elucidate the processes governing its high productivity. In this chapter the onset and evolution of stratification in the spring of 2014 and spring 2015 are analysed and utilised to

explain variability in the surface chlorophyll-a fluorescence signal (Fig. 5.1). Results indicate that the simple view of surface heat supply does not always explain how spring stratification is triggered and maintained.

5.2 Methods

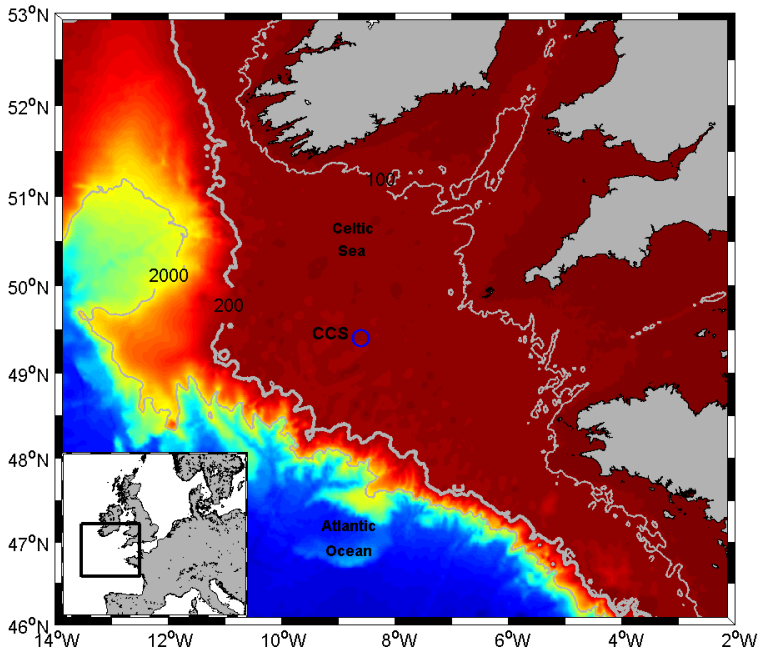

Figure 5.1: Map of the Celtic Sea. Blue circle indicates the location of the Central Celtic Sea mooring. Map in colour represents the bathymetry of the study area with warmer colours indicating relatively shallow regions.

5.2.1 Hydrographic data

At the Central Celtic Sea site (Fig. 5.1) full depth time series of temperature and salinity from moored instruments (Wihsgott et al, 2016) were used to elucidate the mechanisms driving the onset of stratification and the hydrographic variability in the years 2014 and 2015. Time series were interpolated on regular grids with a temporal and spatial resolution of 5 minutes and 2.5 metres. A detailed description on how data were

processed is provided in the previous chapters and in Wihsgott et al. (2016). Conservative temperature, absolute salinity and potential density were calculated (McDougall and Barker, 2011). This chapter focuses on long-term fluctuations, greater or equal to a cycle per day to include the daily fluctuations caused by day and night cycles. Thus, the semi-diurnal signals associated with tidal currents were disregarded by using a low-pass Lanczos filter at each depth with a cut-off frequency of 24^{-1} h^{-1} (Thompson and Emery, 2014). The times analysed in this chapter cover from the 26th of March 2014, when the record started, until the 1st of June 2014 and from the 15th of March 2015 to the 1st of June 2015 (late winter-spring). In the second period there is a 7 day gap between the 5th and 12th of April due to instruments being serviced, thus CTD casts carried out during a research cruise in the Central Celtic Sea were utilised to complement the hydrographic time series.

5.2.2 Horizontal velocities

Horizontal current profiles at the Central Celtic Sea were used to estimate transport. Time series of horizontal velocities from near the bottom up to 20 m depth were recorded from the 26th of March 2014 to the 25th of July 2015. As with temperature and salinity time series, horizontal velocities were interpolated on a regular grid with a temporal and spatial resolution of 5 minutes and 2.5 m, respectively (Wihsgott et al., 2018). As with the hydrographic time series, at each depth a low-pass Lanczos filter was used with a cut off frequency of 24^{-1} h^{-1} (Thompson and Emery, 2014). In contrast to the temperature and salinity time series in the winter-spring 2014 only current data between the 26th of March and 6th of May were analysed due to failure of the battery. For the winter-spring 2015 horizontal velocities were analysed between the 15th of March and the 1st of June 2015.

The depth-averaged flow ($\bar{\mathbf{u}}$) was calculated from the filtered velocities ($\mathbf{u}$) in the form:

$$\bar{\mathbf{u}} = \frac{1}{H}\int_{H}^{0} \mathbf{u} dz \tag{5.1}$$

To assess the velocity anomalies ($\mathbf{u_c}$) (Fig. 5.2 and 5.3) the depth-average flow ($\bar{\mathbf{u}}$) was removed at each time step:

$$\mathbf{u_c} = \mathbf{u} - \bar{\mathbf{u}} \tag{5.2}$$

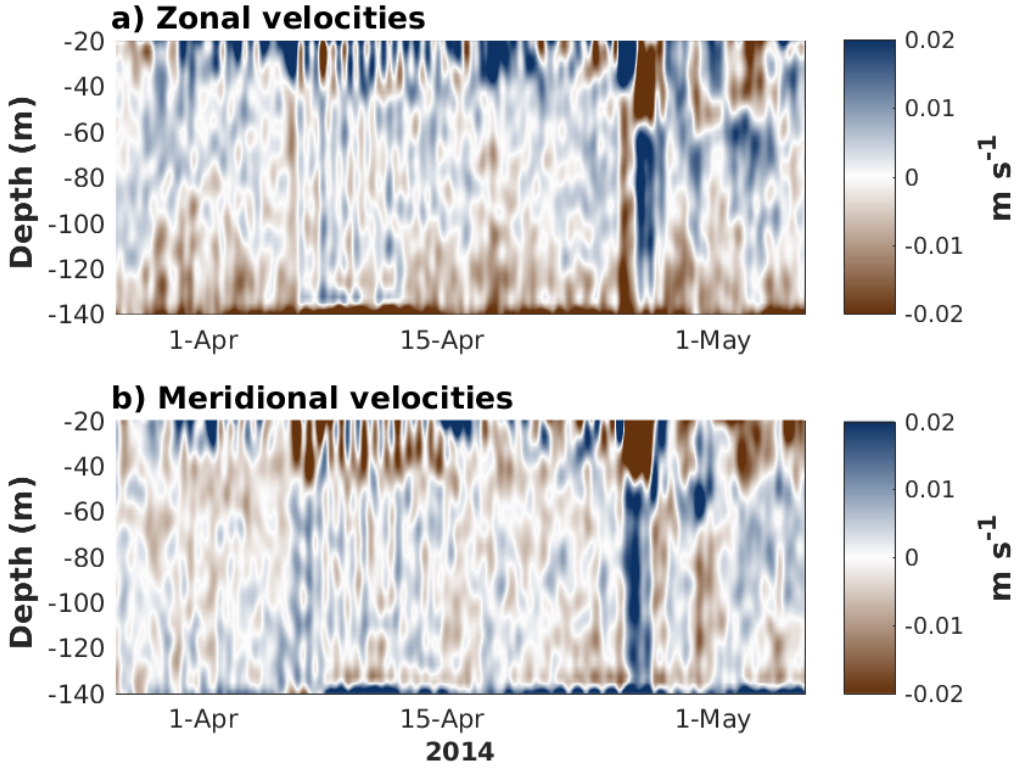

Figure 5.2: a) Zonal and b) meridional component of the velocity anomalies in spring 2014. Positive values indicate eastward and northward flow.

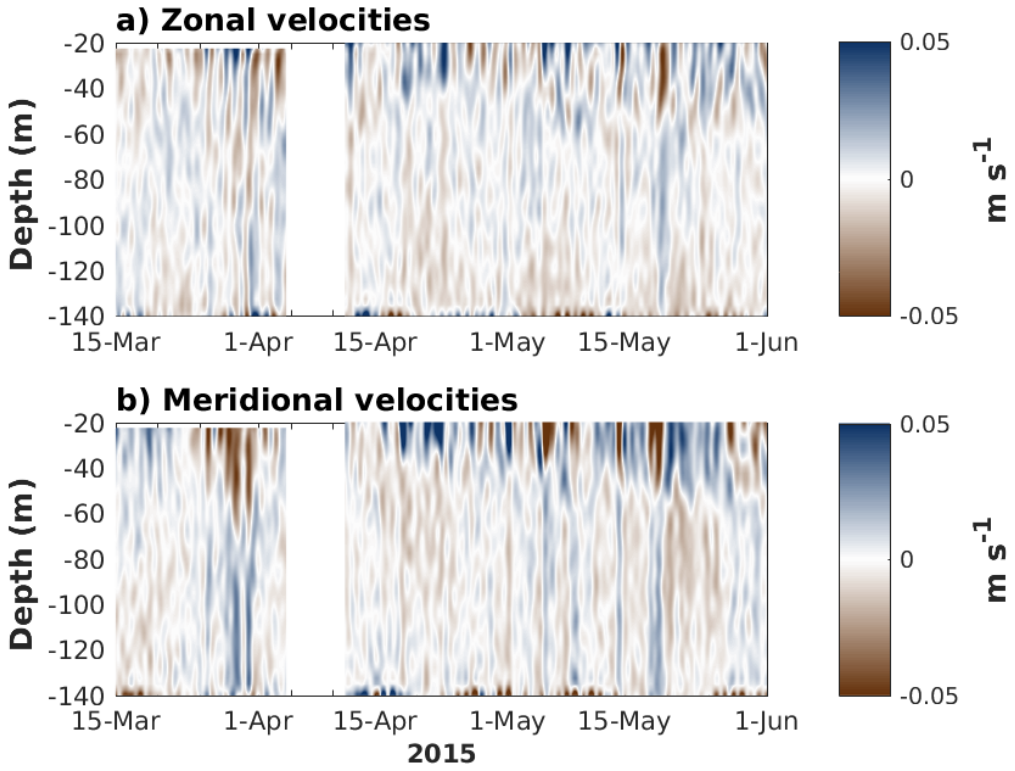

Figure 5.3: a) Zonal and b) meridional component of the velocity anomalies in spring 2015. Positive values indicate eastward and northward flow.

5.2.3 Wind-driven transport

The effects of the wind stress on the water column were analysed using wind data recorded every hour by a meteorological buoy. Wind data was averaged every 48 hours, therefore, only fluctuations greater than the inertial and semidiurnal frequencies were considered. As in previous chapters the zonal (U_w) and meridional (V_w) component of the Ekman transport were calculated in the form:

$$-fV_w = \frac{\tau_x}{\rho_s} \tag{5.3}$$

$$fU_w = \frac{\tau_y}{\rho_s} \tag{5.4}$$

where ρ_s and f represent the surface density and the rotational frequency of the Earth, respectively. The zonal and meridional components of the

wind stress were estimated as:

$$\tau_x = \rho_a Cd|\mathbf{u_w}|u_w \tag{5.5}$$

$$\tau_y = \rho_a Cd|\mathbf{u_w}|v_w \tag{5.6}$$

where u_w and v_w represent the zonal and meridional components of the wind velocity at 10 m above the sea surface. The air density (ρ_a) was assumed to be constant at 1.3 kg m^{-3} and the drag coefficients (Cd) were estimated following Smith and Banke (1975) as in the previous chapters.

5.2.4 Transport in surface layer

The velocity anomalies ($\mathbf{u_c}$) were used to assess the effects of wind-stress on transport in the surface layer. For winter-spring 2014 hydrographic time series indicate the surface layer occupied the upper ∼30 m of the water column. In contrast, hydrographic time series indicate that the surface layer occupied at least the upper 40 m of the water column between the 15th of March and the 5th of April 2015 and the upper 30 m in the period 12th of April-1st of June. For the period 15th of March-5th of April time series of velocity anomalies between 20 and 40 m were used to calculate the averaged velocity ($\bar{\mathbf{u}}_\mathbf{c}$) in the surface layer. For the other periods averaged velocity in the surface layer was estimated using the velocity anomalies time series between 20 and 30 m depth. Therefore, transport in the surface layer was calculated as follows:

$$\mathbf{U} = \bar{\mathbf{u}}_\mathbf{c} h \tag{5.7}$$

where h indicates 30 for the periods March-June 2014 and 12 April -1 of June 2015 and 40 m for the period 15 of March-5 of April; $\bar{\mathbf{u}}_\mathbf{c}$ was defined

as:

$$\bar{\mathbf{u_c}} = \frac{1}{h}\int_h^{20} \mathbf{u_c} dz \tag{5.8}$$

Time series of wind-driven Ekman transport and transport in the surface layer were compared through a Pearson correlation coefficient as described in detail in Chapter 3.

5.2.5 Net heat flux

To analyse the different meteorological agents competing in the onset and maintenance of stratification the net heat flux was calculated in the Central Celtic Sea. Heating and cooling of the water column depend on heat transfer, particularly absorption of solar energy or shortwave radiation (Q_s), evaporation (Q_L), conduction (Q_c), back radiation from the sea surface (Q_b) and horizontal advection of heat (Q_v) (Lynne et al., 2011; Simpson and Sharples, 2012). The combination of these processes leads to the total or net heat flux (Q_T) and is positive when the water column gains heat and negative when it loses heat. The contribution of each process to the heat budget can be resumed in the form:

$$Q_T = Q_s - (Q_b + Q_L + Q_c) + Q_v \tag{5.9}$$

For the analysis in this chapter time series of relative humidity, sea surface temperature, air pressure, wind speed and air temperature recorded by a meteorological buoy at Central Celtic Sea were combined with net surface solar radiation and cloud cover time series obtained from ERA-interim (Dee et al., 2011). An explanation on how each term in eq. (5.9) was calculated from bulk formulae is described below.

Shortwave heat flux (Q_s)

The first term on the right hand side of eq. (5.9) represents the solar radiation that is absorbed by the water column and is always positive. The net shortwave heat flux was estimated following (Gill, 1982; Sharples and Simpson, 2012):

$$Q_s = Q_i\,(1 - A) \tag{5.10}$$

where Q_i is the net amount of solar radiation that reaches the surface and A is the fraction reflected from the sea surface known as albedo. Time series of net heat flux between the 27th and 29th of March 2014 were compared with changes in temperature in the surface mixed layer to determine the value of albedo that better fits the observations. Albedo has been previously estimated to be 0.06 (James and Holt, 1999). Heat loss in the surface layer estimated from hydrographic data was 23 W m^{-2} and using eq. (5.9) with an albedo coefficient of 0.06 - 0.12 leads to a heat loss of 16 - 23.5 W m^{-2}. Thus the albedo was set constant at 0.12.

Back radiation (Q_b)

The gain or loss of energy by back radiation depends on the upward radiation from the sea surface and the returned radiation from the atmosphere back to the ocean. The atmosphere and the sea radiate as black bodies proportionally to the fourth power of their temperatures according to the Stephan-Boltzmann Law (Lynne et al., 2011; Simpson and Sharples, 2012). Thus, following Josey et al. (1999) back radiation (Q_b) was estimated as:

$$Q_b = \varepsilon\gamma_{SB}T_w^4\left(0.39 - 0.05\,(0.01E_wR_h)^{\frac{1}{2}}\right)\left(1 - kC^2\right) + 4\varepsilon\gamma_{SB}T_w^3\,(T_w - T_a) \tag{5.11}$$

where the emittance of the sea surface (ε) was set constant at 0.985 (Holt and James,1999), γ_{SB} is the Stefan-Boltzmann constant (5.67×10^{-8} W

m^{-2} K^{-4}), and are the water and air temperature in degrees Kelvin, k is a latitude-dependant cloud cover coefficient, which increases with latitude and was fixed at 0.73 (Josey et al., 1999), R_h is the relative humidity (%) and C is the fraction of total cloud cover at the Central Celtic Sea. The saturated vapour of pressure (E_w in mbar) can be estimated following James and Holt (1999) and Sharples et al. (2006) in the form:

$$\log_{10} E_w = \frac{0.7859 + 0.03477 T_w}{1.0 + 0.00412 T_w} \tag{5.12}$$

Latent heat flux (Q_L)

The latent or evaporative heat flux implies a loss of heat from the sea surface to the atmosphere. The rate of heat loss is defined as (Lynne et al., 2011; Simpson and Sharples, 2012):

$$Q_L = E_v L_H \tag{5.13}$$

where E_v is the rate of evaporation in kg s^{-1} m^{-2} is the latent heat of evaporation in kiloJoules. For pure water, the latent heat depends on its temperature (^{o}C) $L_H = (2494 - 2.2T)$ $(\frac{kJ}{kg})$ (Lynne et al., 2011). Overall, in the ocean much of the evaporation depends on the diffusion produced by the wind (Lynne et al., 2011) and therefore a semi-empirical formula that depends on the wind speed was used following Holt and James (1999) and Sharples et al. (2006):

$$Q_L = 0.62 \left(1.5 \times 10^{-3}\right) \rho_a w \left(q_w - q_a\right) L_H \tag{5.14}$$

where w is the wind speed, ρ_a is the air density and was set constant at 1.3 kg m^{-3} and L_H is $2.5{\times}10^{-6}$-$2.5{\times}10^{3} T_w$ in J kg^{-1}. Using the saturated vapour pressure of water (E_w) and the vapour pressure of water (E_a), q_w

and q_a were estimated as:

$$q_w = \frac{E_w}{P - 0.38E_w} \tag{5.15}$$

where P is air pressure (mbar). The vapour of pressure of water (E_a) is related to E_w as follows:

$$E_a = 0.001E_wR_h \tag{5.16}$$

Sensible heat flux (Q_c)

Sensible heat flux arises from the differences in temperature between the sea surface and the air above the sea and therefore the gain or loss of heat is proportional to the vertical thermal gradient. For the Central Celtic Sea the sensible heat flux was estimated from (Holt and James, 1999; Sharples et al., 2006):

$$Q_c = c_h\rho_a c_{\rho a} w\,(T_w - T_a) \tag{5.17}$$

where c_h is the Stanton number (1.45×10^{-3}), $c_{\rho a}$ is the specific heat of air (1004 J kg^{-1} k^{-1}) and T_w and T_a are the temperature in Kelvin degrees of the sea surface and air, respectively.

This chapter focuses on the role of positive net heat flux across the surface in the onset of stratification. Therefore the last term (Q_v) in eq. (5.9) was omitted. The annual cycle of the different components of the heat flux across the sea surface at Central Celtic Sea is shown in Fig. 5.4.

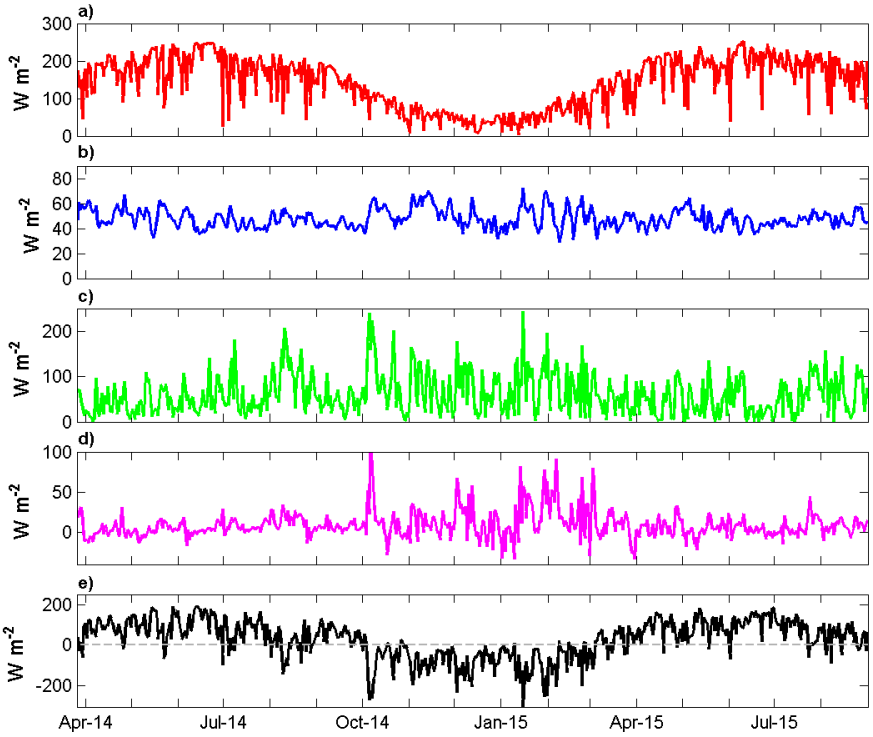

Figure 5.4: Heat fluxes of a) surface net solar radiation, b) back radiation, c) latent heat, d) sensible heat and e) net heat flux.

5.2.6 Chlorophyll *a*

Time series of chlorophyll a fluorescence (Chl-a, hereinafter) measured wiht a Seapoint Chlorophyll Fluorometer at the surface of the Central Celtic Sea site by a Cefas smartbuoy were used to assess the evolution and decay of the spring bloom during 2014 and 2015. Data was recorded every 30 min. The Seapoint Chlorophyll Fluorometer was standarised to arbitrary fluorometry units using fluorescent sulphate microspheres after each deployment at the Cefas laboratories to correct for instrument drift. To disregard quenching only data recorded at night was used. Further details on how the Chl-*a* was processed can be found in Wihsgott et al. (2019). The periods analysed in this chapter cover from the 26th of March to the 1st of June 2014 and from the 5th of March to the 1st of June 2015.

5.2.7 Nutrients

The vertical distribution of the nutrients, nitrate + nitrite, ($NO_3 + NO_2$), referred to nitrate hereinafter, was used to complement the analysis and quantify potential nitrate supply from below the pycnocline to the surface layer. Water samples were collected during a series of research cruises in March 2014 and March, April and May 2015 at Central Celtic Sea and analysed for dissolved inorganic nutrients. Details on how nutrients were analysed can be found in Chapter 2, Woodward (2016) and Poulton et al. (2018).

5.3 Results

5.3.1 Spring 2014

The effects of heat input and the wind on the hydrography of the water column at the Central Celtic Sea are shown in Figure 5.5. Averaged heat loss to the atmosphere occurred between the 27th and 30th of March (Fig. 5a). Afterwards, positive heat flux was persistent until the 25th of April when the water column briefly lost heat to the atmosphere. Following this heat loss event heat input to the water column continued until the 21st -24th of May when a second event of negative heat flux was observed. Before the period of constant positive heat flux (27th-30th of March) westward winds were observed (Fig. 5.5b). During the beginning of constant heat input period, between the 31st of March and 2nd of April, northward winds occurred and turned eastward between the 2nd-10th of April. Overall, throughout the record winds were aligned mainly along the east-west direction. Three events of intensified wind stress were observed on the 25th-27th of April ($\sim$0.23 kg m^{-1} s^{-2}), 12th-17th of May ($\sim$0.18 kg m^{-1} s^{-2}) and 22nd-24th of May ($\sim$0.15 kg m^{-1} s^{-2}) (Fig. 5.5c). Throughout the record the time series of the zonal com-

ponent of transport in the surface layer were not coherent with Ekman transport (Fig. 5.5d) except for the period 27th of March -5th of April 2014 when northward winds occurred and led to a strong correlation (R^2=0.85). The northwards winds generated a weak eastward flow (0.5 m^2 s^{-1}) after the 30th of March. Transport in surface layer and Ekman transport were strongly correlated with each other (R^2=0.77) (Fig. 5.5e). Before the 31st of March a weak northward wind-driven flow occurred (0.3 m^2 s^{-1}) (Fig. 5.5e) and turned eastward between the 31st of March and 2nd of April. Afterwards, between the 2nd and 10th of April a weak southward wind driven flow occurred (0.3 m^2 s^{-1}). The strong westerly wind event (Fig. 5.5b) between the 25th and 27th of April was reflected on the maximum southward transport (>0.5 m^2 s^{-1}).

In the water column the 9.5^{o}C isotherm indicated a two layer system between the 27th and 30th of March (Fig. 5.5f). Temperature in the upper 30 m increased consistently from <9.6^{o}C to >11^o C from the 30th of March to the 25th of April when temperature decreased to ∼10.5^{o}C. The thermocline deepened from 30 to 55 m depth introducing colder waters from the bottom layer and homogenised waters around 10.5 ^{o}C in the upper 55 m. From the 1st of May onwards temperature in the upper 30 m increased from 10.5^{o}C to >12^{o}C by the end of May. The water column was homogenous in salinity before the 2nd of April (∼35.47 g kg^{-1}) (Fig. 5.5g). Afterwards, relatively low salinity (<35.46 g kg^{-1}) in the upper 30 m coincided with westerly wind events in the periods 2nd-10th of April, 27th April-4th of May and 20th of May-1st of June. In contrast, increases in salinity above 30 m depth were observed between the 13th and 20th of April during an easterly wind event. The vertical distribution of temperature and salinity was reflected on density time series (Fig. 5.5h). The water column was stratified before the 27th of March 2014

with the 27.27 kg m^{-3} contour marking the interface between the surface and bottom layers. The inclination of the 27.25 kg m^{-3} density contour, reaching minimum depths on the 30th of March, indicates stratification diminished in the upper 40 m depth. In the period 30th of March-2nd of April salinity remained constant and therefore intensification of stratification was governed by increases in temperature. Afterwards stratification strengthened until the 25th of April when density decreased. As with temperature, the pycnocline deepened down to 55 m and introduced denser waters from below the pycnocline to the surface mixed layer. Between May and June stratification enhanced and mirrored the vertical distribution of temperature. The effects of the relatively strong events of wind stress on the 10th of May delayed the occurrence of waters with densities below 26.9 kg m^{-3} until the 15th of May.

The onset and evolution of stratification was reflected on Chl-*a* time series (Fig. 5.5i). Concentration of Chl-*a* before the 30th of March was at its minimum ($\sim$1 mg m^{-3}) and gradually increased from the 31st of March onwards and peaked (6 mg m^{-3}) between the 10th and 12th of April. As stratification intensified chl-*a* concentration decreased to $\sim$2.5 mg m^{-3} and remained constant from the 15th to the 25th of April. A second peak in Chl-*a* was observed from the 25th of April until the 2nd of May when concentrations reached values above 9 mg m^{-3} and were greater than the first peak.

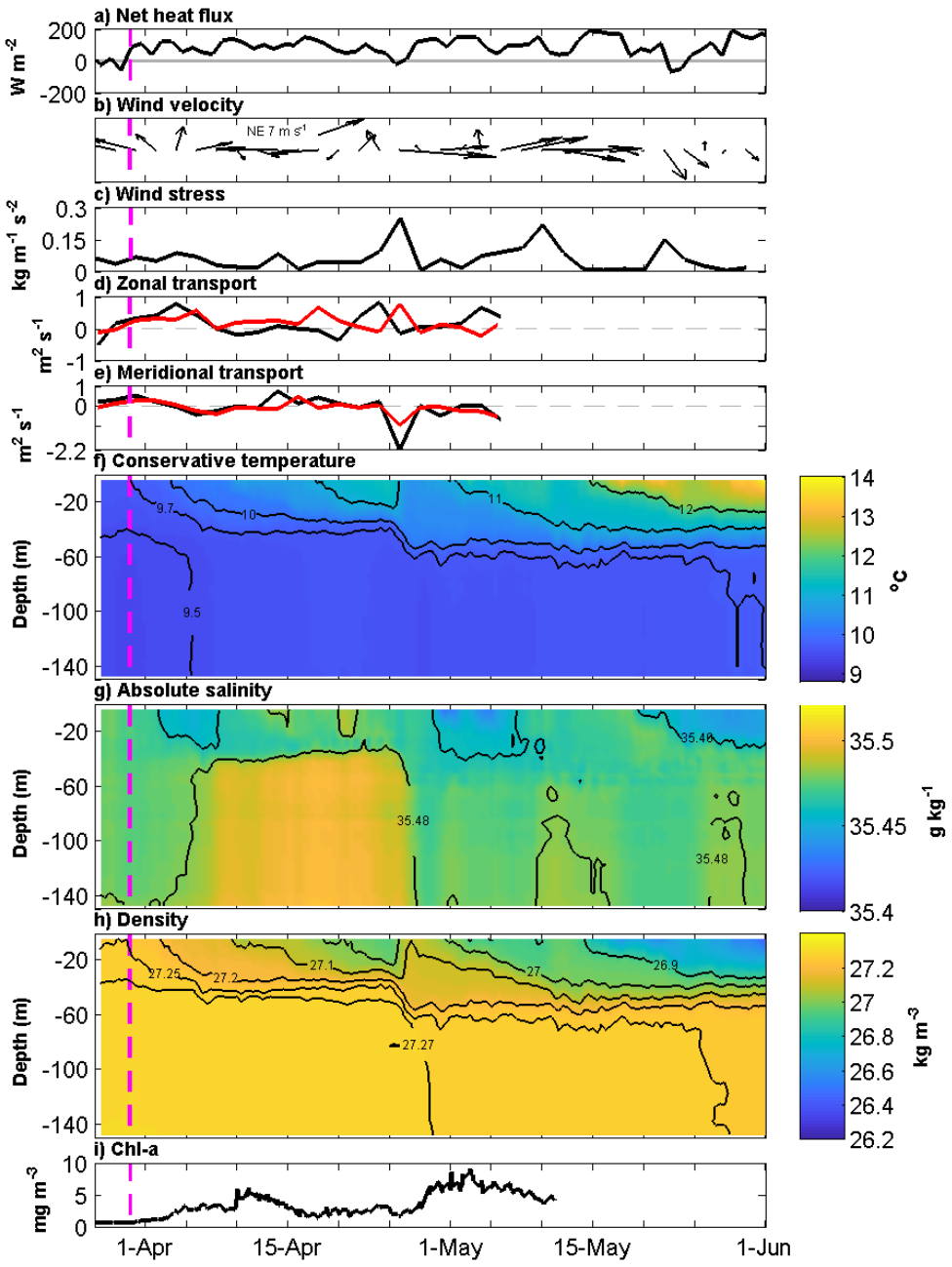

Figure 5.5: Time series between the 27th of March and 1st of June 2014 of a) Net Heat flux b) wind velocity, c) wind stress, d) zonal and e) meridional surface (red) and Ekman transport (black), f) Absolute salinity, g) conservative temperature, h) density, i) Chl-a concentration. Magenta lines indicate the start of constant heat input.

5.3.2 Spring 2015

The effects of the net heat flux and wind stress on the hydrographic conditions of the water column are shown in Figure 5.6. Positive net heat flux was observed between the 16th and 24th of March and was followed

by a heat loss event until the 26th of March (Fig. 5.6a). From the 26th of March onwards, positive net heat flux occurred with a relatively short event of heat loss (1-2 days) on the 18th of April.

Prior to the period of sustained positive net heat flux, northerly winds were observed between the 17th and 26th of March 2015 (Fig. 5.6b). Westerly winds occurred from the 26th of March until the 4th of April and coincided with the beginning of the constant positive net heat flux (Fig. 5.6b). Overall, winds were aligned along the zonal axis with westerly winds being dominant in the periods 3rd-10th of May and 15th-31st of May. In contrast easterly winds occurred in the periods 5th-11th of April, 14th-24th of April, and 28th of April- 2nd of May. Relatively weak wind stress (0.1 kg m^{-1} s^{-2}) occurred during the event of heat loss between the 24th and 26th of April (Fig. 5.6c) and was followed by intensified wind stress (0.26 kg m^{-1} s^{-2}) in the period 26th of April- 1st of May. Transport in the surface layer was coherent with variability in the wind stress. For instance, before the 5th of April strong correlations were found between the surface and Ekman transport of R^2=0.7 and R^2=0.92, for the zonal and meridional components respectively, indicating transports in the upper 40 m were mainly wind-driven (Fig. 5.6d and e). Maximum southward transport (1 m^2 s^{-1}) in the surface layer occurred from the 26th of March to the 4th of April (Fig. 5.6e) and was consistent with the maximum wind stress (Fig. 5.6c). After the 12th of April fluctuations observed in zonal surface transport were not consistent with zonal Ekman transport, as winds were mainly aligned along the east-west direction (Fig. 5.6d). In contrast fluctuations in transport in the surface layer and Ekman transport were strongly correlated (R^2=0.74), influenced by these east-west aligned winds.

In the water column between the 17th and 24th of March short daily increases of temperature above 10^{o}C were observed in the upper 25 m (Fig. 5.6f). Nonetheless, homogenisation of the water column occurred promptly during the night until the period 26th- 29th of March when temperature in the upper 60 m increased and remained above 10^{o}C. Subsequently from the 29th of March until the 5th of April temperature decreased below 10^{o}C in the top 70 m. In contrast, in the bottom 70 m temperature remained above 10^{o}C in the periods 29th of March-2nd of April. From the 11th of April until the 1st of June temperature gradually increased from 10^{o}C to >12^{o}C in the upper 30 m compared to 10-10.5 ^{o}C in the bottom mixed layer.

Salinity time series indicate that the water column was homogeneous in the period 15th- 26th of March (<35.53 g kg^{-1}) (Fig. 5.6g). Between the 28th-29th of March and the 6th of April fresher waters, with salinity below 35.53 g kg^{-1}, occurred. As in the previous year, in the surface layer relatively low salinity waters in the periods 30th of April- 5th of May, 11th - 17th of May and 18th - 24th of May coincided with westerly wind events. In contrast increases in surface salinity and fresher waters below 35.48 g kg^{-1} in the bottom 100 m between the 17th and the 23rd of April were generated by easterly wind events.

The evolution of stratification and the effects on salinity and temperature are observed in the density time series (Fig. 5.6h). Increases in temperature between the 15th and 23rd of March were reflected in density decreases in the upper 25 m. Deepening of the 27.24 kg m^{-3} contour indicates stratification at Central Celtic Sea started on the 26th of March. Despite the gap in the time series, CTD data indicates the vertical distribution of density between the 5th and 11th of April persisted. From

the 11th of April until the 1st of June the vertical distribution of density resembled the temperature time series. Density in the surface layer gradually diminished from >27.24 kg m^{-3} in late-March 2015 to <26.9 kg m^{-3} in June 2015.

The minimum concentration of surface Chl-*a* ($\sim$1 mg m^{-3}) occurred between the 15th and 26th of March (Fig. 5.6i). After the 26th of March, when the stratified period began (Fig. 5.6h), chl-*a* gradually increased and reached a maximum (>10 mg m^{-3}) between the 12th and 19th of April with peaks above 5 mg m^{-3} until the 26th of April. Afterwards chl-*a* concentration gradually diminished and reached minimum values around 1 mg m^{-3} on the 1st of June.

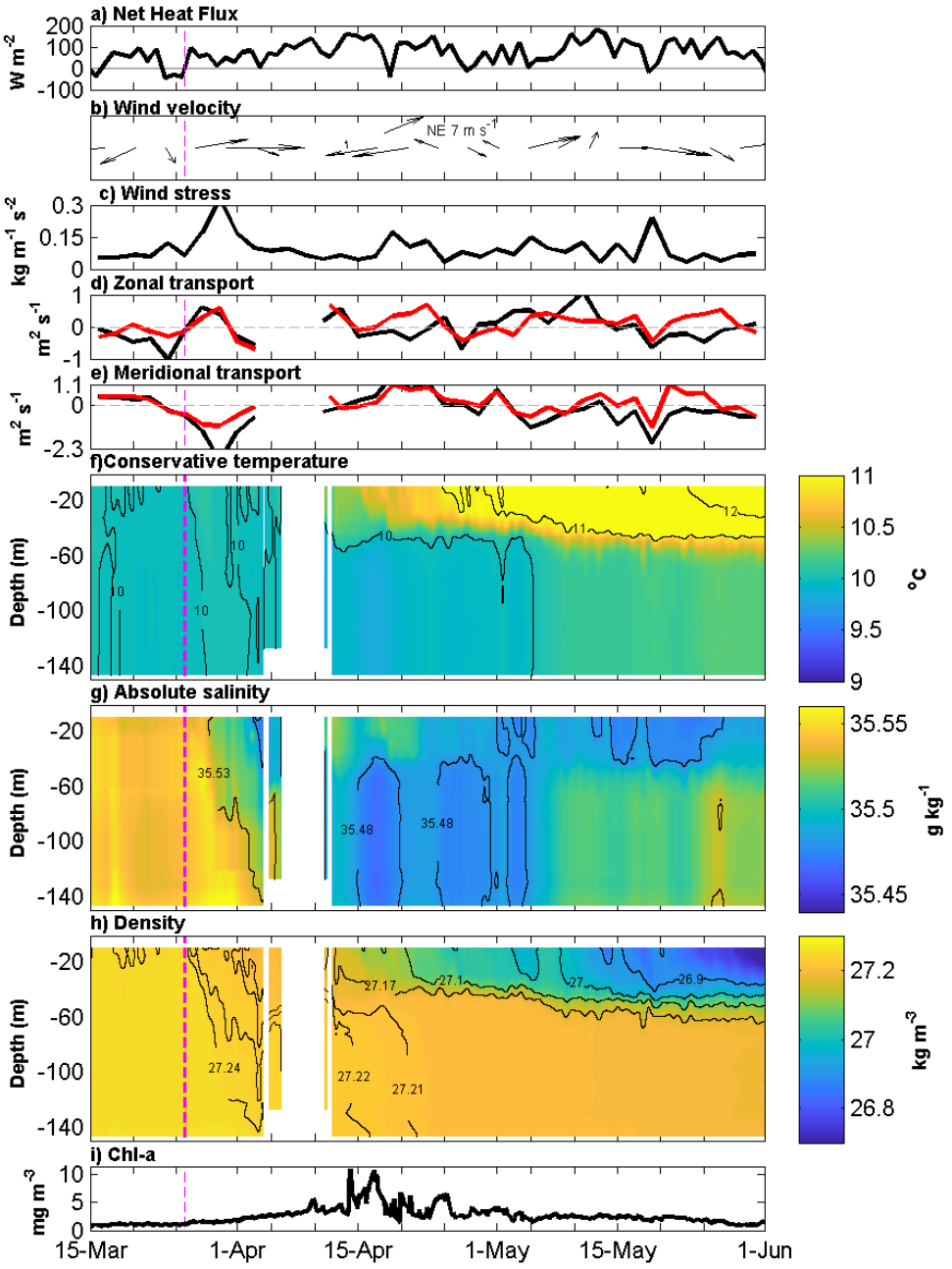

Figure 5.6: Time series between the 15th of March and 1st of June 2015 of a) Net Heat flux b) winds velocity, c) wind stress, d) zonal and e) meridional surface (red) and Ekman transport (black), f) Absolute salinity, g) conservative temperature, h) density, i) Chlorophyll-a concentration. Magenta lines indicate the period of constant heat input.

5.4 Discussion

5.4.1 Spring 2014

Stratification

The vertical distribution of temperature and density indicate stratification in the Central Celtic Sea started before the 26th of March 2014, as described by the 9.5^{o}C isotherm and the 27.27 kg m^{-3} density contour at ∼50 m depth (Fig. 5.5f and h). Between the 27th and 29th of March a heat loss event occurred (Fig. 5.5a), and averaged over the 3 days accounted for 23 W m^2. In the water column temperature decreased in the upper ∼50 m ∼0.02^{o}C leading to a 23 W m^{-2} heat loss (Fig. 5.7a), being similar to the net heat flux across the surface. Therefore, cooling in the upper 50 m of the water column was generated by the atmospheric heat loss event and resulted in surface outcropping of the 27.25 kg m^{-3} density contour (Fig. 5.5h).

Coinciding with this heat loss event, easterly winds were observed between the 27th and 29th of March (Fig. 5.5b) and led to a weak northward surface transport (<0.25 m^2 s^{-1}) with a compensating southward flow in the bottom layer. Prior to the onset of stratification a horizontal gradient in the Celtic Sea resulted in warmer waters at the shelf edge due to faster cooling on shelf (Chapter 4). Therefore colder waters reached the Central Celtic Sea site in the bottom ∼100 m due to wind-driven transport leading to a decrease in temperature of ∼0.02^{o}C (Fig. 5.7a). A comparison between the thicknesses of the surface (∼50 m) and bottom (∼100 m) layers indicate horizontal advection of heat in the bottom was double the heat loss in the surface layer. Hence, in the early stages of stratification horizontal advection has further implications for heat transfer as will be described later for spring 2015.

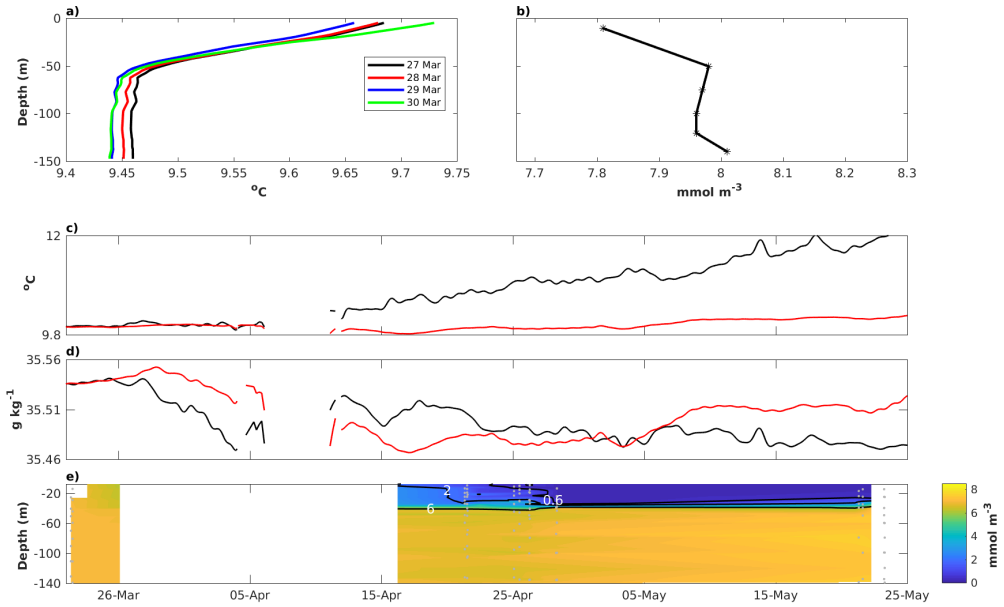

Figure 5.7: Profiles of a) daily averaged temperature between the 27th and 30th of March 2014 and b) nitrate (NO_2+ NO_3) on the 27th of March 2014. Top (black) and bottom (red) time series in spring 2015 of c) temperature and d) salinity and e) Hovmöller diagram of nitrate (NO_3 +NO_2).

A period of constant positive net heat flux began on the 30th of March 2014 and enhanced stratification of the water column. Between the 30th of March and the 2nd of April heat input coincided with southerly winds leading to a eastward wind-driven Ekman transport and a compensatory westward flow in the bottom resulting in negligible cross-shelf advection of salinity and temperature (e.g. chapter 4). Thus, there were no changes in salinity or temperature. Afterwards intensification of the stratification in the upper 30 m was controlled by positive net heat flux despite wind-driven dynamics advecting fresher and relatively high salinity waters across the shelf in the surface and bottom layers. Hence temperature controlled the vertical distribution of density (Brown et al., 2003) and established a pycnocline at ∼35 m which gradually intensified until the 25th of April when a combination of heat loss on the 25th of April (Fig. 5.5a) with enhanced wind stress (Fig. 5.5c) between the 23th and 27th of April mixed the surface layer and deepened the pycnocline up to ∼55 m as described in Wihsgott et al. (2019). Subsequently from the 1st of

May onwards, consistent with positive net heat flux, stratification within the surface layer was re-established.

Implications for phytoplankton growth

Intensification and weakening of stratification had further consequences on phytoplankton growth (e.g. Pingree et al., 1977; Seguro et al., 2017). For instance, the concentration of chl-a prior to the beginning of constant heat input was a minimum around 1 mg m^{-3} despite the water column being stable prior to the 27th of March (Fig. 5.5h). Based on the spring 2015, concentration in chl-a increased 1 mg m^{-3} in 6 days after stratification began (Fig. 5.6i). Potentially, for the spring 2014 stratification of the water column had recently started (Fig.5.5h) resulting in a negligible growth of phytoplankton. With the beginning of consistent positive net heat flux from the 30th of March, a sudden increase in chl-a concentration, up to $\sim$6 mg m^{-3} on the 12th of April, occurred indicating the onset of the spring bloom in the Celtic Sea (e.g. Pingree et al., 1976; Garcia-Martin et al., 2017; Seguro et al., 2017; Wihsgott et al., 2019) whilst nutrients were still available (e.g. Pingree et al., 1976). Following this, the maximum peak concentration of chl-a decreased to 3 mg m^{-3} on the 17th of April, suggesting mortality of phytoplankton due to grazing and nutrients in the surface layer being depleted (Pingree et al., 1976; Poulton et al., 2018). Thus the spring bloom in 2014 lasted $\sim$21 days, a time well aligned with previous observations (Rees et al. 1999). Chl-a concentration remained constant ($\sim$3 mg m^{-3}) until the 25th of April when a combination of enhanced wind stress (Fig. 5.5d) (Whisgott et al., 2019) and heat loss (Fig. 5.5a) deepened the surface layer similar to a storm described in Davis et al. (2014). Consequently nutrients were supplied above the pycnocline from the upper 20 m of the bottom layer. The amount of nitrate(NO_2+ NO_3) introduced into the surface layer can

be estimated from a nitrate profile obtained on the 27th of March (Fig. 5.7b) and accounting for a 0.3 mmol m^{-3} nitrate increase by the 25th of April 2014 due to cross-shelf transport and remineralisation (Fig. 12b in Ruiz-Castillo et al., 2018; Chapter 2). On the 27th of March in the bottom 105 m the averaged nitrate concentration was ∼7.97 mmol m^{-3} and increased to 8.3 mmol m^{-3} by the 25th of April. Therefore a total budget of 871 mmol m^{-2} was observed in the bottom mixed layer before the mixing event (Fig. 5.8, left panel). Waters from the upper 20 m below the pycnocline were introduced into the surface layer and supplied the surface layer with ∼166 mmol m^{-2} which averaged over a layer with a thickness of ∼50 m yielded in 3.3 mmol m^{-3} of nitrate in the upper 50 m (Fig. 5.8, right panel). As a consequence of the mixing event on the 27th of April the concentration of chl-*a* increased and reached a maximum of ∼9 mg m^{-3} on the 3rd of May and suggests a second phytoplankton bloom, which was greater than the previous spring bloom. The concentration of nitrate introduced (∼3.3 mmol m^{-3}) into the surface layer on the 25th of April, compared to the background concentration prior to the spring bloom (7.9 mmol m^{-3}), suggests a greater efficiency of phytoplankton in assimilating the nutrients introduced from the bottom mixed layer. Nonetheless, it occurred later when more light was available. Finally, from the 3rd of May onwards chl-*a* concentration gradually decreased in the surface layer due to grazing and depletion of nutrients (Poulton et al., 2018).

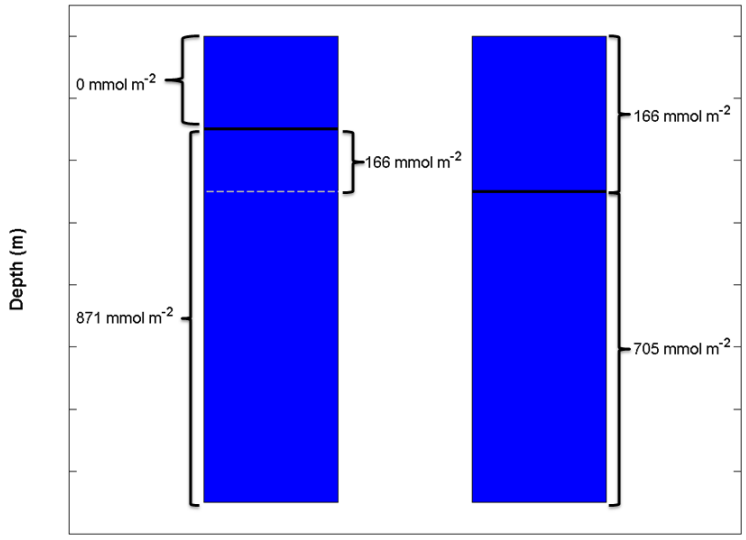

Figure 5.8: Nitrate concentration in the surface and bottom layer before (left column) and after (right column) the enhanced wind stress event. Black line represents the pycnocline.

5.4.2 Spring 2015

Stratification

In shelf seas, far from the coastal domain, the beginning and maintenance of the stratified period is thought to be governed by a competition between heat input and mixing caused by tidal and wind stress (Atkinson and Blanton, 1986). During winter, the Celtic Sea is fully mixed due to heat loss and intensified wind stress (Wihsgott et al., 2019). Nonetheless a cross-shelf gradient occurs with warmer and saltier waters at the shelf edge (Pingree, 1980; Ruiz-Castillo et al., 2018)(Fig. 5.9a). In the Central Celtic Sea events of positive net heat flux between the 15th and 24th of March 2015 increased the temperature in the upper 30 m. However, whilst heat input overcame mixing during the day, heat loss and convective mixing during the night delayed the onset of the sustained thermal stratification until the 26th of March, when a two layer system developed (Fig. 5.6h). From this date onwards positive net heat flux was observed

at the Central Celtic Sea until the 18th of April. However, increases in temperature (>10^{o}C) in the upper 70 m occurred between the 26th and 29th of March. Temperature decreased in the period 29th of March- 5th of April in the upper 70 m below 10^{o}C despite positive net heat flux indicating advection of colder waters. In the Celtic Sea surface and bottom transport is mainly dominated by wind-driven Ekman dynamics (Pingree and Le Cann, 1990; Chapters 3 and 4) and strong correlation for the zonal (R^2=0.7) and meridional (R^2=0.92) components between the 15th of March and 5th of April confirms surface transport was wind-driven at Central Celtic Sea. Consistent with the beginning of the constant positive net heat flux a westerly wind event occurred from the 26th of March to the 5th of April and was favourable for off- and on-shelf flow in the surface and bottom layers respectively. Therefore, southward wind-driven flow advected colder (<10^{o}C) and fresher waters (<35.53 g kg^{-1}) in the surface layer (Fig. 5.6f and g) and warmer (>10^{o}C) and saltier (>35.53 g kg^{-1}) waters were transported by the compensatory bottom flow. The effects of cross-shelf transport are illustrated in Figure 5.9.b. The influence of rain on the changes in salinity can be assessed using ERA-interim data sets (Dee et al., 2011). At the end of the day on the 28th of March salinity in the upper 80 m was 35.536 g kg^{-1}. There was a 0.0016 m of rainfall at the Central Celtic Sea site on the 29th of March. Over the upper 80 m of the water column this would have reduced the salinity to 35.535 g kg^{-1}, which accounts only for 3% of the change in salinity, with averaged salinity being 35.523 g kg^{-1} at the end of the day on the 29th of March. Between the 29th of March and 4th of April the rainwater input accounted for 0.0049 m decreasing salinity down to 35.534 g kg^{-1} greater than the salinity observed (35.486 g kg^{-1}) in the upper 80 m at the end of the day on the 4th of April. Therefore the reduction in salinity between the 28th of March and 4th of April is attributed to

wind-driven transport of fresher waters (<35.53 g kg^{-1}) from the north of the Celtic Sea. Due to wind-driven cross-shelf advection, relatively cold waters were introduced at the Central Celtic Sea in the surface layer and overlaid warmer waters in the bottom (Fig. 5.7c and 5.9b). Nonetheless, a stable water column was maintained (Fig. 5.6h) due to fresher waters occupying the surface layer above relatively high salinity waters as seen in the late stages of the stratified period (Chapter 4). Maximum wind stress ($\sim$0.27 kg m^{-1} s^{-2}) occurred between the 26th of March and 1st of April and was greater than the wind stress ($\sim$0.23 kg m^{-1} s^{-2}) in the spring 2014 that mixed the surface layer. However, the mixing effects in spring 2015 were spread over a 70 m thickness layer, greater than the 35 m thickness of the surface layer in April 2014. Therefore, between the 29th of March and 5th of April stratification was not governed by a competition between heat input and mixing. Stratification was maintained and controlled by cross-shelf advection, particularly wind-driven Ekman transport of relatively low salinity waters (<35.53 g kg^{-1}) in the surface layer (Fig. 5.9b). Subsequently, from the 12th of April onwards the fluctuations in density and intensification of stratification were controlled by heat input and the vertical distribution of temperature (Pingree, 1980; Brown et al., 2003; Wihsgott et al., 2019). Winds were zonally aligned and favourable for off- and on-shelf transport. However, after the 11th of April increases in salinity appeared to have negligible effect on estimating density.

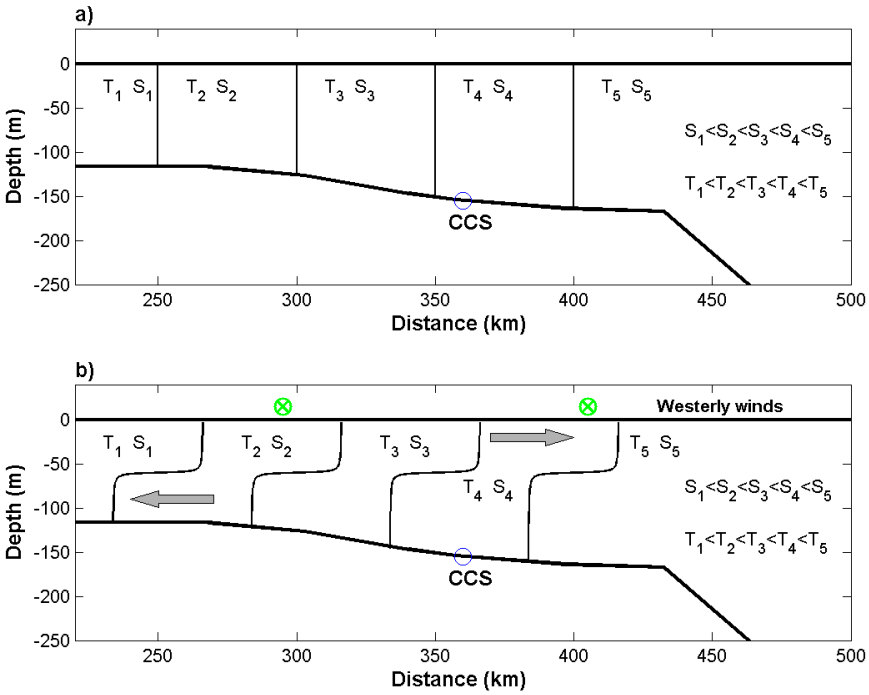

Figure 5.9: Schematics of the cross-shelf distribution of salinity (S) and temperature (T) when a) the water column is mixed (winter) and b) during westerly wind events.

Implications for phytoplankton growth

As in the previous spring, the onset and maintenance of stratification influenced the biology of the Celtic Sea. The chl-*a* concentration was minimum in winter (Fig. 5.6i), as vertical mixing of the water column hindered phytoplankton growth (Pingree et al., 1977). Once the water column stabilised, the concentration of chl-*a* increased on the 26th of March indicating the onset of the spring bloom (Rees et al., 1999). Stratification persisted and therefore chl-*a* concentration gradually augmented and was maximum between the 12th and 19th of April (Garcia-Martin et al., 2017; Seguro et al., 2017; Davis et al., 2018; Wihsgott et al., 2019). Prior to the spring bloom, the nitrate concentration was 6.5 mmol m^{-3} and decreased to <2 mmol m^{-3} on the 20th of April (Fig. 5.7e). Therefore between 4 and 5 mmol m^{-3} were utilised during the sudden growth of phytoplankton. A gradual decrease in nutrients was observed from <2

mmol m^{-3} on the 19th to <0.6 mmol m^{-3} on the 26th of April. Within this period, despite this reduced nutrient concentration smaller peaks (<6 mg m^{-3}) in chl-*a* were observed (Fig. 5.6i; Garcia-Martin et al., 2017). Phytoplankton blooms occurred even though the nutrient concentration was relatively low (<2 mmol m^{-3}). After the 26th of April nutrients were depleted in the surface layer leading to a chl-*a* concentration below 0.6 mmol m^{-3} (Poulton et al., 2018).

Inter-annual variability was observed in the spring blooms of 2014 and 2015. The background nutrient concentration in winter 2015 (7 mmol m^{-3}) was lower than the background nutrient concentration in winter 2014 (8 mmol m^{-3}). However, the spring bloom event was greater in magnitude, by almost a factor 2, than the 2014 spring bloom. Therefore, the amount of phytoplankton growth appeared to be independent of the background nitrate concentration in winter. Therefore, further research should be carried out to elucidate the mechanisms driving inter-annual variability.

5.5 Summary

The mechanisms driving the onset and evolution of the stratification in the Celtic Sea for the spring 2014 and 2015 were analysed and used to assess phytoplankton growth.

In spring 2014 stratification of the water column started before the 27th of March and was intensified by positive net heat flux until the 25th of April when enhanced wind stress and heat loss to the atmosphere mixed the upper 50 m. Stratification in the upper 50 m was re-established from the 1st of May onwards as a result of positive net heat flux.

Associated with the onset of stratification a spring bloom event occurred and was a maximum on the 12th of April. Following the peak in growth, chl-a concentration gradually decreased. During the mixing event on the 25th of April, 3.3 mmol m^{-3} of nitrate were introduced above the pycnocline and triggered a second phytoplankton bloom, which was greater than the previous spring bloom event.

In the spring 2015 constant positive net heat flux from the 26th of March onwards triggered stratification at the Central Celtic Sea site. During positive heat flux between the 28th-29th of March and 5th of April temperature and salinity decreased in the surface layer due to southward wind-driven transport. The onshore compensatory bottom flow advected relatively high salinity waters in the bottom layer. In the early stages of the stratified period a stable water column was not maintained by heat input, but by the vertical distribution of salinity and therefore by cross-shelf advection. From the 11th of April onwards stratification and density were controlled by temperature.

The beginning of the spring bloom in 2015 coincided with the onset of stratification on the 26th of March. There was a relatively constant growth until the 15th- 17th of April. The phytoplankton bloom was greater than the bloom event in the spring 2014 despite lower initial nutrient concentration prior to the onset of stratification. Relatively small blooms were observed between the 20th and 26th of April until the nutrient concentration in the surface layer was below 0.6 mmol m^{-3}.

Phytoplankton growth was enabled between the 29th of March and 5th of April due to stratification being controlled by salinity, i.e. by wind-driven cross-shelf transport of low salinity waters in the surfce layer.

Chapter 6

Summary and discussion

6.1 Summary

The Celtic Sea is a temperate and wide shelf where nutrients are supplied chiefly from the North Atlantic Ocean and to a lesser degree from riverine sources. However, the mechanisms on how and when nutrients are supplied and advected across the shelf are unclear. In this thesis the physical processes leading to seasonal cross-shelf transport and exchange between the Celtic Sea and the North Atlantic Ocean were elucidated. The physical processes occurring in different time-periods are summarised below.

6.1.1 Cross-shelf transport and exchange in summer

At Central Celtic Sea transport variability was bounded by the semidiurnal and inertial frequency bands indicating the influence of internal waves and wind-stress forcing. Within the surface and bottom layers transport variability in the inertial frequency band was greater than the semidiurnal suggesting wind stress forcing was predominant. In contrast, semi-diurnal oscillations governed variability of transport in the pycnocline layer and was attributed to the passing of internal waves.

For each layer transport was separated into Eulerian and Stokes components. Westerly winds predominated and were favourable for surface off-shelf (southward) transport and an onshore (northward) compensatory bottom flow. Wind-driven Ekman transport accounted for most of the Eulerian transport in the surface and bottom layers with both transports strongly correlated (R^2 >0.7). In addition, their variability was aligned in the same direction. Therefore, off-shelf transport in the surface layer was wind-driven whilst onshore transport in the bottom layer resulted from the wind-driven compensatory flow (Fig. 6.1).

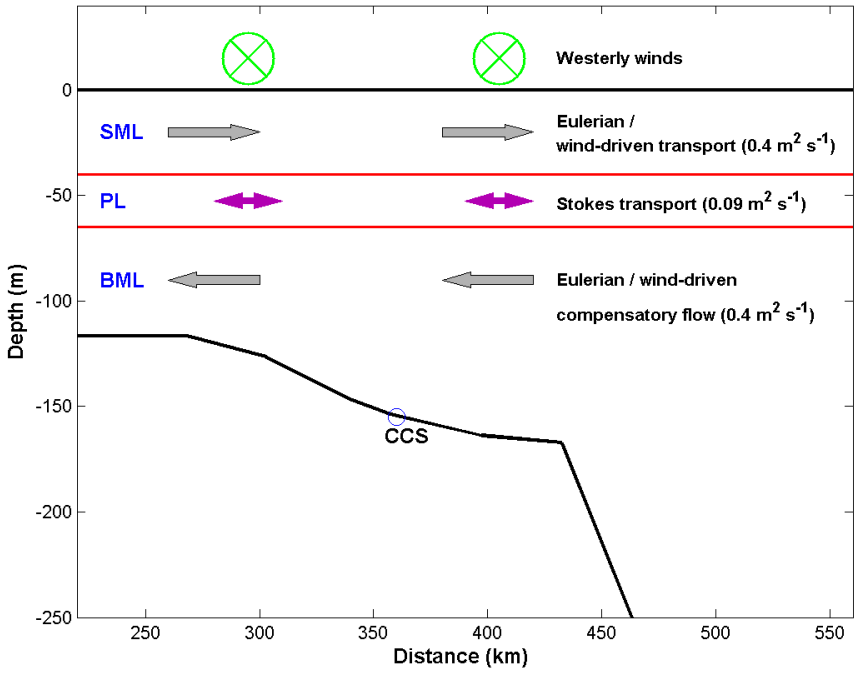

Figure 6.1: Schematics of the main mechanisms leading to cross-shelf transport and exchange between the Celtic Sea and the North Atlantic Ocean.

A horizontal salinity and temperature gradient, with salinity and temperature increasing towards the shelf edge and North Atlantic Ocean, was set in winter. During the onset of stratification the horizontal temperature gradient in the surface layer vanished. However, below the pycnocline the gradient was maintained throughout summer. As a consequence of wind-driven dynamics in the bottom layer high salinity and

warmer waters from the North Atlantic were advected on-shelf and intruded between 80 and 110 km in a 7-8 month period. Similarly, the compensatory flow of wind-driven dynamics led to onshore advection of relatively high salinity waters from the shelf throughout summer until winter mixing.

Throughout summer evidence of relatively high salinity waters intruding on-shelf and low salinity waters being exported off-shelf within the pycnocline was indicative of cross-slope exchange. The on- and off-shelf transport resulted from Stokes transport, which was greater than the Eulerian transport within the pycnocline, and was mainly aligned orthogonally to the shelf edge. Exchange between the Celtic Sea and the North Atlantic Ocean within the pycnocline layer was attributed to the Stokes transport generated by internal waves (Fig. 6.1).

Wind-driven cross-shelf transport has been observed globally in shelf seas. However, the Celtic Sea is a unique region. On narrow shelves ($\sim$50 km) surface divergence generated by wind-driven transport results in vertical and surface outcropping of the pycnocline at the shelf edge (e.g. Torres and Gomez-Valdes, 2015). In addition, in shelf seas due to surface divergence relatively cold water from the subsurface is expected to upwell along the coast (e.g. Ruiz-Castillo et al., 2016). For the wide Celtic Sea (>500 km) surface off-shelf transport at the shelf break was replenished by waters from further on the shelf and therefore vertical velocities and/or upwelling of deeper waters at the shelf break seems to be negligible. In addition, relatively cold waters are not observed along the coast. Stratification prevailed throughout summer in the relatively deep inner shelf hindering mixing so that high salinity and relatively cold waters from the bottom are not observed in the surface. Instead,

the relatively high salinity waters from near the shelf edge may entrain the cyclonic circulation in the north of the Celtic Sea (Horsbourgh et al., 1998; Brown et al., 2003).

6.1.2 Cross-slope exchange in late-autumn and winter

In NW European shelf cross-slope exchange in autumn and winter has been typically thought to be important for removing carbon from the shelf that has been fixed during the stratified period (Thomas et al., 2004; Painter et al., 2017). In the Celtic Sea in December evidence of Ekman drainage beneath the poleward along-slope current and wind-driven transport across the shelf and towards the shelf edge was observed. The Ekman transport resulted in convergence of waters at the shelf edge. However, the hydrographic sections suggested that the Ekman drain exported only shelf edge water into the deeper slope waters. The wind-driven transport of fresher waters towards the shelf edge appeared to recirculate onshore in the bottom layer (Fig. 6.2). In shelf seas interaction between wind-driven and bottom Ekman dynamics occurring simultaneously at the shelf edge has been observed before (e.g. Roughan and Middleton, 2002). However, in the Celtic Sea the interaction between wind-driven transport and Ekman drainage results in bottom recirculation of surface waters, a novel process that has not been observed previously.

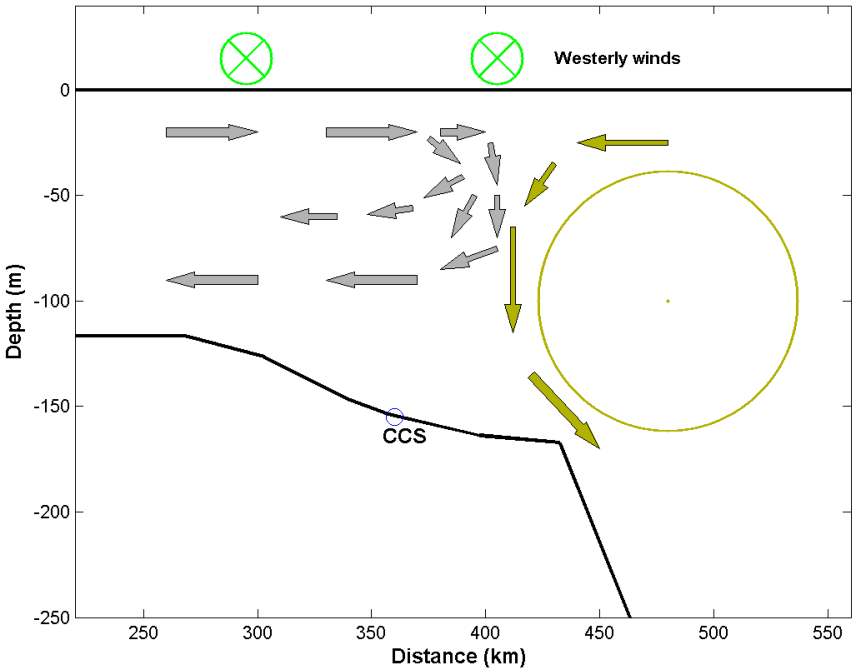

Figure 6.2: Schematics of the interaction between wind-driven and bottom Ekman drainage processes at the shelf edge.

Throughout summer, the along-slope current seems to be absent (van Aken, 2002) or even reverses (Porter et al., 2016). Westerly winds predominate in the Celtic Sea and are favourable for off-shelf surface transport. Thus, during the stratified period wind-driven dynamics govern cross-slope exchange in the Celtic Sea and would be enhanced by the along-slope current heading southward. In contrast, when the poleward along slope current occurs Ekman drainage dynamics would inhibit wind-driven cross-slope. A combination of westerly winds during periods (autumn) when dynamics at the shelf edge are governed by the poleward along slope current may result in recirculation of surface waters in the bottom layer as described in this thesis. Thus, in autumn bottom recirculation of surface fresher waters may be a regular feature in the Celtic Sea.

In winter westerly winds and the poleward along-slope current occur simultaneously. However, hydrographic and current time series indicate

that the mixing effect of wind and tidal stresses overcame wind-driven cross-shelf advection. Thus, recirculation of surface fresher waters in the bottom layer is not plausible.

Southward depth-averaged flow of relatively low salinity waters was observed at the Celtic Deep and Central Celtic Sea sites in winter 2014-2015. Overall, there was no evidence of exchange between the Celtic Sea and the North Atlantic Ocean. Shelf waters seemed to not be exported into the North Atlantic Ocean.

6.1.3 Onset of stratification

In shelf seas, far from riverine influence, stratification is thought to be maintained by a competition between heat input into the sea surface and mixing generated by wind and tidal stresses (Simpson, 1981). The onset and maintenance of stratification was assessed in spring 2014 and 2015. In spring 2014, stratification strengthened due to positive net heat flux. Similarly, in spring 2015 the onset of stratification was triggered by positive net heat flux. However, in the early stages of the stratified period in spring 2015, temperature above and below the pycnocline decreased and increased, respectively, despite the positive net heat flux into the sea surface. This temperature inversion was caused by wind-driven transport advecting cold and relatively low salinity surface waters from further north in the Celtic Sea. In this case the stratification of the water column was maintained by the vertical distribution of salinity, with greater salinity from near the shelf edge occupying the bottom layer. In the absence of stable thermal stratification this vertical salinity gradient stimulated phytoplankton growth.

Advection of fresher and colder waters in the surface due to wind driven

transport is highly expected due to the Celtic Sea experiencing predominantly westerly winds. Nonetheless, in late winter and early spring outburst of cold and intensified easterly wind events, locally known as the "beast from the east" may occur and have further implications on the water column stratification and therefore on the timing and duration of the spring bloom. These easterly winds are favourable for onshore surface transport and an off-shelf compensatory bottom flow, opposite to westerly wind events. In the early stages of spring easterly winds combined with the horizontal salinity gradient would advect relatively high salinity and warm waters in the surface layer. The vertical distribution of salinity may generate an unstable water column if salinity has a greater effect than temperature on controlling density. Moreover, cold temperatures are associated with the easterly wind events. Therefore, surface temperature may decrease and contribute to an unstable water column. Instability of the water column inhibits phytoplankton growth and therefore spring blooms would be halted and/or delayed.

6.2 Discussion

The results in this thesis have important consequences in particular for three aspects of shelf sea biogeochemical cycles: (1) the supply of nutrients to shelf sea phytoplankton, (2) the export of carbon from the shelf sea, and (3) the triggering and maintenance of stratification.

6.2.1 Supply of nutrients to shelf sea phytoplankton

The background nutrient concentration for both the northern and southern Celtic Sea is set in winter, when the water column is fully mixed, and determines nutrient availability for the following spring bloom. At the Bristol Channel and shelf edge boundaries the nutrient sources are

variable between years. In the Bristol Channel riverine nutrient input is a maximum in winter (Uncles and Radford, 1980; Jonas and Millward, 2010; Uncles, 2010) and eventually, after nitrogen removal (Seitzinger et al., 2006), nutrients from riverine origin reach the Celtic Sea. At Central Celtic Sea and Celtic Deep nutrients were estimated to account for 10% and 30% of the nitrate available, respectively. At the shelf edge and shelf break the depth of the winter mixed layer is variable as well (Hydes et al., 2004; Hartman et al., 2014). For the winter 2014-2015 mixing down to 500 m depth autumn nitrate profiles at the shelf break resulted in a similar background concentration to the nitrate observed at the shelf edge and shelf break for the spring 2015. Therefore, winter mixing set the amount of nutrients at the shelf break and the background nutrient concentration that would be transported northward in the bottom mixed layer throughout the stratified period by wind-driven dynamics. During the stratified period bottom nitrate-rich waters were transported northward/onshore by Ekman dynamics until winter mixing occurred and distributed nitrate from below the pycnocline throughout the water column. Therefore, far from the nutrient sources, i.e. far from the Bristol Channel and the shelf edge, in the interior of the Celtic Sea a combination of the northward transport with winter mixing set the background nutrient concentration for the following spring bloom.

The high productivity of the Celtic Sea (Seguro et al., 2017) can only be maintained whilst nutrients are available (Pingree et al., 1976). Evidence presented here indicates that in the bottom layer waters from the shelf break are introduced ∼80-100 km onshore by wind-driven dynamics in a 7-8 month period, before winter mixing. Therefore, for the wide Celtic Sea nutrients from oceanic origin will be advected north of Central Celtic Sea in at least 2 years and would reach the coast in a 2-5 year period,

a time-scale consistent with previous estimates (Hydes et al., 2004). At the northern boundary, nutrients supplied from the Bristol Channel are expected to be diverted northward (Uncles, 2010) and therefore its influence over the wide Celtic Sea is expected to be limited. Thus, in order to maintain the high productivity the biogeochemical system of the Celtic Sea seems to be very efficient at recycling nutrients. About 50-60% of the nutrients located at Central Celtic Sea and within the outer shelf were recycled in the water column between March and mid-November. Hence, even though nitrate is chiefly supplied from the North Atlantic Ocean, and to a lesser extent, from the Bristol Channel, into the Celtic Sea, in the interior of the shelf the nitrate availability resulted from a combination of wind-driven bottom onshore advection of recycled nutrients from the previous years.

6.2.2 Export of carbon from the shelf sea

Temperate shelf seas, are considered to be CO_2 carbon sinks (Thomas et al., 2004; Painter et al., 2017), particularly the Celtic Sea (Hartman et al., 2018). In the NW European shelf export of carbon from shelf seas in the form of DIC is thought to be driven by Ekman drainage generated by the poleward along slope current, particularly from the Hebridean shelf northwards (Souza et al., 2001; Simpson and Mcandliss, 2013; Painter et al., 2017). For instance, recent estimates for the Hebridean shelf quantified that 2.18Tg C day^{-1} was exported into the North Atlantic through an Ekman drain mechanism in November and December 2014 with the export being significant compared to the air-sea CO_2 fluxes (Painter et al., 2017). However, south of the Hebridean shelf in the Celtic Sea previous observations indicate that in summer the along slope current weakens and even reverses and flows in the equatorward direction (Pingree and Le Cann, 1989; Porter et al., 2016), or seems to be absent (van Aken,

2002). Furthermore, shelf-ocean exchange throughout the stratified period is governed by wind-driven dynamics and on average supply oceanic waters onto the shelf in the bottom layer. Therefore, it is unlikely that Ekman drain is significant for the Celtic Sea throughout most of the stratified period. In contrast, in late autumn and winter the along-slope current occurs in the poleward direction (Pingree and Le Cann, 1989; Souza et al., 2001; Simpson and McCandliss, 2013) and appears to be a continuous flow from the Bay of Biscay to the north of the Hebridean Shelf (Painter et al., 2017) and in a favourable direction for export of shelf waters in the bottom boundary layer. However, whilst this study did find a surface Ekman transport of shelf water towards the shelf edge in late autumn, only the outer 10-20 km of the shelf waters appeared to gain access to the shelf edge, and the water that did reach the shelf edge seemed to be recirculated back onto the shelf in the bottom compensatory flow indicating a negligible off-shelf carbon export.

In winter the water column was fully mixed and there was no evidence of cross-slope exchange. At Central Celtic Sea velocity anomalies were consistent with wind-driven dynamics and headed towards the right of the direction of the wind in the upper 70-80 m with the compensatory flow occupying the bottom 70-80 m resulting in a negligible net cross-shelf exchange of carbon once mixing occurred. At the shelf break hydrographic evidence indicates the water column was fully mixed reaching depths below the bottom depth of the shelf slope. If Ekman drain occurred in the bottom boundary layer at the shelf slope, a compensatory flow would had transported waters on-shelf above the bottom boundary layer, but again would result in negligible net exchange of carbon, once the water column mixes. Thus, whilst in the Hebridean Shelf significant export of carbon (DIC) occurs (Painter et al., 2017) and in the North Sea seems to

take place (Thomas et al., 2004), off-shelf export seems negligible along the shelf edge of the Celtic Sea. Furthermore, if Ekman drain dynamics governed at the shelf slope, its influence over the wide Celtic Sea (>500 km) would be limited to the vicinity of the shelf slope (10-20 km). For instance, a rough estimate of the volume of the Celtic Sea and the region influenced by Ekman drain dynamics in the bottom 60 m yields 5.68×10^{12} and 4.1×10^{11} m^3 with the latter accounting for only 7% of the total volume of the Celtic Sea. Therefore, off-shelf export of DIC in the bottom layer of the whole Celtic Sea cannot be produced by the Ekman drain mechanism. Particularly if the along-slope current is in the poleward direction between mid-autumn and spring only (Pingree and Le Cann, 1989; van Aken, 2002). Overall, export of DIC through Ekman drain is negligible at the shelf edge of the Celtic Sea implying that DIC is either accumulating within the shelf, or probably is exported northward through the Irish Sea in time scales longer than 2 years.

6.2.3 Triggering and maintenance of stratification

Finally, wind-driven transport had further implications for the onset and maintenance of stratification of the water column in the Celtic Sea. The canonical view of shelf sea stratification away from freshwater sources is that surface heating is the key driver (e.g.Brown et al., 2003; Young et al., 2004; Wihsgott et al., 2019). For the spring 2015 positive net heat flux occurred at the same time as the onset of the stratified period. However, despite this heat input the temperature of the surface layer decreased and overlaid warmer waters in the bottom layer due to wind-driven cross-shelf advection of a horizontal temperature and salinity gradient. The onset of stratification coincided with the beginning of a westerly wind event that advected relatively cold, low salinity surface waters from further north into the Central Celtic Sea and high salinity and warm waters within

the compensatory bottom onshore flow. Potentially the initial onset of spring stratification in 2015 arose from the wind-driven advection of the horizontal salinity gradient; stratification may have occurred earlier than it would have done in the absence of the westerly winds.

At the end of the summer stratified period evidence was also found of the winds extending the period of stratification. In December 2014-January 2015 the stratified period was prolonged despite vertical thermal instability. Heat loss to the atmosphere cooled waters in the surface layer generating relatively low temperature waters to overlay warmer waters in the bottom. A stable water column was maintained by the wind-driven advection of relatively high salinity and fresher waters in the bottom and surface layers respectively, and therefore again by wind-driven Ekman transport. Overall, the role of the wind acting on the horizontal salinity gradients across the shelf, both in triggering and in extending stratification, underlines the importance of regional shelf sea models being able to accurately simulate horizontal salinity distributions as well as air-sea heat fluxes if they are to track the biogeochemical cycles of the shelf sea system.

References

Allen, S. E., X. Durrieu de Madron. 2009. A review of the role of submarine canyons in deep-ocean exchange with the shelf. Ocean Sci. 5, 607-620.

Austin, J. A. S. J. Lentz. 2002. The inner shelf response to wind-driven upwelling and downwelling.J. Phys. Oceanogr. 32, 2171-2193.

Behrenfled, M. J., E. Boss, D. A. Siegel, D. M. Shea. 2005. Carbon-based ocean productivity and phytoplankton physiology from space. Global Biogeochem. Cycles. 19, GB1006.

Blanc, T. V. 1987. Accuracy of bulk-method-determined flux, stability, and sea surface roughness. J. Geoph. Res. 92 (C4), 3867-3876.

Bowers, D.G., E. M. Roberts, M. White, B. D. Moate. 2013. Water masses, mixing, and the flow of dissolved organic carbon through the Irish Sea. Cont. Shelf Res. 58, 12-20.

Brown, J., L. Carrillo, L. Fernand, K. J. Horsburgh, A. E. Hill, E. F. Young, K. J. Medler. 2003. Observations of the physical structure and seasonal jet-like circulation of the Celtic Sea and St. Georges Channel of the Irish Sea. Cont. Shelf Res. 23, 533-561.

Carr, N., C. Davis, S. Blackbird, L. R. Daniels, C. Preece, M. Woodward, C. Mahaffey,. 2018. Seasonal and spatial variability in the optical characteristics of DOM in a temperate shelf sea. In press.
https://doi.org/10.1016/j.pocean.2018.02.025

Centurioni, L. R., P. P. Niiler, D-K. Lee. 2004. Observations of inflow of Phillippine Sea surface water into the South China Sea through the Luzon Strait. J. Phys. Oceanogr. 34, 113-121.

Chen CT.A.. 2010. Cross-Boundary Exchanges of Carbon and Nitrogen in Continental Margins1. In: Liu KK., Atkinson L., Quiones R., Talaue-McManus L. (eds) Carbon and Nutrient Fluxes in Continental Margins. Global Change - The IGBP Series. Springer, Berlin, Heidelberg".

Cooper, L. H. N., D. Vaux. 1949. Cascading over the continental slope of water from the Celtic Sea. Journal of the Marine Biological Association of the United Kingdom, 28 (3), 719-750.

Cushman-Roisin B, J. M. Beckers. 2009. Introduction to geophysical fluid dynamics. physical and numerical aspects. elsevier.

Davis, C. E., C. Mahaffey, G. A. Wolff, J. Sharples. 2014. A storm in a shelf sea: Variation in phosphorus distribution and organic matter stoichiometry, Geophys. Res. Lett., 41 (23), 8452-8459. doi:10.1002/2014GL061949.

Dee, D. P., S. M. Uppala, A. J. Simmons, P. Berrisford, P. Poli, S. Kobayashi, U. Andrae, M. A. Balmaseda, G. Balsamo, P. Bauer , P. Bechtold, A. C. M. Beljaars, L. van de Berg, J. Bidlot, N. Bormann, C. Delsol, R. Dragani, M. Fuentes, A. J. Geer, L. Haimberger, S. B. Healy, H. Hersbach, E. V. Hlm, L. Isaksen, P. Kllberg, M. Khler, M. Matricardi, A. P. McNally, B. M. Monge-Sanz, J.-J. Morcrette, B.-K. Park, C. Peubey, P. de Rosnay, C. Tavolato, J.-N. Thpaut, F. Vitart. 2011. The ERA-Interim reanalysis: configuration and performance of the data assimilation system. Q. J. R. Meteorol. Soc., 137: 553-597. doi:10.1002/qj.828

Ekman, V. W. 1905. On the influence of the earth's rotation on ocean currents. Arkiv Mat. Astron. Fysik. 2 (11).

Fasham, M. J. r, P. M. Holligan,P. R. Pugh, 1983. The spatial and temporal development of the spring phytoplankton bloom in the Celtic Sea, April, 1979. Prog. Oceanogr.12 (1), 87-145.

Garcia-Martn, E.E., C. J. Daniels, K. Davidson, J. Lozano, K. M. J. Mayers, S. McNeill, E. Mitchell, A. J. Poulton, D. A. Purdie, G. A. Tarran, C. Whyte, C. Robinson. 2017. Plankton community respiration and bacterial metabolism in a North Atlantic Shelf Sea during spring bloom development (April 2015). Progress in Oceanography. In press. http://dx.doi.org/10.1016/j.pocean.2017.11.002

Gill, A. Atmosphere-Ocean Dynamics. In International Geophysics Series, volume 30. Academic Press, 1982.

Green, J. A. M., J. H. Simpson, S. Legg, M. R. Palmer. 2008. Internal waves, baroclinic energy fluxes and mixing at the European shelf edge. Cont. Sh. Res. 28(7), 937-950.

Gomez-Valdes, J., G. Jeronimo. 2009. Upper mixed layer temperature and salinity variability in the tropical boundary of the California Current, 19972007, J. Geophys. Res., 114, C03012, doi:10.1029/2008JC004793.

Gowen, R. J., B. M. Stewart. 2005. The Irish Sea: nutrients status and phytoplankton. J. Sea Res. 54, 36-50.

Hartman, S. E., M. C. Hartman, D. J. Hydes, Z-P. Jiang, D. Snythe-Wright, C. Gonzalez. 2014. Seasonal and inter-annual variability in nutrient supply in relation to mixing in the Bay of Biscay. Deep-Sea Res. II, 106, 68-75. http://dx.doi.org/10.1016/j.dsr2.2013.09.032

Hartman, S. E., M. P. Humphreys, C. Kivimäe, E. M. S. Woodward, V. Kitidis, T. McGrath, D. J. Hydes, N. Greenwood, T. Hull, C. Ostle, D. J. Pearce, D. Sivyer, B. M. Stewart, P. Walsham, S. C. Painter, E. McGovern, C. Harris, A. Griffiths, A. Smilenova, J. Clarke, C. Davis, R. Sanders, P. Nightingale. 2018. Seasonality and spatial heterogeneity of the surface ocean carbonate system in the northwest European continental shelf. Progr. Oceanogr. In press. https://doi.org/10.1016/j.pocean.2018.02.005

Henderson, S. M.. 2016. Upslope internal-wave stokes drift, and compensating downslope Eulerian mean currents, observed above a lake bed. J. Phys. Oceanogr. 46, 1947-1961.

Hickman, A. E., C. M. Moore, J. Sharples, M. I. Lucas, g. H. Tilstone, v. Krivtsov, P. M. Holligan, 2012. Primary production and nitrate uptake within the seasonal thermocline of a stratified shelf sea. Mar. Ecol. Prog. 463,39-57.

Hickman et al. 2018. Seasonal variability in size-fractionated chlorophyll-a and primary production in the Celtic Sea. Progr. Oceanogr. In press.

Hill, A. E., K. J. Horsburgh, R. W. Garvine, P. A. Gillibrand, G. Slesser, W. R. Turrell, R. D. Adams. 1997. Observations of a density-driven recirculation of the scotish coastal current in the Minch. Est. Coas. and Sh. Sci. 45 (4), 473-484.

Hill, A. E., A. Souza, K. Jones, J. H. Simpson, G. I. Shapiro, R. Mcandllis, H. Wilson, J. Leftley. 1998. The Malin cascade in winter. J. Mar. Res. 56(20), 87-106.

Holligan, P. M., Williams P. J., Purdie D., Harris R. P. 1984. Photosynthesis, respiration and nitrogen supply of plankton populations in stratified, frontal and tidally mixed shelf waters. Mar. Ecol. Prog. Ser. 17, 201-213

Holt, J., I. D. James. 1999. A simulation of the southern North Sea in comparison with measurements from the North Sea Project Part 2 Suspended Particulate matter. Cont. Sh. Res. 19 (12), 1617-1642.

Holt, J., S. Wakelin, J. Huthnance. 2009. Downwelling circulation of

the northwest European continental shelf: A driving mechanism for the continental shelf carbon pump. Geophys. Res. Lett. 36. L14602

Hopkins, J., G. R. Stephenson Jr., J. A. M. Green, M. E. Inall, M. R. Palmer. 2014. Storms modify baroclinic energy fluxes in a seasonally stratified shelf sea: Inertial-tidal interaction. J. Geoph. Res, 119, 6863 - 6883.

Hopkins, J., J. Sharples, J. M. Huthnance. 2012. On-shelf transport of slope water lenses within the seasonal pycnocline. Geophys. Res. Lett. 39, L08604. doi:10.1029/2012GL051388,

Horsburgh, K. J., A. E. Hill, J. Brown, L. Fernand, R. W. Garvine, M. M. P. Angelico. 2000. Seasonal evolution of the cold pool gyre in the western Irish Sea. Prog. Oceanog. 46, 1-58.

Horsburgh, K. J., A. E. Hill, J. Brown. 1998. A summer Jet in the St. Georges Channel of the Irish Sea. Estuar. Coast. Shelf Sci. 47, 285 - 294.

Houghton, R. W., R. D. Vaillancourt, J. Marra, D. Hebert, B. Hales. 2009. Cross-shelf circulation and phytoplankton distribution at the summertime New England shelf break front. J. Mar. Syst. 78, 411-425.

Hull, T., D. Sivyer, D. Pearce, N. Greenwood, N. Needham, C. Read, E. Fitton. 2017. Shelf Sea Biogeochemistry - Celtic Deep 2 SmartBuoy. Centre for Enviroment Fisheries and Aquaculture Science, UK. doi:10.14466/CefasDataHub.39.

Hsueh, Y., H-J. Lie, H. Ichikawa. 1996. On the branching of the kuroshio west of kyushu. J. Geophys. Res., 101, 3851 - 3857.

Huthnance, J. M. 1995. Circulation, exchange and water masses at the ocean margin: The role of physical processes at the shelf edge, Prog. Oceanogr. 35, 353-431.

Huthnance, J. M., H. Coelho, C. R. Griffiths, P. J. Knight, A. P. Rees, B. Sinha, A. Vangriesheim, M. White, P. G. Chatwin. 2001. Physical structures, advection and mixing in the region of Goban spur. Deep-Sea Res. II 48, 2979-3021.

Huthnance, J. M., J. T. Holt, S. L. Wakelin. 2009. Deep ocean exchange with west-European shelf seas. Ocean Sci., 5. 621-634.

Hydes, D. J., Gowen, R. J., Holliday, N. P., Shammon, T. M., Mills, D.. 2004. External and internal control of winter concentrations of nutrients (N, P and Si) in north west European Shelf Seas. Estuar. Coast. Shelf Sci. 59, 151-161.

Inall, M., G. I. Shapiro, T. J. Sherwin. 2001. Mass transport by non-linear internal waves on the Malin Shelf. Cont. Sh. Res. 21(13-14), 1449-1472.

Inall, M., D. Aleynik, T. Boyd, M. Palmer, J. Sharples. 2011. Internal tide coherence and decay over a wide shelf sea. Geophys. Res. Lett. 38, L23607. doi:10.1029/2011GL049943

Inall, M. E., D. Aleynik, C. Neil. 2013. Horizontal advection and dispersion in a stratified shelf sea: The role of inertial oscillations. Progr. Oceanogr. 117, 25-36.

IOC, SCOR, IAPSO, 2010. The international thermodynamic equation of seawater -2010: Calculations and use of thermodynamic properties. Intergovernmental Oceanographic Commission, Manuals and Guides No. 56, UNESCO, 196 pp.

Ivanov, V. V., G. I. Shapiro, J. M. Huthnance, D. L. Aleynik, P. N. Golovin. 2004. Cascades of dense water around the world ocean. Prog. Oceanogr. 60, 47-98.

Jahnke, R. A. 2010. Global synthesis in Carbon and Nutrient Fluxes in a Global Context, in Carbon and nutrient fluxes in continental margins. A global Synthesis. Pp. 741.

Jonas, P. J. C., G. E. Millward. 2010. Metals and nutrients in the Severn Estuary and Bristol Channel: Contemporary inputs and distributions; Mar. Pollut. Bull. 61, 52-67.

Josey, S. A., E. C. Kent, P. K. Taylor, 1999. New insights into the Ocean Heat budget closure problem from analysis of the SOC Air-Sea Flux climatology. J. Clim. 12, 2856-2880.

Kara, A. B., P. A. Rochford, and H. E. Hurlburt. 2000. An optimal definition for ocean mixed layer depth, J. Geophys. Res., 105 (C7), 16803 - 16821.

Lavin, M., G. Gaxiola-Castro, J. M. Robles, K. Richter. 1995. Winter water masses and nutrients in the Gulf of California. J. Geophys. Res. 100(C5), 8587-8605.

Lentz, S. J. 2003. A climatology of salty intrusions over the continental shelf from Georges Bank to Cape Hatteras. J. Geophys. Res. 108(C10), 3326.

Linden, P. F., J. E. Simpson. 1988. Modulated mixing and frontogenesis in shallow seas and estuaries. Cont. Shelf Res., 8, 1107-1127.

Liu, K. K., L. Atkinson, R. A. Quiones, L. Talaue-McManus. 2010. Biogeochemistry of Continental Margins in a Global Context, in Carbon and nutrient fluxes in continental margins. A global Synthesis. Pp. 741.

Liu, K-K., T. Y. Tang, G. C. Gong, L. Y. Chen, F. K. Shiah. 2000. Cross-shelf and along-shelf nutrients fluxes derived from flow fields and chemical hydrography observed in the southern East China Sea off northern Taiwan. Cont. Shelf Res. 20, 493-523.

Marchesiello, P., P. Estrade. 2010. Upwelling limitation by onshore geostrophic flow. J. Mar. Res. 68, 37-62.

McDougall, T.J. P.M. Barker. 2011: Getting started with TEOS-10 and the Gibbs Seawater (GSW) Oceanographic Toolbox, 28pp., SCOR/IAPSO WG127, ISBN 978-0-646-55621-5.

Moliniari, R.L., J. Morrison. 1988. The separation of the Yucatan current from the Campeche bank and the intrusion of the loop current into the Gulf of Mexico. J. Geophys. Res. 93 (C9), 10645-10654.

New, A. L. 1988. Internal tidal mixing in the Bay of Biscay. Deep-Sea Res. 35 (5), 691-709.

New, A. L., R. D. Pingree. 1990. Evidence for internal mixing near the shelf break in the Bay of Biscay. Deep-Sea Res. 37(12), 1783-1803.

Oke, P., J. Middleton. 2000. Topographically induced upwelling off eastern Australia. J. Phys. Oceanogr. 30, 512-531.

Painter S, S. Hartman, C. Kivimae, L. A. Salt, N. M. Clargo, Y. Bozec,c. J. Daniels, S. C. Jones, V. S. Hemsley, L. R. Munns, S. R. Allen. 2017. Carbon exchange between a shelf sea and the ocean: The Hebrides Shelf, west of Scotland. J. Geophys. Res. Oceans, 121, 4522-4544

Pedlosky, J. 2007. The coastal bottom boundary layer: a note on the model of Chapman and Lentz. J. Phys. Oceanogr. 37, 2776-2784.

Palmer, M. R., M. E. Inall, J. Sharples. 2013. The physical oceanography of Jones Bank: A mixing hotspot in the Celtic Sea. Prog. Oceanogr. 117, 9-24.

Pemberton, K., A. P. Rees, P. I. Miller, R. Raine, I. Joint. 2004. The influence of water body characteristics on phytoplankton diversity and production in the Celtic Sea. Cont. Shelf Res. 24(17), 2011-2028.

Pingree, R. D., P. M. Holligan, G. T. Mardell, R. N. Head. 1976. The influence of physical stability on spring, summer and autumn phyto-

plankton blooms in the Celtic Sea. Journal of the Marine Biological Association of the United Kingdom. 56, 845-873.

Pingree, R.D. L. Maddock, E. I. Butler. 1977. The influence of biological activity and physical stability in determning the chemical distributions of inorganic phosphate, silicate and nitrate. Journal of the Marine Biological Association of the United Kingdom. 57(4), 1065-1073.

Pingree, R. D. 1980. Physical Oceanography of the Celtic Sea and English Channel. In The North-West European Shelf Seas: the sea bed and the sea in motion II. Physical and Chemical Oceanography, and Physical Resources. Ed F. T. Banner, M. B. Collins and K. S. Massie. Elsevier Oceanography Series.

Pingree, R. D., B. Le Cann. 1989. Celtic and Armorican slope and shelf residual currents. Prog. Oceanog. 23, 303-338.

Pingree, R. D., B. Le Cann. 1990. Structure, strength and seasonality of the slope currents in the Bay of Biscay. Journal of the Marine Biological Association of the United Kingdom. 70 (4), 857-885.

Polton, J. A. 2015. Tidally induced mean flow over bathymetric features: A contemporary challenge for highresolution widearea models. Geophysical and Astrophysical Fluid Dynamics, 109, 207-215.

Pingree, R. D., A.L. New. 1995. Structure, seasonal development and sunglint spatial coherence of the internal tide on the Celtic and Armorican shelves and in the Bay of Biscay. Deep-Sea Res. Part 1. 42(2), 245-284.

Porter, M., M. E. Inall, J. Hopkins,M. R. Palmer, A. C. Dale, D. Aleynik,J. A. Barth, C. Mahaffey, D. A. Smeed. 2016. Glider observations of enhanced deep water upwelling at a shelf break canyon: A mechanism for cross-slope carbon and nutrient exchange. J. Geophys. Res.,121, 7575-7588, doi:10.1002/2016JC01208

Porter, M., M. Inall, J. Green, J. Simpson, A. Dale, P. Miller. 2016. Drifter observations in the summer time bay of Biscay slope current, J. Mar. Syst., 157, 65-74.

Poulton A. J., C. E. Davis, C. J. Daniels, K. M. J. Mayers, C. Harris, G. A. Tarran, C. E. Widdicombe, E. M. S. Woodward. 2018. Seasonal phosphorous and carbon dynamics in a temperate shelf sea (Celtic Sea). Progr. Oceanogr. In press. https://doi.org/10.1016/j.pocean.2017.11.001

Preisendorfer, R. W., C. D. Mobley. 1998. Principal component analysis in meteorology and oceanography. Elsevier Science and technology.

Rees, A. P., I. Joint, K. M. Donald. 1999. Early spring bloom phytoplankton-nutrient dynamics at the Celtic Sea Shelf Edge, Deep-Sea Res. I, 46, 483-510.

Rossi, V., M. Feng, C. Pattiaratchi, M. Roughan, A. M. Waite. 2013. On the factors influencing the development of sporadic upwelling in the Leeuwin current system. J. Geophys. Res. 118, 1-14.

Roughan, M., J. H. Middleton. 2002. A comparison of observed upwelling mechanisms off the east coast of Australia. Cont. Shelf Res. 22, 2551-2572.

Roughan, M., J. H. Middleton. 2004. On the East Australian current: variability, encroachment and upwelling. J. Geophys. Res. 109 (C7), C07003.

Ruiz-Castillo, E., J. Gomez-Valdes, J. Sheinbaum, R. Rioja-Nieto. 2016. Wind-driven coastal upwelling and westward circulation in the Yucatan shelf. Cont. Sh. Res. 118, 63-76.

Ruiz-Castillo, E., J. Sharples, J. Hopkins, M. Woodward. 2018. Seasonality in the cross-shelf physical structure of a temperate shelf sea and the implications for nitrate supply. In press.
https://doi.org/10.1016/j.pocean.2018.07.006

Sanders, T. M., R. W Garvine. 2001. Freshwater delivery to the continental shelf and subsequent mixing: An observational study. J. Geophys. Res. 106 (C11), 27087-27101.

Schaeffer, A., M. Roughan, 2015. Influence of a western boundary current on shelf dynamics and upwelling from repeat glider deployments. Geophys. Res. Lett., 42, 121-128.

Shapiro, G. I., A. E. Hill. 1997. Dynamics of dense water cascades at the shelf edge. J. Phys. Ocean. 27, 2381-2394.

Seguro, I., A. D. Marca, S. J. Painting, J. D. Shutler, D. J. Sugget, J. Kaiser. 2017. High-resolution net and gross biological production during a Celtic Sea spring bloom. Progr. Oceanogr. In press.
https://doi.org/10.1016/j.pocean.2017.12.003

Seitzinger, S., J. A. Harrison, J. K. Bohlke, A. F. Bouwman, R. Lowrance, B. Peterson, C. Tobias, G. V. Drecht. 2006. Denitrification across landscapes and waterscapes: a synthesis. Ecological Applications, 16, 2064-2090.

Sharples, J., M. C. Moore, T. P. Rippeth, P. M. Holligan, D. Hydes, N. R. Fisher, J. H. Simpson. 2001. Phytoplankton distribution and sur-

vival in the thermocline. Limn. Oceanogr. 46 (3), 486-496.

Sharples, J., O. N. Ross, B. E. Scott, S. P. R. Greenstreet, H. Fraser. 2006. Inter-annual variability in the timing of stratification and the spring bloom in the north-western north sea. Cont. Sh. Res., 26, 733-751.

Sharples, J., C. M. Moore, E. R. Abraham. 2001. Internal tide dissipation, mixing, and vertical nitrate flux at the shelf edge of NE New Zealand. J. Geophys.l Res., 106, 14069 - 14081.

Sharples, J., F. Tweddle, J. A. Mattias Green, M. R. Palmer, Y-N Kim, A. E. Hickman, P. M. Holligan, C. M. Moore, T. P. Rippeth, J. H. Simpson, V. Krivtsov. 2007. Springneap modulation of internal tide mixing and vertical nitrate fluxes at a shelf edge in summer. 52 (5), 1735-1747.

Sharples, J., J. Middelburg, K. Fennel, T. D. Jickkels. 2017. What proportion of riverine nutrients reaches the open ocean? Global Biogeochem. Cycles. 31, 39-58. doi: 10.1002/2016GB005483.

Simpson, J. H. 1976. A Boundary Front in the Summer Regime of the Celtic Sea. Estuar. Coast. Mar. Sci. 4, 71-81.

Simpson, J. H. 1981. The Shelf-sea fronts: implications of their existence and behaviour. Phil. Trans. R. Soc. Lond. A. 302, 531-546.

Simpson, J., J. Sharples. Introduction to the Physical and Biological Oceanography of Shelf Seas. Cambridge University Press. 2012. Pp 424.

Simpson J. H, R. R. McCandliss. 2013. "The Ekman drain": a conduit to the deep ocean for shelf material. Oc. dynam.63 (9-10), 1063-1072.

Smith, S. D., E. G. Banke. 1975. Variation of the sea surface drag coefficient with wind speed. Royal Meteorological society. 101 (429), 665-673.

Souza, A. J., J. H. Simpson, M. Harikrishnan, J. Malarkey. 2001. Flow structure and seasonality in the Hebridean slope current. Oc. Acta. 24 (1), 63-76.

Spingys, C., 2016. Volume exchange across the shelf edge: the role of the internal tide and other physical processes. PhD thesis.

Thomas, H.,Y. Bozec, K. Elkalay, H.J. W. de Baar. 2004. Enhances open ocean storage of CO_2 from shelf sea pumping. Science. 304 (5673), 1005-1008.

Thompson C. E. L., B. Sillburn, M. E. Williams, T. Hull, D. Sivyer,

L. O. Amoudry, S. Widdicombe, J. Ingels, G. Carnovale, C. L. McNeill, R. Hale, C. Laguionie Marchais, N. Hicks, H. E. K. Smith, J. K. Klar, J. G. Hiddink, J. Kowalik, V. Kitidis, S. Reynolds, E. M. S. Woodward, K. Tait, W. B. Homoky, S. Krger, S. Bolam, J. A. Godbold, J. Aldridge, D. J. Mayor, N. M. A. Benoist, B. J. Bett, K. J. Morris, E. R. Parker, H. A. Ruhl, P. J. Statham, M. Solan. 2017. An approach for the identification of exemplar sites for scaling up targeted field observations of benthic biogeochemistry in heterogeneous environments. Biogeochemistry (135) 1-34. DOI 10.1007/s10533-017-0366-1

Talley, L. D., G. L. Pickard., W. J. Emery, J. H. Swift. 2011. Descriptive Physical Oceanography: An introduction. Sixth Edition, Elsevier.

Thompson C. E. L., M. E. Williams, L. Amoudry, T. Hull, S. Reynolds, A. Panton, G. R. Fones. 2017. Cont. Shelf. Res., In press, doi: 10.1016/j.csr.2017.12.005

Thompson, R., W. Emery. Data Analysis Methods in Physical Oceanography. 3rd Edition. Elsevier, Amsterdam, 2014. Pp 701

Tilburg, C. E. 2003. Across-shelf transport on a continental shelf: do across shelf winds matter? J. Phys.Oceanogr. 33, 2675-2688.

Torres, H. S., J. G. Gomez-Valdes. 2015. Coastal circulation driven by short-period upwelling-favorable winds in the northern Baja California region. Deep Sea Res. I. 98, 31-42.

Townsend, D. W., L. M. Cammen, P. M. Holligan, D. E. Campbell, N. R. Pettigrew. 1994. Causes and consequences of variability in the timing of spring phytoplankton blooms. Deep Sea Res.I. 41(5-6) 747-765.

Uncles, R. J. 1984. Hydrodynamics of the Bristol Channel. Mar. Pollut. Bull. 15 (2), 47-53.

Uncles, J. 2010. Physical properties and processes in the Bristol Channel and Severn Estuary. Mar. Pollut. Bull. 61, 5-20.

Uncles, R. J., P. J. Radford. 1980. Seasonal and spring-neap tidal dependence of axial dispersion coefficients in the Severn - a wide, vertically mixed estuary. J. Fluid Mech. 98 (4), 703-726.

Uncles, R. J., J. A. Stephens. 2007. SEA 8 Technical Report- Hydrography.

Unesco, SCOR,ICES, IAPSO, Joint panel on oceanographic tables and standards. 1983. Algorithms for computation of fundamental properties of seawater.

van Aken, H. M. 2002. Surface currents in the Bay of Biscay as observed with drifters between 1995 and 1999. Deep Sea Res. I., 49 (6) 1071-1086.

Venegas, S.A.. 2001. Statistical methods for signal detection in climate. Tech. Rep.,76, Danish Center for Earth Systems science.

Vlasenko, V., C. Guo, N. Stashchuk. 2012. On the mechanism of A-type and B-type internal solitary wave generation in the northern south China Sea. Deep. Sea Res. I. 69, 100-112.

Walsh, J. J. 1991. Importance of continental margins in the marine biogeochemical cycling of carbon and nitrogen. Nature. 350, 53-55

Wihsgott, J. U.,J. Sharples, J. E. Hopkins, E. Malcolm, S. Woodward, N. Greenwood, T. Hull, D. B. Sivyer. 2019. Observations of vertical mixing in autumn and its effect on the autumn phytoplankton bloom. Progr. Oceanogr. In press. https://doi.org/10.1016/j.pocean.2019.01.001

Wihsgott J., J. Hopkins, J. Sharples, E. Jones, C. A. Balfour. 2016. Long-term mooring observations of full depth water column structure spanning 17 months, collected in a temperate shelf sea (Celtic Sea). British Oceanographic Data Centre - Natural Environment Research Council, UK. doi:10/bqwf.

Wihsgott J., J. Hopkins, J. Sharples , C. A. Balfour, E. Jones. 2018. Long-term, full depth observations of horizontal velocities spanning 17 months, collected in a temperate shelf sea (Celtic Sea) on the NW European Shelf. British Oceanographic Data Centre - Natural Environment Research Council, UK. doi:10/cjrh.

Williams, C., J. Sharples, C. Mahaffey, T. Rippeth. 2013. Wind-driven nutrient pulses to the subsurface clorophyll maximum in seasonally stratified shelf seas. Geophys. Res. Lett. 40, 5467-5472.

Winant, C.D.. 1980. Downwelling over the southern California Shelf. J. Phys. Oceanogr. 10, 791-799

Woodward, E.M.S. 2016. Discrete inorganic nutrient samples collected from the Celtic Sea during RRS Discovery cruise DY026B in August 2014. British Oceanographic Data Centre - Natural Environment Research Council, UK. doi:10/bhpg.

Young, E. F., J. Brown, J. N. Aldridge, K. J. Horsburgh, L. Fernand. 2004. Development and application of a three-dimensional baroclinic model to the study of the seasonal circulation in the Celtic Sea. Cont. Sh. Res., 24, 13-36.